UNIVERSITÀ DEGLI STUDI DI TRENTO
Facoltà di Scienze Matematiche Fisiche e Naturali
Scuola di Dottorato in Fisica

Tesi per il conseguimento del titolo di
Dottore di Ricerca

Light Propagation in Ultracold Atomic Gases

Relatore: Dr. Iacopo CARUSOTTO

Candidato:
Francesco BARIANI

XXII CICLO - Anno Accademico 2008-2009

To my Family:
Graziano, Luisa and Fabio.

In memory of Nicola Fambri.

Contents

Introduction

After the development of laser sources, atomic gases have been used as an optical medium to study non-linear processes. Via the presence of atoms an intense laser beam can influence its own properties or those of other beams [1]. The gaseous samples allow to treat directly the discrete and well-known energetic structure of atoms to carry out *ab initio* calculations starting from the interaction between light and a single atom. These predictions can be experimentally tested with high precision by means of spectroscopic techniques.

Later on, light has been demonstrated as a very powerful tool not only to study atoms but also to manipulate them. During the last thirty years, in the field of *Atomic Molecular Optical* (AMO) Physics the development of laser cooling and trapping of neutral atoms [2] has lead to an impressive series of achievements related to the investigation of the outstanding properties of ultracold matter. Among these, the experimental realization of *Bose Einstein Condensation* (BEC) is the most famous [3].

The combination of these reciprocal interactions induces back-action effects that result in surprising phenomena. For instance, the kick given by the probe light to the interrogated atoms in the precision spectroscopy experiment of [4] was able to shift the position of the resonance fluorescence line of a significant amount. Furthermore, in the first experiments with optical lattices [5, 6], the change in the lattice constant due to the effective index of refraction of the atomic sample itself was detected via Bragg spectroscopy [7].

More recently, the mutual effects arising from atom-laser interaction in an ultracold sample were shown in a most clean way by the cavity optomechanics experiment [8]. In this setup a BEC is put inside an optical cavity and then a laser beam is shined which is far off-resonant with respect any electronic transitions of atoms while it is resonant with a cavity mode. The excitation of the cavity mode induces an effective lattice potential for the condensate which is then modulated in density. The refractive index

due to the presence of the atomic medium is then accordingly spatially modulated resulting in a shift of the cavity frequency. This interplay has a sharp signature in the oscillating transmission spectrum of the cavity.

The use of ultracold matter as an efficient tool to manipulate light is the key idea of the present work. We start from an optical point of view: we have investigated the features of ultracold atomic gases as an extremely dispersive and tunable medium for light propagation. Inspired by the development in solid-state systems of structures designed to have a specific optical response such as *Photonic Crystals* [9] or metamaterials [10], we have joined the sharp features of cold samples with the intriguing effects deriving from spatially modulated geometries and coherent dressing of atomic states. The focus is the proof of principle of techniques which may be important in view of optical information processing. Cold matter allows to get rid of spurious effects present in solid-state devices and then to address the underlying physics in these phenomena. Cold gases take also advantage from the suppression of Doppler broadening with respect hot atomic vapor.

Before the achievement of BEC, some attention was paid to the study of coherent scattering of photons by the atoms in the condensate phase to determine the refractive index of the sample [11–13]. The use of light which is resonant with some atomic transition enhances dramatically the atom-photon coupling: the strong coupling regime is reached when the matrix element for the interaction is bigger then the linewidth of the atomic transition. While in semiconductors this coupling leads to mixed radiation-matter excitations called *polaritons*, in gaseous atomic media resonant light is usually strongly absorbed preventing the observation of the Rabi splitting.

The achievement of *Mott Insulator* (MI) phase for a BEC loaded into a deep optical lattice [14] has opened an interesting perspective in order to observe polariton physics in ultracold samples: the strong localization of atoms at the lattice sites is in fact responsible for a quenching of absorption [15]. In a modern perspective, the atomic MI can be seen as a sort of extremely resonant photonic crystal. A key point discussed in literature is the existence of a complete photonic band gap in such structures [16–18]. The interplay of conventional polariton (Rabi) splitting and the diffraction due to the lattice arrangement is at basis of different regimes for the optical response [19]. Although the radiation-matter coupling is much weaker than in solid-state dielectric structures, the high regularity of MI strongly decreases the dephasing mechanisms.

The response of this systems around the resonance frequency is dominated by both strong reflectivity and absorption processes which result in light being forbidden from propagating through the medium. By exploiting

dark resonances in dressed atomic gases it is possible to overcome this limitation. The existence of non absorbing resonances in three-level atomic systems pumped by two laser beams was first discovered during spectroscopic experiments in sodium vapors [20]. Thanks to the interference between different excitation processes, atoms are driven into a coherent superposition of states that is eventually decoupled from radiation: this is the essence of the *Coherent Population Trapping* [21]. Furthermore, the coherent control of the optical response of a medium by means of a strong laser field allows for the optical switching of the propagation of a second weak probe beam, leading to the so called *Electromagnetically Induced Transparency* (EIT) [22–24]. Among the different realizations, ultracold samples offer a unique environment which is protected from decoherence: this is favourable even in the case of such a robust phenomenon as EIT.

The propagation of light through otherwise optically opaque media can be described within a polariton treatment in the three-level system. Beyond the conventional resonant polaritons typical of two-level atoms, a narrow branch appears at resonance: this is the *Dark Polariton* (DP) which consists of a coherent mixing of radiation and atomic excitations corresponding to a two-photon Raman resonance [25–27]. The DP is responsible for EIT and shows interesting properties: it is long-living because of the suppression of absorption, it suffers no reflection at the boundaries of the system and, most remarkably, its group velocity can be optically tuned by means of the control beam down to very small values [28]. The complete turn off of the control beam provides a full mapping of the probe pulse into atomic (spin-like) excitations. The process can be reversed resulting in a light storage and retrieval from atoms [29]. Both ultraslow light and light storage were demonstrated in cold atomic samples [30,31] while more recently the use of an atomic MI has shown a promising increase of the storage time up to some hundreds of milliseconds [32].

The increase of the interaction time due to the small speed of probe pulses joined with the tunability of the optical response enhances the possibilities to perform a dynamic modulation of the light signal. Such modulations are the goal of *Dynamic Photonic Structures* (DPS) [33]. The general concept of DPS is based on a pulsed experiment where the optical response of a medium is varied in time while the probe signal is inside the structure. This configuration allows for an efficient manipulation at both classical and quantum level. The perturbation of the medium can be applied through a control laser beam (all-optical technique) or by means of other mechanisms (e.g. injection of carries or magnetic field ramps).

Although the more complete modern theories implies that both light and matter are represented by quantum fields, radiation-matter interaction can still be treated within a semi-classical picture in a lot of situations:

the electro-magnetic (e.m.) field is considered as a classical object and the energetic structure of matter is quantized. This formalism dates back to the birth of quantum mechanics and can be applied to all the processes in which the quantum nature of light is still hidden such as e.g. the stimulated emission, up to many aspects of laser physics [34]. In particular, at the level of linear optics, i.e. for weak e.m. fields, classical Maxwell's theory fully describes the dynamics of the radiation field. Within this formalism the effect of radiation on the matter appears through the minimal coupling replacement into the Schrödinger's equation. Vice versa, the presence of matter generates a polarization term into the Maxwell's equations which gives the refractive properties of the material. The self-consistent connection between the two formalisms is given by a density matrix representation of the atomic evolution which allows to transfer the results of the Schrödinger's equation into Maxwell's. Dissipative effects due to vacuum fluctuations (i.e. spontaneous emission) are included within a master equation treatment.

The propagation of light through an ultracold atomic gas is the main topic of the present work.
The thesis consists of two parts.
In Part I (Chapters 1,2,3), we give a complete description of the 1D photonic bands of a MI of two-level atoms paying attention to both band diagrams and reflectivity spectra. The role of regular periodicity of the system is addressed within a polariton formalism. The scattering on defects inside lattices of three-level atoms is also studied in view of optical detection of impurities in such structures. The light is used as a probe of systems engineered by the use of other laser beams.
Part II (Chapters 4,5) is devoted to the development of a general framework for the time-dependent processing of a propagating slow DP in a spatially inhomogeneous system. The coherently tunable atomic gas acts as a DPS. Applications of this concept concerning wavelength conversion and reshaping of the pulse are also discussed.

The theoretical tools used to face the semi-classical theory of radiation-matter interaction in the systems under investigation are: *Maxwell-Bloch* (MB) formalism [35] and *Transfer Matrix* (TM) technique [36].
We have restricted to a 1D geometry with transverse polarized probe beams which allows to consider e.m. radiation as a scalar field. We have solved the photonic band problem by means of TM that give the stationary response of 1D layered dielectric structures starting from the susceptibility of each single layer. The interest in this technique is related to its simplicity, numerical stability and to the fact that it allows to simultaneously calculate both dispersion law and reflectivity spectra.
The study of the time evolution of a pulse injected and propagating through an EIT medium is performed by means of MB equations for the

coupled electric and atomic polarization fields. The use of a modified version of the conventional *Slowly Varying Envelope Approximation* (SVEA) makes possible to handle the problem of reflection at interfaces in a unified treatment without the need for coupled mode theory.

The thesis is organized as follows.
In Chapter 1, we briefly review the semi-classical theory for atom-laser interaction by using *Optical Bloch Equations* (OBE). The general form for the evolution of atomic coherences and the corresponding resonant cases are reported in order to derive the dispersive susceptibility for both two-level and three-level atoms. It is also discussed the difference between the response of a single atom as compared to a cloud (Clausius-Mossotti formula).

The photonic bands of an atomic MI are studied in Chapter 2. Two distinct regimes are individuated depending on the relative position of the resonant and Bragg frequencies with respect to polariton splitting. The band diagram as well as reflectivity spectra are discussed. For the reflection properties, two different geometries are addressed: the semi-infinite system and the finite slab. The variation of resonant reflectivity from a single atom to a long lattice is also highlighted.

In Chapter 3, the EIT phenomenon in an atomic gas is introduced and its main features are discussed in terms of a polariton dispersion. The reflectivity dip corresponding to the slow DP is used to study the scattering on defects of the atomic system such as lack of atoms at some sites of a MI. The defect can be seen as a cavity which supports localized modes. Furthermore, by using an atomic defect instead of a vacuum region, a peak appears and it can be moved within the EIT window.

A complete MB formalism is developed in Chapter 4 aiming to study the propagation of a pulse through a generic inhomogeneous and time-dependent structure composed of alternating layers of vacuum and EIT media. The *modified SVEA* (mSVEA) is presented and its main features and limitations are pointed out. The pulse propagation is investigated in two geometries: a homogeneous layer and an interface, in both static and dynamic situations. An effective equation for the flow of the electric field intensity is derived.

Finally, in Chapter 5 we describe some relevant physical aspects of DPS. The chapter is divided in three parts. The first one deals with the problem of the effective coupling between different polariton bands, induced by the time-evolution of the system parameters. In the second part, we propose the scheme for a cold gas *Photon Energy Lifter* [37] which performs a wavelength conversion of a DP pulse. In the last part, it is presented the general idea of a inhomogeneous structure (*EIT chain*) devoted to the reshaping of the electric field of a light signal. At the level of linear optics,

this is equivalent to the manipulation of photon wavefunction. Both for the photon lifter and the EIT chain, realistic values extracted from current experiments are used in the simulations.

The acronyms and physical constants used in the thesis are summarized in the final appendix *Notation*.

Part I

Probing Structures

CHAPTER 1

Resonant atom-light interaction

The interaction between atoms and light is mainly determined by the resonances related to the discrete structure of the energetic levels. The separation in energy between the different levels and the use of light sources with a reduced spread in frequency (i.e. lasers) allow to play selectively with one or few of these levels. Dilute cold gases offer the possibility to study the optical response of the whole medium with simple techniques starting from the atomic behavior.

In Section 1, we summarize the derivation of the optical response of an atom to a probe field via a density matrix approach. The resulting *Optical Bloch Equations* (OBE) are presented.

In Section 2, we calculate the stationary situations at linear order in the probe field in order to obtain the susceptibility of an ensemble of two-level atoms. From the general case, we specify the atomic susceptibility for a resonant radiation and we introduce a generalized oscillator strength f as an adimensional parameter describing the atom-photon coupling.

We apply the same procedure to the case of a three-level Λ atomic configuration in Section 3. In this case the response of the atomic gas is tailored by the intensity of a control laser beam.

In Section 4, we show a brief derivation of the Clausius-Mossotti correction for the susceptibility of a dense atomic bulk. It results in an effective shift of the atomic resonance frequency.

1.1 Optical Bloch Equations

We consider a semi-classical picture in which the (light) electric field $E(x,t)$ is a classical object while the atomic transitions are represented through operators (i.e. the density matrix). We specify the density matrix only to the relevant atomic levels, i.e. the initial state, the levels coupled through some light field to the ground state and the levels which can be reached through decay mechanisms. In the weak excitation regime, the dynamics of the atomic ensemble under the action of resonant or quasi-resonant coherent (laser) fields can be described using a linearized form of the OBE [21, 35]. The general form of OBE is:

$$i\hbar\frac{\partial\hat{\rho}}{\partial t} = [\hat{H},\hat{\rho}] + \mathcal{L}(\hat{\rho}). \tag{1.1}$$

The first term in the LHS is the usual Von Neumann commutator for the evolution of the density matrix $\hat{\rho}$ under the action of a radiation-matter Hamiltonian $\hat{H}$. In order to describe the real evolution of the atomic system, the OBE include dissipative terms, $\mathcal{L}(\hat{\rho})$. These terms come from a master equation treatment and are responsible for the loss of coherence in the radiation-matter interaction as well as spontaneous emission [24]. In fact, the relevant quantities for our purposes are the so called *coherences* ρ_{ab}, i.e. the off-diagonal elements of the atomic density matrix $\hat{\rho} = \sum_{a,b}\rho_{ab}\left|a\right\rangle\left\langle b\right|$, where a and b label the internal atomic states [1]. In terms of the coherences ρ_{lg} the atomic polarization reads

$$P(x,t) = \sum_{l} n(x,t)\, d_{lg}\ \left(\rho_{lg}(x,t) + \rho_{gl}(x,t)\right). \tag{1.2}$$

Here, d_{gl} is the electric dipole moment of the transition from the ground $|g\rangle$ state to a generic excited state $|l\rangle$; $n(x,t)$ is the atomic density of the medium. The susceptibility is then determined from its definition

$$\mathcal{P}(\omega) = \epsilon_0\chi(\omega)\mathcal{E}(\omega), \tag{1.3}$$

which is given here in the frequency domain. In the following we will consider two cases: the two-level atom and the three-level Λ configuration, shown in Fig. 1.1.

[1] From now on, we drop the symbol '^' from the notation wherever it is clear which quantities are operators.

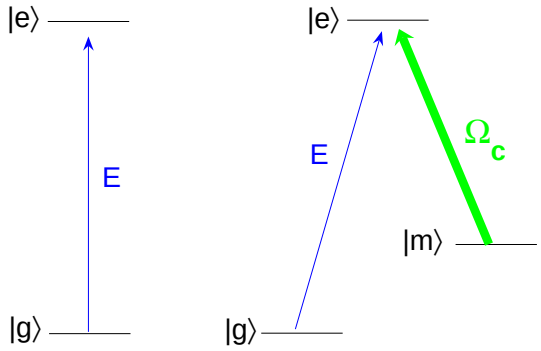

FIGURE 1.1: Excitation schemes: on the left, 2-level atom; on the right, 3-level Λ scheme.

1.2 Resonant Susceptibility for two-level atom

We consider the electric field of a laser $E(t) = \mathcal{E}\left(e^{-i\omega t} + c.c.\right)$ that interacts with the transition between two levels of an atom: the ground state $|g\rangle$ and an excited state $|e\rangle$. We suppose that the other levels are far from probe frequency ω which is tuned near the transition frequency $\omega_{eg} = \omega_e - \omega_g$. The Hamiltonian of the system consists of an atomic part,

$$H_A = \hbar\omega_g \left|g\right\rangle \left\langle g\right| + \hbar\omega_e \left|e\right\rangle \left\langle e\right|, \tag{1.4}$$

and a radiation-matter interaction part,

$$H_{AR} = -d_{eg}\mathcal{E}\left(e^{-i\omega t}\left|e\right\rangle \left\langle g\right| + h.c.\right). \tag{1.5}$$

Within the rotating wave approximation [34, 35], we are only considering the resonant terms for interaction. The first term in the RHS of equation (1.1), that corresponds to the usual Von Neumann equation, gives

$$i\hbar\frac{d\rho_{gg}}{dt} = -d_{eg}\mathcal{E}\left(\rho_{eg}e^{i\omega t} - \rho_{ge}e^{-i\omega t}\right), \tag{1.6a}$$

$$i\hbar\frac{d\rho_{ee}}{dt} = -d_{eg}\mathcal{E}\left(\rho_{ge}e^{-i\omega t} - \rho_{eg}e^{i\omega t}\right), \tag{1.6b}$$

$$i\hbar\frac{d\rho_{eg}}{dt} = \hbar\left(\omega_e - \omega_g\right)\rho_{eg} + d_{eg}\left(\rho_{ee} - \rho_{gg}\right)\mathcal{E}e^{-i\omega t}, \tag{1.6c}$$

$$i\hbar\frac{d\rho_{ge}}{dt} = -\hbar\left(\omega_e - \omega_g\right)\rho_{eg} - d_{eg}\left(\rho_{ee} - \rho_{gg}\right)\mathcal{E}e^{i\omega t}. \tag{1.6d}$$

We eliminate the exponential factors by introducing the reduced coherences $\tilde{\rho}_{eg} = \rho_{eg}e^{i\omega t}$ and $\tilde{\rho}_{ge} = \rho_{ge}e^{-i\omega t}$, while ρ_{ee} and ρ_{gg} are unchanged:

$$i\hbar\frac{d\rho_{gg}}{dt} = -d_{eg}\mathcal{E}\left(\tilde{\rho}_{eg} - \tilde{\rho}_{ge}\right), \tag{1.7a}$$

$$i\hbar\frac{d\rho_{ee}}{dt} = -d_{eg}\mathcal{E}\left(\tilde{\rho}_{ge} - \tilde{\rho}_{eg}\right), \tag{1.7b}$$

$$i\hbar\frac{d\tilde{\rho}_{eg}}{dt} = \hbar\left(\omega_{eg} - \omega\right)\tilde{\rho}_{eg} + d_{eg}\mathcal{E}\left(\rho_{ee} - \rho_{gg}\right), \tag{1.7c}$$

$$i\hbar\frac{d\tilde{\rho}_{ge}}{dt} = -\hbar\left(\omega_{eg} - \omega\right)\tilde{\rho}_{eg} - d_{eg}\mathcal{E}\left(\rho_{ee} - \rho_{gg}\right). \tag{1.7d}$$

We use the second term in the RHS of equation (1.1) to introduce the lifetime of the atomic level γ which determines the decay of the excited state population ρ_{ee} and the lose of coherence during the interaction process. The OBE then read

$$\frac{d\rho_{gg}}{dt} = i\frac{d_{eg}\mathcal{E}}{\hbar}\left(\tilde{\rho}_{eg} - \tilde{\rho}_{ge}\right) + \gamma\rho_{ee}, \tag{1.8a}$$

$$\frac{d\rho_{ee}}{dt} = i\frac{d_{eg}\mathcal{E}}{\hbar}\left(\tilde{\rho}_{ge} - \tilde{\rho}_{eg}\right) - \gamma\rho_{ee}, \tag{1.8b}$$

$$\frac{d\tilde{\rho}_{eg}}{dt} = -i\left(\omega_{eg} - \omega\right)\tilde{\rho}_{eg} - i\frac{d_{eg}\mathcal{E}}{\hbar}\left(\rho_{ee} - \rho_{gg}\right) - \frac{\gamma}{2}\tilde{\rho}_{eg}, \tag{1.8c}$$

$$\frac{d\rho_{ge}}{dt} = +i\left(\omega_{eg} - \omega\right)\tilde{\rho}_{eg} + i\frac{d_{eg}\mathcal{E}}{\hbar}\left(\rho_{ee} - \rho_{gg}\right) - \frac{\gamma}{2}\tilde{\rho}_{ge}. \tag{1.8d}$$

From the first two equations, it is visible the conservation of the trace of the density matrix, while the latter two equations state that the density matrix is always hermitian. For this reason, we need only one from the last two equations. We also note the quantity $\Omega = -(d_{eg}\mathcal{E})/\hbar$ which is usually called the *Rabi frequency* of the laser field. If we consider a gas of atoms which are in the ground state at the intial time and we assume the electric field to be weak, at linear order in $\mathcal{E}$ we obtain $\rho_{gg} = 1$ and $\rho_{ee} = 0$ from (1.8). We are interested in particular in the stationary solution of the equation (1.8c):

$$\tilde{\rho}_{eg} = -i\frac{d_{eg}\mathcal{E}}{\hbar}\frac{1}{i(\omega - \omega_{eg}) - \gamma/2} = \tag{1.9}$$

$$= \frac{d_{eg}\mathcal{E}}{\hbar}\frac{1}{\omega_{eg} - \omega - i\gamma/2}. \tag{1.10}$$

By using (1.2) and (1.3), we obtain the susceptibility of a gas of two-level atoms:

$$\chi(\omega) = \frac{nd_{eg}^2}{\epsilon_0\hbar}\frac{1}{\omega_{eg} - \omega - i\gamma/2}. \tag{1.11}$$

We remind that this result is valid in the range of frequency near the resonance.

1.2.1 The oscillator model

To get the susceptibility far off-resonance it is possible to model the atomic transition as an harmonic oscillator with proper frequency ω_{eg} subject to a forcing term due to the probe field E and affected by a dissipative term based on γ. To write the equation of motion of such a system we introduce the mass m_e and charge e of the electron and we assume z as the direction of oscillation:

$$m_e \frac{d^2 z}{dt^2} = eE - m_e \omega_{eg}^2 z - m_e \gamma \frac{dz}{dt}. \tag{1.12}$$

By switching to the frequency domain, we obtain

$$-m_e \omega^2 z + m_e \omega_{eg}^2 z - i m_e \gamma \omega z = eE. \tag{1.13}$$

The polarization of the atomic gas is given in terms of the dipole moment of the single atom

$$P = nez = \epsilon_0 \chi E, \tag{1.14}$$

where n is the atomic density. From (1.13) and (1.14), we obtain the

$$\chi(\omega) = \frac{ne^2}{m_e \epsilon_0} \frac{1}{\omega_{eg}^2 - \omega^2 - i\gamma\omega} \tag{1.15}$$

which is the so called *Drude-Lorentz* formula. The factor

$$\omega_p^2 = \frac{ne^2}{m_e \epsilon_0} \tag{1.16}$$

is the square of the *plasma frequency* of the atomic gas. In the limit of resonant excitation, ($\omega \to \omega_{eg}$), the linearized form of (1.15) gives the expression (1.11) and it is possible a comparison with the measurable quantities related to a real atom. In general, the plasma frequency is used to express the numerator of the susceptibility by defining the adimensional *oscillator strength* f [38]:

$$\chi(\omega) = \frac{f\omega_p^2}{\omega_{eg}^2 - \omega^2 - i\gamma\omega}. \tag{1.17}$$

Throughout the present work, we decide to use the slightly different formulation

$$\chi(\omega) = \frac{f\omega_{eg}^2}{\omega_{eg}^2 - \omega^2 - i\gamma\omega}, \tag{1.18}$$

which keeps the adimensionality of f, but it uses the transition frequency instead of ω_p. From the comparison of (1.15) and (1.11), we obtain:

$$\frac{f\omega_{eg}}{2} = \frac{nd_{eg}^2}{\epsilon_0 \hbar}. \tag{1.19}$$

In the following we will always refer to the oscillator strength as a crucial parameter to determine the strength of radiation-matter interaction.

1.3 Resonant Susceptibility for three-level atom

In the case of the Λ scheme depicted in Fig. 1.1, we also consider the level $|m\rangle$ that is coupled to the excited state via a (generally) strong coherent field, represented through its Rabi frequency Ω_c. This field is addressed as the *control* or *dressing* field to distinguish from the probe field E. The optical transition between the state $|m\rangle$ and the ground state is forbidden for symmetry rules: the state is then long-living with respect $|e\rangle$ and therefore it is called *metastable*. It means that $\gamma_m \ll \gamma_e$, where the subscripts clearly refer to the different atomic states. We also assume the excited state to have the same decay rate γ_e towards both the ground and metastable states. The Hamiltonian for the three-level Λ configuration is given by

$$\begin{aligned} H_A &= \hbar\omega_g |g\rangle\langle g| + \hbar\omega_e |e\rangle\langle e| + \hbar\omega_m |m\rangle\langle m|, && \text{(1.20a)} \\ H_{AR} &= -d_{eg}\mathcal{E}\left(e^{-i\omega t}|e\rangle\langle g| + h.c.\right) + \\ &\quad + \hbar\frac{\Omega_c}{2}\left(e^{-i\omega_c t}|e\rangle\langle m| + h.c.\right). && \text{(1.20b)} \end{aligned}$$

As the density matrix is hermitian, the general form of the OBE equations is given by the six equations:

$$\begin{aligned} i\hbar\frac{d\rho_{gg}}{dt} &= -d_{eg}\mathcal{E}\left(\rho_{eg}e^{i\omega t} - c.c.\right) + i\frac{\hbar\gamma_e}{2}\rho_{ee}, && \text{(1.21a)} \\ i\hbar\frac{d\rho_{ee}}{dt} &= d_{eg}\mathcal{E}\left(\rho_{eg}e^{i\omega t} - c.c.\right) + \frac{\hbar\Omega_c}{2}\left(\rho_{me}e^{-i\omega_c t} - c.c.\right) + \\ &\quad -i\hbar\gamma_e\rho_{ee}, && \text{(1.21b)} \\ i\hbar\frac{d\rho_{mm}}{dt} &= -\frac{\hbar\Omega_c}{2}\left(\rho_{me}e^{-i\omega_c t} - c.c.\right) + i\frac{\hbar\gamma_e}{2}\rho_{ee}, && \text{(1.21c)} \\ i\hbar\frac{d\rho_{eg}}{dt} &= \hbar\omega_{eg}\rho_{eg} + d_{eg}\mathcal{E}e^{-i\omega t}(\rho_{ee} - \rho_{gg}) + \frac{\hbar\Omega_c}{2}\rho_{mg}e^{-i\omega_c t} + \\ &\quad -i\frac{\hbar\gamma_e}{2}\rho_{eg}, && \text{(1.21d)} \\ i\hbar\frac{d\rho_{mg}}{dt} &= \hbar\omega_{mg}\rho_{mg} + \frac{\hbar\Omega_c}{2}\rho_{eg}e^{i\omega_c t} - d_{eg}\mathcal{E}e^{-i\omega t}\rho_{me} + \\ &\quad -i\frac{\hbar\gamma_m}{2}\rho_{mg}, && \text{(1.21e)} \\ i\hbar\frac{d\rho_{me}}{dt} &= \hbar\omega_{me}\rho_{me} + \frac{\hbar\Omega_c}{2}e^{i\omega_c t}(\rho_{ee} - \rho_{mm}) - d_{eg}\mathcal{E}e^{i\omega t}\rho_{mg} + \\ &\quad -i\frac{\hbar\gamma_e}{2}\rho_{me}. && \text{(1.21f)} \end{aligned}$$

At the linear order in the amplitude of the electric field $\mathcal{E}$ only the ground state is populated: $\rho_{gg} = 1$ while $\rho_{ee} = \rho_{mm} = 0$. Furthermore the coherence ρ_{me} is a term of second order in the amplitude of the probe field as

can be seen from (1.21f) and (1.21e). By exploiting these observations, we are left with the equations (1.21d) and (1.21e) in order to determine the linear susceptibility:

$$i\hbar\frac{d\rho_{eg}}{dt} = \hbar\omega_{eg}\rho_{eg} - d_{eg}\mathcal{E}e^{-i\omega t} + \frac{\hbar\Omega_c}{2}\rho_{mg}e^{-i\omega_c t} - i\frac{\hbar\gamma_e}{2}\rho_{eg}, \quad (1.22a)$$

$$i\hbar\frac{d\rho_{mg}}{dt} = \hbar\omega_{mg}\rho_{mg} + \frac{\hbar\Omega_c}{2}\rho_{eg}e^{i\omega_c t} - i\frac{\hbar\gamma_m}{2}\rho_{mg}. \quad (1.22b)$$

To eliminate the exponential phases we define new coherence variables: $\tilde{\rho}_{eg} = \rho_{eg}e^{i\omega t}$ and $\tilde{\rho}_{mg} = \rho_{mg}e^{i(\omega-\omega_c)t}$. The equations then become

$$\frac{d\tilde{\rho}_{eg}}{dt} = -\left(\frac{\gamma_e}{2} + i\delta_e\right)\tilde{\rho}_{eg} + i\frac{d_{eg}\mathcal{E}}{\hbar} - i\frac{\Omega_c}{2}\tilde{\rho}_{mg}, \quad (1.23a)$$

$$\frac{d\tilde{\rho}_{mg}}{dt} = -\left(\frac{\gamma_m}{2} + i\delta_R\right)\tilde{\rho}_{mg} - i\frac{\Omega_c}{2}\tilde{\rho}_{eg}. \quad (1.23b)$$

Here we have defined the one-photon detuning from the excited state $\delta_e = \omega_{eg} - \omega$ and the detuning $\delta_R = \omega_{mg} + \omega_c - \omega$ from the two-photon *Raman* transition that connects the ground to the metastable state. The stationary solution of the reduced system (1.23) reads

$$\tilde{\rho}_{mg} = -\tilde{\rho}_{eg}\frac{i\Omega_c/2}{\gamma_m/2 + i\delta_R}, \quad (1.24a)$$

$$\tilde{\rho}_{eg} = \frac{d_{eg}\mathcal{E}}{\hbar}\left[\delta_e - i\gamma_e/2 - \frac{\Omega_c^2}{4}\frac{1}{\delta_R - i\gamma_m/2}\right]^{-1}. \quad (1.24b)$$

As in the previous case, it is straightforward to obtain the linear susceptibility

$$\chi(\omega) = \frac{f\omega_{eg}}{2}\left[\delta_e - i\gamma_e/2 - \frac{\Omega_c^2}{4}\frac{1}{\delta_R - i\gamma_m/2}\right]^{-1}, \quad (1.25)$$

where we have introduced the oscillator strength (1.19).

1.3.1 Coupled Oscillators model

We calculate the off-resonance susceptibility by using a coupled harmonic oscillators model. For simplicity we consider the Raman resonance condition, which consists of using the same frequency for both the harmonic oscillators. We start from the single oscillator model (1.12) and we add a second harmonic oscillator through the coupling constant given by the control Rabi frequency Ω_c. The Newton's equation for this system are

$$m_e\frac{d^2z}{dt^2} = -m_e\omega_{eg}^2 z + eE - m_e\omega_{eg}\Omega_c y - m_e\gamma\frac{dz}{dt} \quad (1.26)$$

$$m_e\frac{d^2y}{dt^2} = -m_e\omega_{eg}^2 y - m_e\omega_{eg}\Omega_c z - m_e\gamma_m\frac{dy}{dt}, \quad (1.27)$$

where the friction term for the second oscillator is proportional to the dephasing rate. By considering an oscillatory forcing field $E(t)$ at frequency ω, we solve the model. From the second equation we obtain

$$y(-\omega^2 + \omega_{eg}^2 - i\gamma_m\omega) = \omega_{eg}\Omega_c z. \tag{1.28}$$

By substituting this result into (1.26), we express the oscillating dipole in terms of the forcing electric field

$$d = ez = \frac{e^2}{m_e}\left(\omega_{eg}^2 - \omega^2 - i\gamma\omega - \frac{\Omega_c^2\omega_{eg}^2}{\omega_{eg}^2 - \omega^2 - i\gamma_m\omega}\right)^{-1} E. \tag{1.29}$$

The dielectric susceptibility is then

$$\chi(\omega) = \frac{ne^2}{m_e\epsilon_0}\left[\omega_{eg}^2 - \omega^2 - i\gamma\omega - \frac{\Omega_c^2\omega_{eg}^2}{\omega_{eg}^2 - \omega^2 - i\gamma_m\omega}\right]^{-1}, \tag{1.30}$$

which gives, in the resonant limit $\omega \to \omega_{eg}$ and by introducing the oscillator strength, the expression (1.25).

1.4 Clausius - Mossotti Susceptibility

In the previous sections, we have calculated the dielectric response of the atomic medium starting from the single atom behavior given by the Bloch equations and then by multiplying the atomic density n. This procedure automatically identifies two different quantities: the susceptibility χ we have mentioned up to now, and the polarizability α. The first quantity is defined in relation to *macroscopic* fields, namely the polarization of a region containing a huge number of atoms and the mean electric field, while the latter gives the polarization of a single atom in terms of the *local* electric field acting on it. Strictly speaking the OBE give the atomic polarizability and in the calculations we have assumed that

$$\chi = n\alpha. \tag{1.31}$$

This relation is a sort of first order approximation which holds for dilute systems. To obtain the correct relation between the two quantities, we need to consider the difference between the mean electric field E and the local one E_{loc}. The local electric field acting on the single atom we are considering is given by the mean field contribution E, minus the average polarization induced by the region (macroscopically small, but with a large number of atoms) surrounding it E_P, plus the detailed effect of the same atoms E_{det}:

$$E_{loc} = E - E_P + E_{det}. \tag{1.32}$$

It is demonstrated that the global effect of a set of dipoles arranged in a cubic lattice on one of them vanishes: $E_{det} = 0$ [39]. On the other hand, the average effect of a homogeneous polarization P inside a spherical cavity round the atom gives [39]

$$E_{loc} = E + \frac{4\pi}{3}P. \tag{1.33}$$

Then the susceptibility results

$$\chi = \frac{n\alpha}{1 - \frac{4\pi}{3}n\alpha}. \tag{1.34}$$

This formula is know as the *Clausius-Mossotti* or *Lorentz-Lorenz* correction[2]. If we substitute (1.11) to α in (1.34) we get

$$\chi = \frac{f\omega_{eg}}{2}\left[\omega_{eg} - \omega - i\frac{\gamma}{2} - \frac{4\pi}{3}\frac{f\omega_{eg}}{2}\right]^{-1}. \tag{1.35}$$

The typical value of f in the ultracold atomic gases is of the order of 10^{-10} to 10^{-8}: this shift in the position of the resonance frequency, which is in the MHz to GHz range, is to be considered in the experiments. In the following we always refer to the (shifted) resonance frequency for the considered atomic gas as ω_{eg}. As we have seen above, the calculation of this shift depends on the particular geometry under investigation and its derivation on specific cases is beyond the aim of this work.

[2] A detailed derivation of this effect in the case of a lattice of atoms can be found in [18, 40].

chapter 2

Optical response of a Mott Insulator of two-level atoms

After the achievement of *Bose Einstein Condensation* (BEC) [3] in alkali atoms, one of the most important trends emerged in the field of laser trapping are *Optical Lattices* [5,6]: the trapping effect of light intensity is in this case modulated via the interference of countepropagating laser beams. Atoms are trapped in the nodes or anti-nodes of the stationary wave via a dynamical Stark effect [41]. In this way it is possible to modulate in a periodic way the atomic density. Optical lattices can be combined with other trapping techniques (e.g. dipole traps) to shape the periodicity along one, two or three dimensions.

During the same years, strong efforts were put in the theoretical modeling and experimental realization of the so called *Photonic Crystals* [9, 42]. The well known concept of interference of light diffracted from a periodic arrangement of atoms, which is at the basis of the X-ray optics [43] and all the related studies on the crystalline structures [44], was then renewed by noticing the similarities between the roles of the dielectric constant in the Maxwell's equations and the potential in the Schrödinger's equation. The Floquet-Bloch theorem [45] for the e.m. field in periodic dielectric structures states that the dispersion law for light contains propagation bands and forbidden gaps [46] in close analogy with the case of electrons in crystalline structures. The scalability of Maxwell's equations then allows to built up structures which works in different frequency domains, from microwave to visible light.

Optical lattices allow an engineering of periodic atomic structures; a spatial modulation of the optical response of the atomic medium in the range of optical wavelengths means that these structures can be used as photonic crystals [47, 48]. Furthermore, the observation of strong resonant light-matter coupling, which is forbidden by absorption processes in homogeneous gases, can be studied in *Mott Insulator* (MI) systems where absorption is suppressed because of localization of atoms [15, 40]. The simultaneous occurrence of narrow optical resonances and the periodic arrangement of atoms offers the possibility to study the mixing of these effects in the building up of photonic bands and in the relative reflectivity spectra. The atomic MI is then a remarkable example of resonant photonic crystal.

Section 1 contains a brief summary about the MI phase of an ultracold atomic sample trapped in an optical lattice: this is the structure that we investigate in the following.

In Section 2, we introduce the *Transfer Matrix* (TM) technique for the study of the optical response of a layered dielectric structure. We model the MI of two-level atoms as a 1D chain of atomic sheet with resonant susceptibility.

In Section 3, we discuss the band diagram of the system. Two distinct regimes are discriminated depending on whether the atomic resonant frequency and the Bragg frequency are close or far away in terms of the resonant light-atoms coupling.

Section 4 is devoted to the study of the reflectivity spectra in both the regimes previously determined. Two different geometries are discussed: a semi-infinite system and a finite slab, where the multiple reflections of a polariton inside the structure give rise to Fabry-Perot fringes in the spectrum. We also discuss the crossover between the Lorentzian reflectivity of a single atom and the formation of forbidden gaps for long lattices.

2.1 The Mott Insulator phase

The modulation of the atomic density in an optical lattice generally depends on the intensity of the trapping field. In particular this value fixes the tunneling rate J between neighboring sites: the ratio between J and the local atomic repulsive interaction U, which depends on the atomic species, estimates the mobility of an atom throughout the optical lattice in the Bose-Hubbard model [49]. Below a critical value of this ratio, for commensurate fillings, a quantum phase transition between a superfluid and a MI state takes place. The MI is characterized by a fixed number of atoms in each site without coherence between the wavefunction of atoms

sitting at the different sites as it was experimentally observed [14, 50, 51]. The strong localization of atoms at lattice sites can be estimated by comparing the oscillator length of a single site:

$$a_{ho} = \sqrt{\frac{\hbar}{2m\omega_{tr}}}, \tag{2.1}$$

where m is the atomic mass and ω_{tr} is the trapping frequency, with the trapping wavelength. If we express the trapping frequency in terms of the recoil energy

$$E_r = \frac{\hbar^2 k_L^2}{2m} = \frac{h^2}{\lambda_L^2}\frac{1}{2m}, \tag{2.2}$$

we obtain

$$a_{ho} = \sqrt{\frac{\hbar}{2mN(E_r/\hbar)}} = \frac{\lambda_L}{2\pi\sqrt{N}}. \tag{2.3}$$

Here λ_L is the wavelength of the trapping laser. While in the first realizations of MI, N was of the order of 20 [14], it is nowadays possible to reach much deeper lattices with $N = 130$ [52]. For this reason it is a good approximation to assume the atoms to have a point-like structure.

The absence of fluctuation in the occupation number of the lattice sites ensures the extreme regularity of the periodic structure. This fact has a crucial role in the radiation-matter interaction: the resulting discrete translational symmetry imposes a modification of the e.m. vacuum which results in a suppression of the absorption process [15, 40]. Furthermore the presence of an energy gap for the many-body excitation of the system protects the radiation-matter interaction against decoherence processes.

2.2 Transfer Matrix technique

To study the propagation of monochromatic light through a MI of atoms, we model the system as a one-dimensional chain of atomic planes separated by a distance a (*lattice constant*): each of these planes has a superficial homogeneous density $\sigma_n = na$. The wavevector of light is normal to the atomic planes. To get the band diagram and the reflectivity spectra, we consider the stationary solution of the Maxwell's equations given by the TM technique [36].

The basic idea of this algorithm is the discretization of an arbitrary complex 1D dielectric structure in many homogeneous layers. The spatial part of the electric field is expanded in terms of the two counterpropagating waves at a fixed energy $\hbar\omega$:

$$E(x,t) = \left(E_+ e^{ik_+ x} + E_- e^{ik_- x}\right) e^{-i\omega t}, \tag{2.4}$$

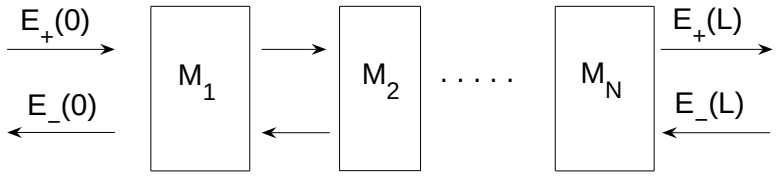

FIGURE 2.1: Pictorial representation of how the TM technique works.

and it is then represented by a two-component vector $\vec{E} = (E_+, E_-)$. In a homogeneous layer with refractive index n_1 and length d, these plane waves have wavevectors

$$k_\pm = \pm n_1 \frac{\omega}{c}, \tag{2.5}$$

where c is the speed of light in vacuum. The plane waves acquire a phase $e^{ik_\pm d}$ during the path through the layer. The electric field at the end of the layer $\vec{E}(d)$ is then calculated by applying the matrix

$$M_{n_1,d}(\omega) = \begin{pmatrix} e^{in_1kd} & 0 \\ 0 & e^{-in_1kd} \end{pmatrix} \tag{2.6}$$

to the vector $\vec{E}(0)$ corresponding to the origin of the layer; here $k = \omega/c$. The passage through an interface between neighboring layers with different refractive indeces n_1 and n_2 gives rise to reflection and transmission according to the continuity condition for the electric field, as expressed by Fresnel laws [39]

$$t_{n_1 \to n_2} = \frac{E'_+}{E_+} = \frac{2n_1}{n_1 + n_2}, \tag{2.7a}$$

$$r_{n_1 \to n_2} = \frac{E_-}{E_+} = \frac{n_1 - n_2}{n_1 + n_2}. \tag{2.7b}$$

Here the $'$ denotes the quantities in the layer with index n_2. The transfer matrix of the interface is then given by

$$M_{n_1 \to n_2} = \begin{pmatrix} \frac{n_1 + n_2}{2n_2} & \frac{n_2 - n_1}{2n_2} \\ \frac{n_2 - n_1}{2n_2} & \frac{n_2 + n_1}{2n_2} \end{pmatrix}. \tag{2.8}$$

By using the matrices (2.6) and (2.8), it is possible to describe every 1D structure[1] as it is depicted in Fig. 2.1.

[1] In fact, a continuous variation of the dielectric properties can also be described as long as the discretization step is chosen much shorter than the radiation wavelength, according to the spatial derivative of the refractive index.

2.2.1 Application to periodic structures

TM technique is very powerful in the case of periodic structures: in fact, by diagonalizing the TM describing the *elementary cell* for each frequency ω, it is possible to obtain the band diagram and the electric field for the propagating modes of an infinite structure.

If there is no absorption (i.e. the dielectric constant $\epsilon \in \mathbb{R}$) and the cell is symmetric, the structure is invariant for time and space reversal, which is always the case in the systems we are presently investigating. Because of these symmetries, the eigenvalues λ_1 and λ_2 of the TM of the elementary cell show peculiar properties:

1. space reversal invariance implies that $det(M) = 1$ which gives $\lambda_1 = (\lambda_2)^{-1}$;
2. time reversal invariance implies $\lambda_1 = \lambda_2^*$.

Under these assumptions, the general form of the eigenvalues of the TM is

$$\lambda_\pm = e^{\pm iK(\omega)a}, \tag{2.9}$$

where a is the length of the elementary cell. By looking at the expression of these eigenvectors, it is clear that they are either real or complex conjugated. If they are real, then the Bloch wavevector has two possible forms:

$$K(\omega) = 0 + i\beta, \tag{2.10}$$

$$K(\omega) = \frac{\pi}{a} + i\beta(\omega); \tag{2.11}$$

where β is real. The electric field is evanescent inside the structure with extinction length

$$\ell_{ext} = \frac{1}{\beta}, \tag{2.12}$$

and the propagation is forbidden in an infinite system: these solutions correspond to the gaps in the band spectrum. If instead the eigenvalues $\lambda_\pm$ are complex conjugated, the band diagram is determined through the formula

$$K(\omega) = \frac{1}{a}\, arcos\left(\frac{Tr(M(\omega))}{2}\right), \tag{2.13}$$

where $K(\omega)$ belongs to the first Brillouin zone (fBz), $-\pi < Ka < \pi$. In the present analysis, the bands show a symmetry for opposite wavevectors corresponding to the same frequency (i.e. energy) and for this reason we usually show in the figures only half the fBz.

2.2.2 Transfer Matrix for an atomic plane

We consider the scattering of light on a single atomic plane to derive the related TM: we model the atomic sheet as a Dirac-like impurity embedded in vacuum in the origin of propagation axis [53], $x = 0$. Its susceptibility can be written by using the expression for the two-level atomic gas (1.11):

$$\chi(\omega, x) = \frac{f\omega_{eg}}{2}\frac{1}{\omega_{eg} - \omega}\, a\, \delta(x) = P_R(\omega)\, \delta(x), \tag{2.14}$$

where we have introduced the refractive power $P_R(\omega)$. We use this expression to calculate the polarization which appears into the wave equation for the propagation of the electric field [39]

$$\frac{\partial^2 E(x)}{\partial x^2} + k^2 \left(1 + \epsilon_0 \chi(\omega, x)\right) E(x) = 0. \tag{2.15}$$

We integrate in space between the symmetric boundaries $-l$ and $+l$ and then let $l \to 0$; the δ-like polarization generates a discontinuity in the first derivative of the electric field:

$$\left(\left.\frac{\partial E}{\partial x}\right|_{x=0^+} - \left.\frac{\partial E}{\partial x}\right|_{x=0^-} \right) = -P_R(\omega) k^2 E(0). \tag{2.16}$$

We note that, differently form its derivative, the electric field is continuous through the atomic defect, exactly as it happens in the case of the wavefunction and its spatial derivative for a δ-like potential in the Schrödinger's equation. By imposing the boundary condition, we calculate the electric field components at the opposite sides of the atomic plane: from these values we get the elements of the TM. The product with the TM of a vacuum layer of length a generates the TM for the elementary cell of the structure under analysis:

$$M(\omega) = \begin{pmatrix} e^{ika}\left(1 + i\dfrac{P_R(\omega)k}{2}\right) & e^{-ika}\left(i\dfrac{P_R(\omega)k}{2}\right) \\ e^{ika}\left(-i\dfrac{P_R(\omega)k}{2}\right) & e^{-ika}\left(1 - i\dfrac{P_R(\omega)k}{2}\right) \end{pmatrix}. \tag{2.17}$$

2.3 Photonic Bands

To get a simple physical understanding of the system, it is useful to concentrate our discussion on the simplest case of a 1D geometry: most effects related to resonant light-matter interaction are in fact independent from the dimensionality of the system under consideration [40, 54, 55]. In particular we concentrate on the interplay between the periodicity of the system

and the resonant behavior of the optical response which has never been studied in a systematic way. Interesting discussions of the optical properties of different kinds of 1D resonant PCs can be found in [48, 56–61].

A challenging question in the study of photonic bands is the search for a complete (i.e. 3D) photonic band gap [62, 63] which allows to stop the incoming radiation despite its direction and polarization in a certain frequency region: the debate for the case of atomic samples is still open and continues to attract interest [15–18, 64], but this is beyond our aim.

As introduction to the periodic case, we briefly discuss the properties of the resonant susceptibility (1.11) which describes a homogeneous system. In all the figures, the shaded regions indicate the forbidden gaps.

2.3.1 Bulk of resonant atoms

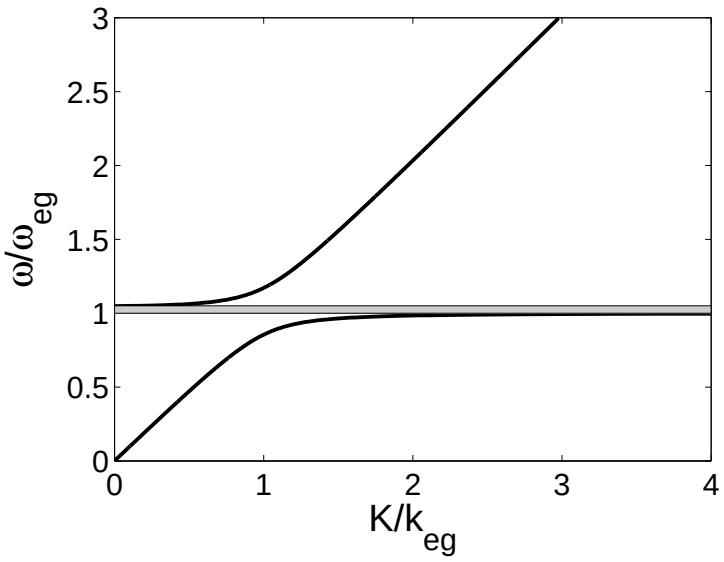

FIGURE 2.2: Polariton dispersion for a bulk of non-absorbing two-level atoms: the oscillator strength is $f = 10^{-1}$. The gray area indicates the polariton gap. For the sake of clarity, the dipole moment has been exaggerated with respect to actual values of atomic systems.

As we stated above, the characteristic element in the dispersion law of a bulk of non-absorbing two-level atoms is the polariton gap which appears above the resonance frequency ω_{eg}. As we neglect the absorption, the dielectric constant is always real. The gap opens up where $\epsilon(\omega) = 1 + \chi(\omega)$ is negative, i.e. for $[\omega_{eg} - \omega + (f/2)\omega_{eg}] < 0$. In fact, in this case the refractive index of the medium $n(\omega) = \sqrt{\epsilon(\omega)}$ is imaginary and therefore the field is

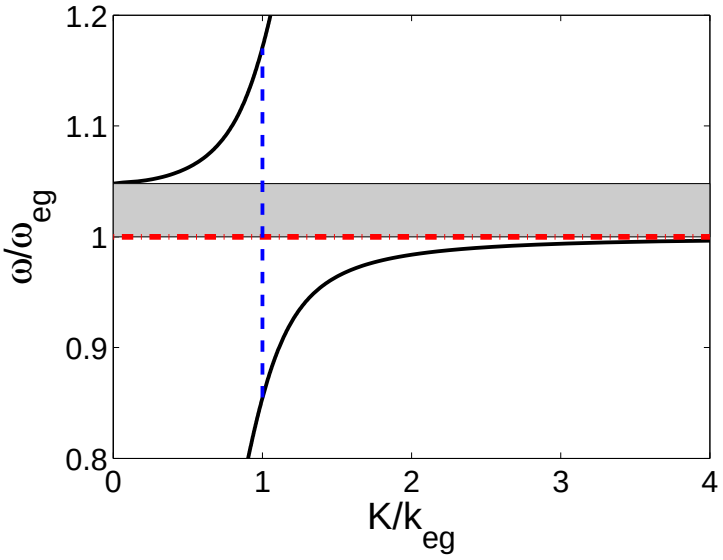

FIGURE 2.3: Polariton dispersion of a two-level atomic gas: zoom on the region near the polariton gap. The red dot-dashed line is the resonant frequency and the blue dashed line shows the Rabi splitting. Same parameters as in Fig. 2.2.

evanescent. We immediately see that the width of the gap is fixed by the oscillator strength:

$$\Delta\omega_{pol} = \frac{f}{2}\omega_{eg}. \tag{2.18}$$

The other important quantity is the width of the *Rabi splitting* which opens corresponding to the crossing between the transition frequency and the vacuum dispersion of light: it indicates the strength of the radiation-matter coupling. This splitting can be calculated from the general form of the light dispersion[2]:

$$\epsilon(\omega)\frac{\omega^2}{c^2} = K^2, \tag{2.19}$$

where we substitute the resonant wavevector $K = k_{eg}$. Because we are looking for the splitting near the resonant frequency, we solve the equation for the frequency detuning $\delta_e = (\omega_{eg} - \omega)$ and we retain terms up to the second order in $\delta_e, (f/2)\omega_{eg} \ll \omega_{eg}$. By substituting the appropriate values,

[2]We use different notations depending on the variable which is the independent through the calculation: the Capital letters (Ω, K) refer to the dependent variables, vice versa for the small ones (ω, k).

we obtain:

$$\begin{aligned}\left(1+\frac{f\omega_{eg}}{2\delta_e}\right)(\omega_{eg}-\delta_e)^2 &= \omega_{eg}^2 \\ \delta_e^2+\delta_e\frac{f}{2}\omega_{eg}-\frac{f}{4}\omega_{eg}^2 &= 0. \end{aligned} \tag{2.20}$$

The leading order of the solution in terms of f is given by

$$\delta_e = \pm\frac{\sqrt{f}}{2}\omega_{eg}. \tag{2.21}$$

The different width of the gap and the Rabi splitting is clearly shown in Fig. 2.3.

2.3.2 Band diagram of a Mott Insulator

In the analysis of the band diagram of the MI, two frequency scales are to be considered: the atomic resonance frequency ω_{eg}, and the Bragg frequency $\omega_{Br} = c\pi/a$ of the lattice which carries information on the periodicity of the lattice and derives from the famous Bragg condition for diffraction spectroscopy [44]. As we have seen in the introductory discussion, the width of the frequency region in which radiation and matter strongly interact is determined by the Rabi splitting (2.21). Starting from this consideration, two different regimes can be distinguished according to the ratio between the detuning $\omega_{eg}-\omega_{Br}$ and the Rabi splitting.

Purely excitonic regime

The *purely excitonic* regime corresponds to the case when the resonance frequency ω_{eg} and the Bragg frequency ω_{Br} are well separated $|\omega_{Br}-\omega_{eg}| \gg \sqrt{f}\omega_{eg}$. An example of polaritonic dispersion for this regime is shown in Fig. 2.4 for $\omega_{eg} < \omega_{Br}$.

Two main features characterize this regime: the region of the polariton gap and the foldings of the light line at the edges of the fBz. Near the resonant frequency, the polariton dispersion shows the usual Rabi splitting: in fact the wavelength of the radiation is much bigger than the periodicity and the system can be considered for many aspects as a bulk. Far from this region, the polaritonic modes tend to almost purely radiation or matter modes. At the edges of the fBz, for frequencies multiple of ω_{Br}, the vacuum dispersion of light crosses itself because of the periodicity of the system: this is a pictorial representation of Bragg scattering processes on the atomic lattice. In this case the far off-resonance value of the susceptibility (1.15) represents the effective interaction between counterpropagating light modes induced by the presence of atoms.

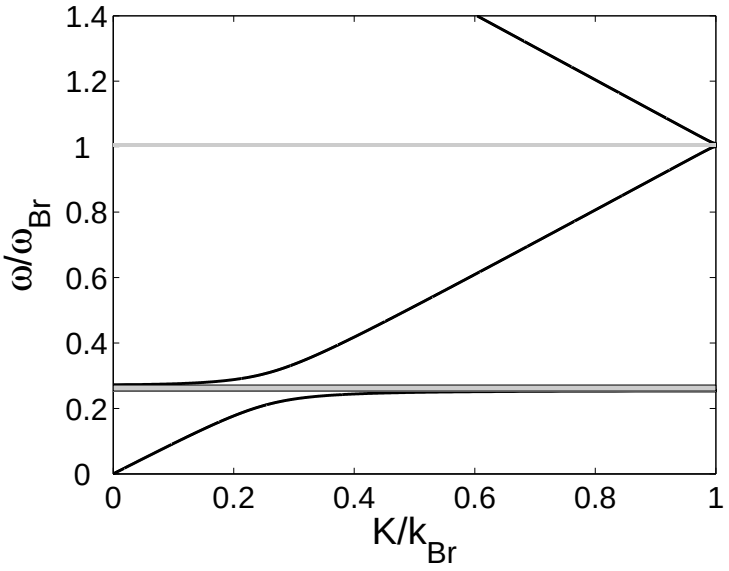

FIGURE 2.4: Polariton dispersion in a 1D lattice of two-level atoms. Purely excitonic regime: $f \approx 3.6 \cdot 10^{-2}(\omega_{Br}/\omega_{eg})$, $\omega_{Br}/\omega_{eg} \approx 4$.

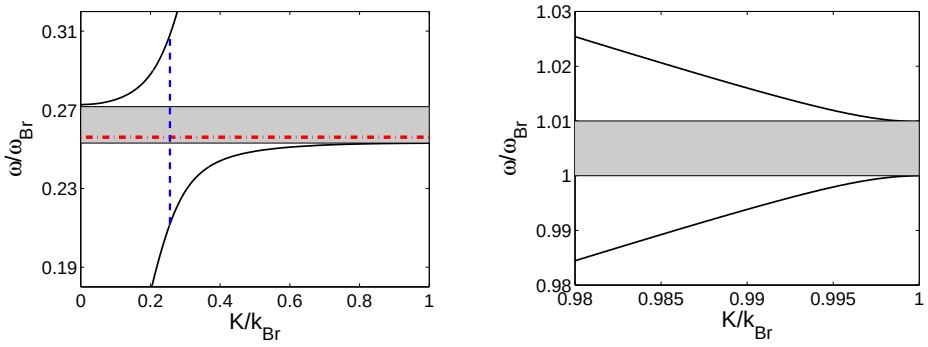

(a) (b)

FIGURE 2.5: Polariton dispersion in a 1D lattice of two-level atoms: zoom on the two lower-lying gaps. Purely excitonic regime: parameters as in Fig. 2.4. (a) Excitonic gap near the resonance frequency (red dot-dashed line), the blue dashed line shows the Rabi splitting. (b) First Bragg gap.

The anticrossings due to these processes result in the opening of gaps at the edges of the fBz as shown in Fig. 2.5. Around ω_{eg}, there is the usual polaritonic gap of resonant dielectrics [39], while just above ω_{Br} we have the first of the gaps due to Bragg scattering. There is a small difference from the bulk case: the former gap extends on both sides of ω_{eg} because of the limited size of the fBz. As long as the detuning between the two frequency scales diminishes, this gap passes from above to below ω_{eg}. Its width remains of the order of the oscillator strength (2.18). The latter one is instead located strictly above ω_{Br}. Its lower edge is exactly at ω_{Br} and corresponds to a propagating modes which is unaffected by the presence of the atoms that are located at the electric field nodes. As usual, the polaritonic density of states vanishes inside the gaps, and radiative propagation at these frequencies is forbidden.

Mixed Exciton-Bragg regime

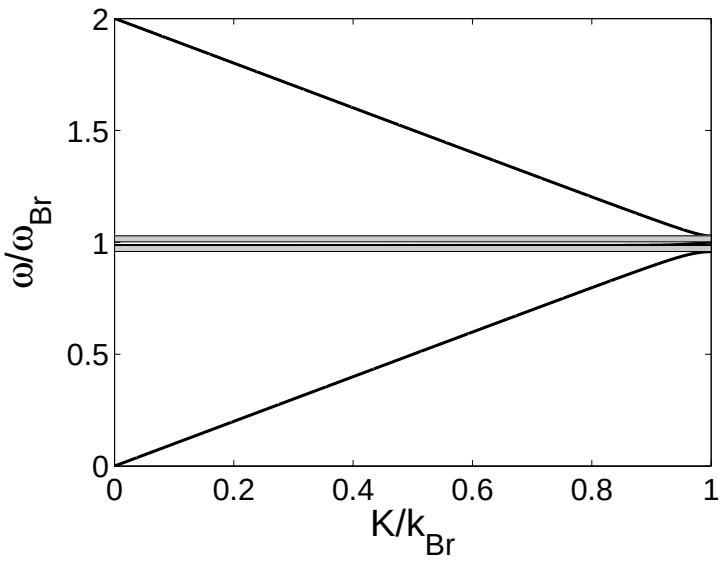

FIGURE 2.6: Polariton dispersion in a 1D lattice of two-level atoms. Mixed exciton-Bragg regime: $f \approx 2.4 \cdot 10^{-3}(\omega_{Br}/\omega_{eg})$ and $1 - (\omega_{eg}/\omega_{Br}) \approx 1.4 \cdot 10^{-2}$.

The condition $(\omega_{Br} - \omega_{eg}) \lesssim \sqrt{f}\omega_{eg}$ defines the *mixed exciton-Bragg* regime. The name suggests the strong interplay between the periodicity and the atomic resonance in the frequency spectrum. In fact, three modes are simultaneously mixed: the two counterpropagating e.m. modes, the incoming one at k and the first Bragg diffracted at $k - 2\pi/a$, and the atomic excitation.

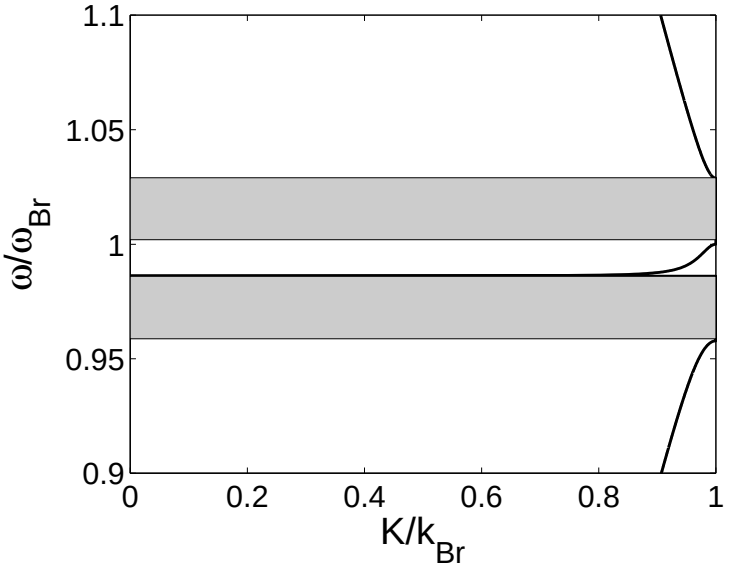

FIGURE 2.7: Polariton dispersion in a 1D lattice of two-level atoms: zoom on the gap region near ω_{Br}. Mixed exciton-Bragg regime: same parameters as in Fig. 2.6.

Differently from the previous case, the Rabi splitting is now located close to the edges of the fBz. As one can see in Fig. 2.6, this results in much wider forbidden gaps of the order of the splitting. It is interesting to note the presence of a mini-band which ranges between ω_{eg} and ω_{Br}: the squeezing effect due to the reduced detuning between the two main frequencies induces a very flat dispersion over most of the fBz. As in the previous regime, the polariton dispersion touches the vacuum light line at the Bragg frequency because of the electric field showing nodes at the atomic locations.

The maximum extension of the two gaps is $\sqrt{f/2}\omega_{eg}$ and it corresponds to the complete squeezing of the mini-band, $\omega_{Br} = \omega_{eg}$. The separation in frequency between the modes at k_{Br} is $\sqrt{2f}\omega_{eg}$ and there is a factor $\sqrt{2}$ with respect the usual Rabi splitting: this factor comes from the structure of the electric field that contains a superposition of equal weights of the two Bragg reflected plane waves.

2.4 Reflectivity spectra

The band diagram describes the physics of an infinite structure with a full discrete translational invariance: there are propagating modes corresponding to the bands separated by gaps of forbidden energy. Most spectroscopic

experiments, however, involve light beams which are incident onto finite systems and therefore require a description of the interfaces between regions of different optical properties, namely the external vacuum and the atomic lattice. Maxwell's theory requires in fact the continuity of both the electric field and its spatial derivative. We consider plane waves in vacuum and polariton modes (eigenvectors of the TM) inside the atomic structure. By imposing suitable boundary conditions, we calculate the reflectivity spectra of the system [48, 55, 56, 58–61]. Two geometries will be considered: a semi-infinite lattice, and a finite slab.

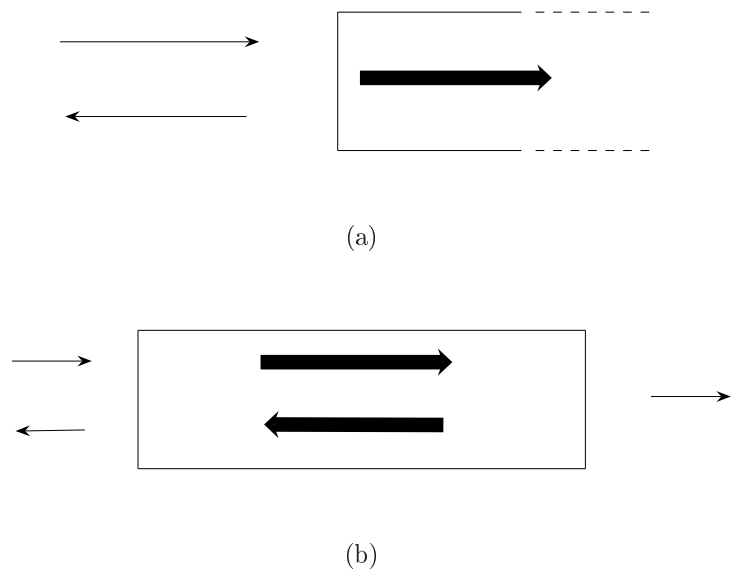

FIGURE 2.8: Geometries considered for the reflectivity spectra. Panel (a): semi-infinite system (vacuum on the left, lattice on the right). Panel(b): finite slab (vacuum at both side of a finite lattice). Thin arrows indicate the plane waves in vacuum and thick arrows indicate polariton eigenmodes in the lattice.

Semi-infinite geometry

In this configuration illustrated in Fig. 2.8(a), there is a single interface, dividing the space in two semi-infinite regions: vacuum and lattice.

We first consider the *input* problem with an incoming and a reflected plane wave in the vacuum and a single transmitted polariton Bloch mode in the lattice. We fix the wavevector $k = \omega/c$ of the plane wave and then we choose the polariton mode with Bloch wavevector $K(\omega)$ in order to satisfy energy conservation. We calculate the electric field and its derivative by considering a symmetric elementary cell with the atomic plane at its cen-

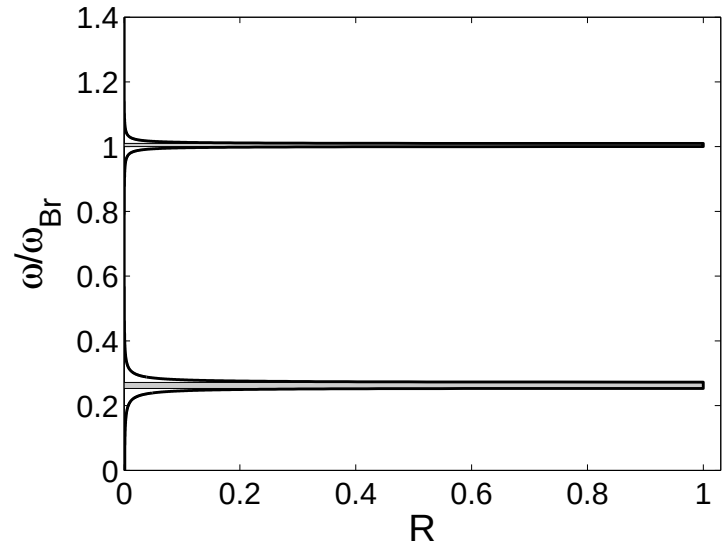

(a)

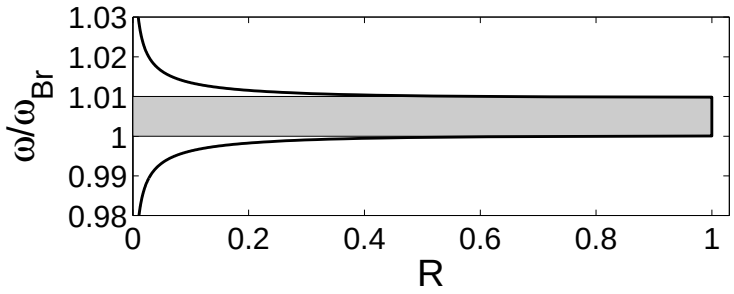

(b)

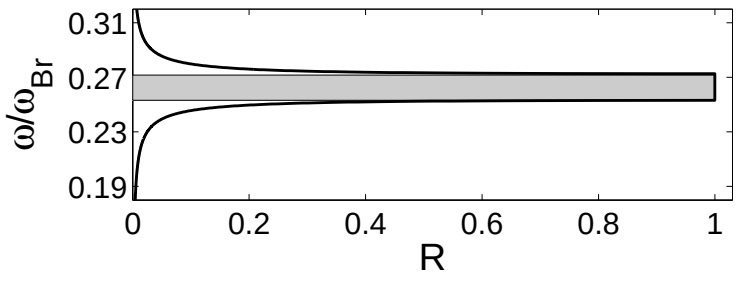

(c)

FIGURE 2.9: Upper panel (a): Reflectivity spectra in the purely excitonic regime for a semi-infinite lattice. Lower panels: (b) Bragg gap. (c) Excitonic gap. Parameters as in Fig. 2.4.

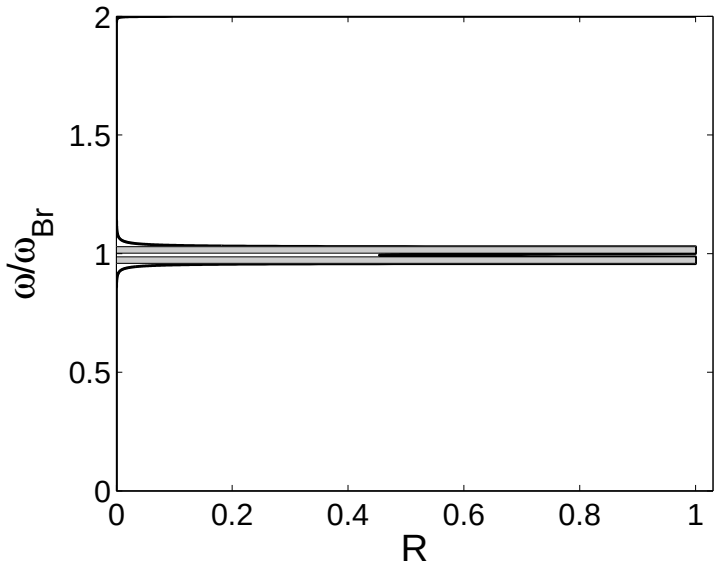

(a)

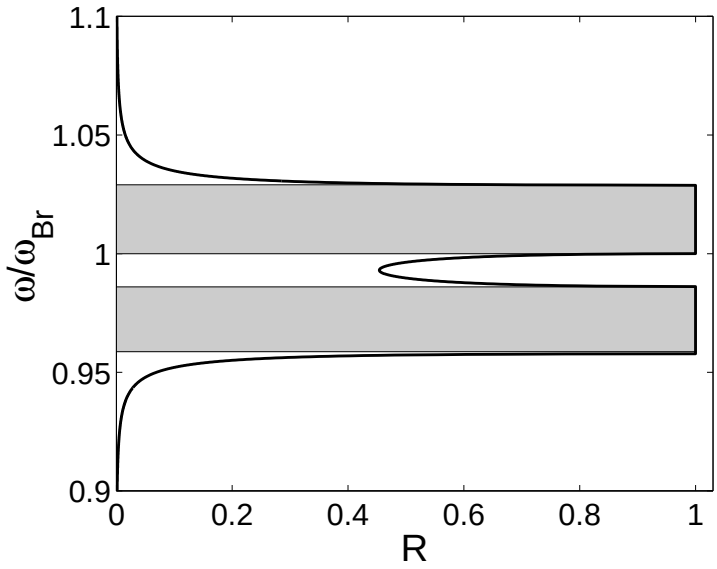

(b)

FIGURE 2.10: Upper panel: Reflectivity spectra in the mixed exciton-Bragg regime for a semi-infinite lattice. In the bottom panel: zoom on the gap region and mini-band reflectivity. Parameters as in Fig. 2.4.

ter: this way, also the derivative is continuous through the interface. The reflection amplitude r_{in} is then expressed in terms of the ratio between the wavevectors inside and outside the lattice:

$$r_{in} = \frac{E(0) + (i/k)E'(0)}{E(0) - (1/k)E'(0)}, \tag{2.22}$$

where the $'$ denotes the spatial derivative of the electric field. The mismatch between the wavevectors of the polariton state and the incoming wave determines the reflectivity $R_{in} = |r_{in}|^2$ shown in Fig. 2.9 and Fig. 2.10: this is significant around the gaps where the incoming wave is strongly interacting with the atomic resonance [Fig. 2.9(b)], the Bragg diffracted wave [Fig. 2.9(c)], or both [Fig. 2.10(b)]. In the mixed exciton-Bragg regime, we note that the reflectivity remains quite large in between the two gaps: the flatter the middle-polariton branch, the higher the corresponding reflectivity. It is then hard to exploit the slow light properties of this mini-band because the amount of light that can be coupled into the system is small. In the present semi-infinite geometry, reflectivity is complete for frequencies corresponding to the gaps where the wave vector becomes imaginary and the field inside the lattice consists of an evanescent wave.

The *output* problem corresponds to two counterpropagating Bloch modes with the same energy inside the lattice, let's call them[3] E^+ and E^-, and a single transmitted plane wave in the external vacuum. The reflectivity is given by $R_{out} = |r_{out}|^2$ with

$$r_{out} = -\frac{E^+(0) + (i/k)E'^+(0)}{E^-(0) + (i/k)E'^-(0)}. \tag{2.23}$$

It is straightforward to note that the reflectivity is the same in input and output case: in fact, $E^+ = (E^-)^*$ which is a consequence of the system being invariant under time reversal and spatial parity.

Finite slab

Reflectivity spectra for a finite system [Fig. 2.8(b)] are shown in Fig. 2.11 and Fig. 2.12. There are two main differences with respect to the semi-infinite case: the propagation takes place also in the intervals of frequency corresponding to the gaps for an infinite system and there are fast oscillations on top of the reflectivity spectrum around the main gaps. In this case light can propagate through the system also in the ranges of frequency in which the Bloch wavevector K is imaginary: it is the ratio of the length

[3] We use here the superscript to distinguish the propagating modes from their components within the TM formalism that are labeled below.

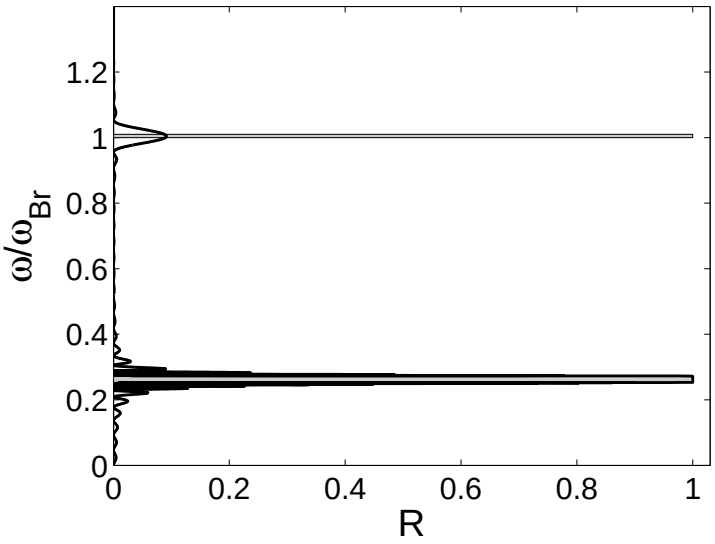

(a)

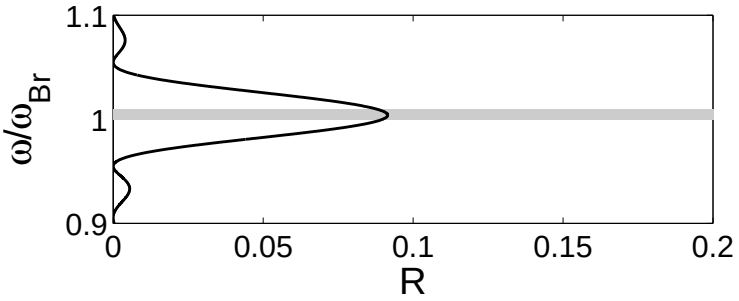

(b)

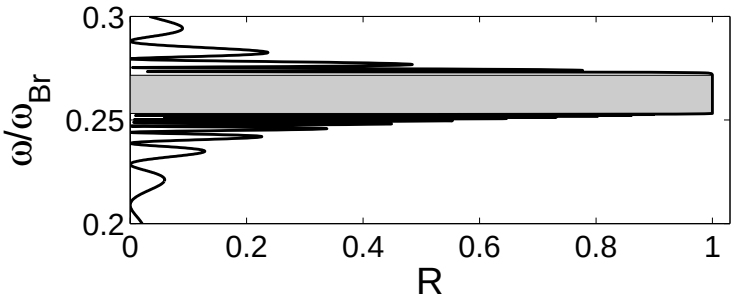

(c)

FIGURE 2.11: Upper panel: Reflectivity spectra in the purely excitonic regime for a finite slab of atomic planes with $N = 20$ cells. Lower panels: (b) Reflectivity peak at ω_{Br} (c) Gap near the resonant frequency. Parameters as in Fig. 2.4. The gray regions correspond to the gaps for the infinite system.

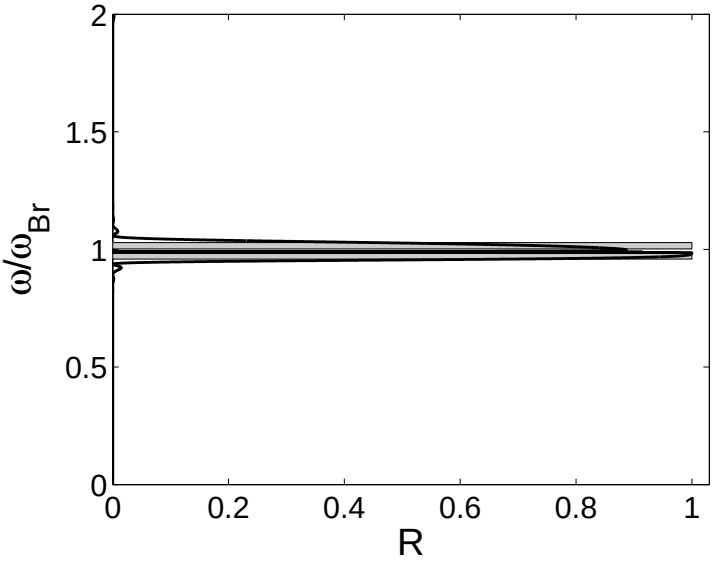

(a)

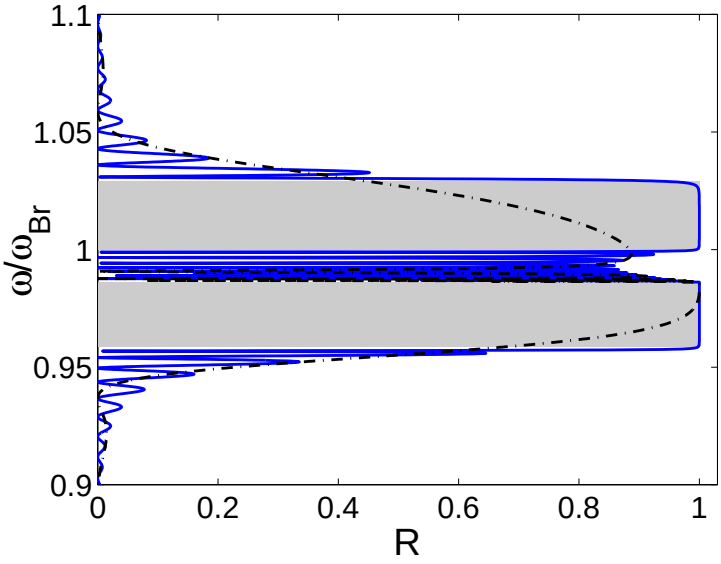

(b)

FIGURE 2.12: Upper panel: Reflectivity spectra in the mixed exciton-Bragg regime for a finite slab of atomic planes with $N = 20$ cells. Bottom panel: zoom on the region near ω_{Br} for the case $N = 20$ (black dot-dashed line) and $N = 100$ (blue solid line). Parameters as in Fig. 2.4. The gray regions correspond to the gaps for the infinite system.

of the lattice L on the extinction length $1/K$ which discriminates between a short system, $KL \ll 1$, and a long one, $KL \gg 1$. The crucial role of the parameter KL for a Bloch wavevector either real or imaginary, is clear from the expression for the reflectivity of a system composed by N elementary cells [57]:

$$R_N = \left| \frac{m_{1,2} sin(KaN)}{m_{2,2} sin(KaN) - sin(Ka(N-1))} \right|^2, \tag{2.24}$$

where the m coefficients represents the elements of the elementary cell and we have $L = Na$.

In the *short lattice* case, the spectrum is mainly characterized by a Lorentzian peak corresponding to the atomic resonance. The paradigm of this regime is the single atomic plane which gives the reflectivity:

$$\begin{aligned} R &= \left| -\frac{m_{1,2}}{m_{2,2}} \right|^2 = \\ &= \left[1 + \left(\frac{\omega - \omega_{eg}}{\omega_{eg}} \frac{4}{f} \frac{1}{ka} \right)^2 \right]^{-1}. \end{aligned} \tag{2.25}$$

The width of the peak is fixed by the oscillator strength and the corresponding Lorentzian shape is shown in Fig. 2.13. As the number of atomic planes grows the peak initially acquires a width proportional to N. For $N \to \infty$, the reflectivity reaches value 1 into the whole gap regions and not only at the resonance frequency. The development of these stop bands is not uniform along the spectrum, in fact the extinction length is proportional to the susceptibility and it becomes small near ω_{eg} while it is much bigger in other regions of frequency corresponding to a gap in the infinite system. For example, the far off-resonant gaps develop slower as compared to the polaritonic gap. This is the case depicted in Fig. 2.11(b) and Fig. 2.11(c): we compare the strength of the reflectivity peaks respectively near resonance and at Bragg frequency, in the purely excitonic regime. For this reason the short and long lattice cases depends also on the range of frequency under investigation.

In the *long lattice* regime, the appearance of the fringes at the gap edges can be explained by considering the slab geometry of the system. Two interfaces at respectively $x_{fr} = -((N-1) + 1/2)a$ and $x_{back} = a/2$ now separate three regions of space: the vacuum with the incident and reflected plane waves, the finite-size lattice with counterpropagating polaritons, and again vacuum with now only a transmitted plane wave. The field in the last cell ($x \in [-a/2, a/2]$) is determined by the output problem considered above to be

$$E_{st}(x) = E^+(x) + r_{out} E^-(x). \tag{2.26}$$

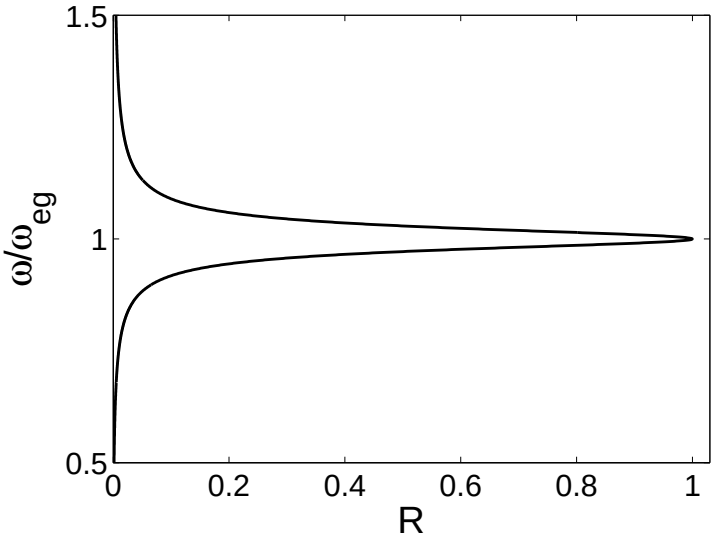

FIGURE 2.13: Typical Lorentzian reflectivity peak for a single atomic plane. Parameters as in Fig. 2.4.

As both $E^{\pm}(x)$ are Bloch states, the field in the first cell (taking $x \in [-((N-1)+1/2)a, -((N-1)-1/2)a]$) has the simple form

$$\tilde{E}_{st}(x) = E_{+}(x+(N-1)l)\, e^{-ikl(N-1)} + r_{out} E_{-}(x+(N-1)l)\, e^{ikl(N-1)}. \quad (2.27)$$

By solving the continuity conditions at the front interface at $x = x_{fr}$, we get

$$r_{slab} = e^{2i(\omega/c)x_{fr}} \frac{\tilde{E}_{st}(x_{fr}) + i(c/\omega)\tilde{E}'_{st}(x_{fr})}{\tilde{E}_{st}(x_{fr}) - i(c/\omega)\tilde{E}'_{st}(x_{fr})}. \quad (2.28)$$

Because of the phase factors in (2.27), fast oscillations occur in the reflectivity (2.28) due to the Fabry-Perot-like interference of Bloch waves which undergo multiple reflections at the lattice boundaries. The period $\Delta\omega$ of these oscillations is fixed by the group velocity $v_{gr} = d\omega/dK$ and the total length of the system L,

$$\Delta\omega = \frac{\pi}{L}\, v_{gr} : \quad (2.29)$$

the slower v_{gr}, the closer the peaks. This relation clarifies the fact that the fringes appear near the gaps where the interaction between radiation and matter mostly deforms the vacuum dispersion of light.

It is instructive to compare the envelope of this oscillations with the spectrum in the semi-infinite geometry. We can consider a simplified model where the lattice is replaced by a bulk medium of refractive index n. In this case, the reflectivity for a single interface separating vacuum and

medium is

$$R_{int} = \left(\frac{1-n}{1+n}\right)^2 . \tag{2.30}$$

For a slab of thickness L, the reflectivity is [65]

$$R_{slab} = \frac{(n-1/n)^2 \, \sin^2(\omega n L/c)}{4\cos^2(\omega n L/c) + (n+1/n)^2 \sin^2(\omega n L/c)} \tag{2.31}$$

Fabry-Perot oscillations are apparent, with a maximum reflectivity at the peaks equal to

$$R_{slab}^{max} = \left(\frac{1-n^2}{1+n^2}\right)^2 . \tag{2.32}$$

In the limit $n \to 1$, the ratio $(R_{slab}^{max}/R_{int}) \to 4$: this is due to the presence of two counterpropagating Bloch modes in the slab as compared to the single propagating mode in the semi-infinite case. This factor 4 provides a good approximation in the lattice case as well, as one can easily see in the low-reflectivity tails of the spectra shown in Fig. 2.14.

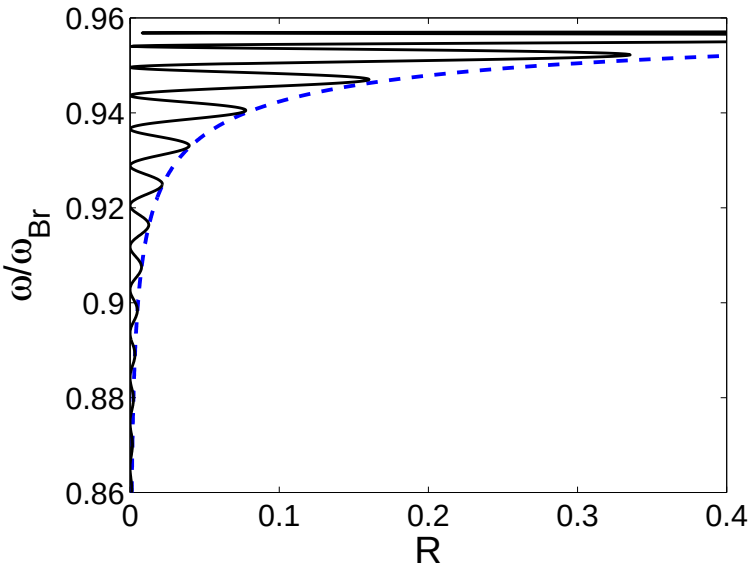

FIGURE 2.14: Comparison between the low reflectivity tails of the spectra below the resonance frequency for the semi-infinite case (dashed blue line is 4 times R) and the finite slab (solid black line) with $N = 100$ (long lattice limit). Parameters as in Fig. 2.6.

CHAPTER 3

Scattering of slow light on defects

In Chapter 2, we have noticed the formation of a squeezed mini-band in the photonic spectrum of a *Mott Insulator* (MI) of two-level atoms in the mixed exciton-Bragg regime. The width of this mini-band is fixed by the detuning between the resonant and Bragg frequencies and it is then in principle tunable by acting on these atomic degrees of freedom. The reduced slope of the dispersion means that the polaritonic propagating modes are slow as compared to the vacuum speed of light. This *slow light* [28] behavior is very interesting: if the electric field propagates slowly, the interaction time with the underlying medium is enhanced opening a rich variety of possibilities to probe the system as well as to manipulate the propagating radiation. However, high reflection at interfaces in the corresponding frequency range inhibit the use of such a feature [39, 48, 56, 66, 67].

The so called Λ excitation scheme for a three-level atomic system, discussed in the Chapter 1, generates a peculiar dispersion for the probe beam which joins together slow light behavior, a good impedance matching at interfaces and strong suppression of absorption [21]. The crucial ingredient is the strong dressing of the transition between the metastable and the excited state via the control (or dressing) field: the application of a resonant probe in fact drives the atoms into a coherent superposition of the lower-lying and long living states that is decoupled from the excited level. The resulting *Electromagnetically induced transparency* (EIT) [22–24] offers fascinating perspectives to coherently play with light.

The reflectivity dip can be used to inject slow light into the structure as a probe. In the case of atomic MI is of great interest the possibility to detect the presence of defects, such as lack of atoms at some lattice site: we then expect a change in the optical response of the system.

In Section 1, we introduce the resonant behavior of a three-level system by using the susceptibility derived in Chapter 1. We present and discuss the expressions for the group velocity, reflectivity and absorption corresponding to the two-photon Raman resonance.

Section 2 is instead devoted to the study of the reflection of the slow *Dark Polariton* (DP) on defects embedded in a lattice of three-level atoms. The vacuum defect is shown to behave like an empty cavity with proper localized modes. On the other hand, the presence of a two-level atomic impurity along the 1D system with resonant frequency corresponding to the EIT reflectivity dip gives rise to complete reflection. Effect of absorption is also discussed.

3.1 EIT Dispersion

The dispersion arising from the resonant susceptibility (1.25) is characterized by three polaritonic branches [26, 27, 29] as shown in Fig. 3.1. The bands are calculated by using the general law for light dispersion in matter (2.19).

In the regime $\sqrt{f} \gg \Omega_c/\omega_{eg}$, the upper (UP) and lower (LP) polaritons have a structure similar to the two-level case and the leading order of the Rabi splitting is given by the oscillator strength. The presence of the metastable state and the control field results in the appearance of a third central band: the DP (or middle polariton) carries all the nice properties related to EIT. The width of the central band is controlled by the amplitude of the dressing field, Ω_c.

We focus the analysis on the susceptibility at Raman resonance, $\delta_R = 0$, to obtain the relevant quantities that describe the propagation of a DP. In particular we consider a resonant dressing of the transition from the metastable state to the excited state, $\delta_e = \delta_R$. The expressions for the susceptibility and its first and second order derivatives with respect

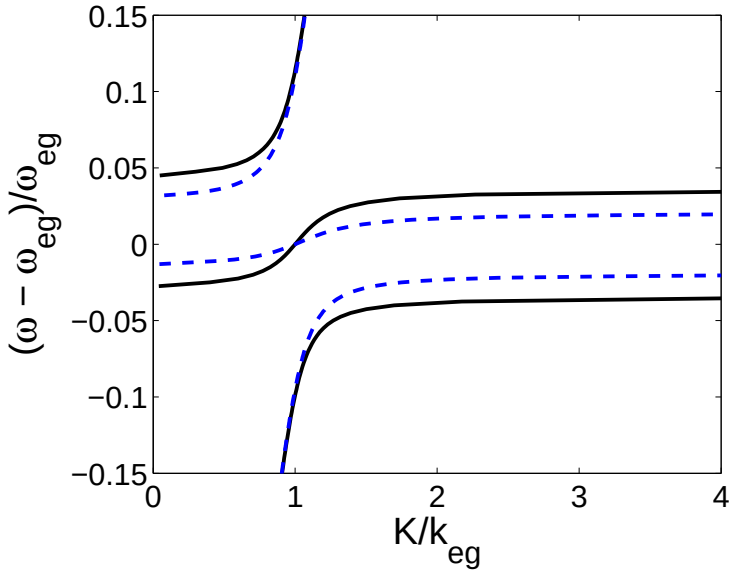

FIGURE 3.1: Polaritonic dispersion in an EIT atomic medium near resonance. Oscillator strength: $f = 0.04$. Rabi frequency of the control field: $\Omega_c = 0.07\,\omega_{eg}$ (black solid line), $\Omega_c = 0.04\,\omega_{eg}$ (blue dashed line).

frequency are [68]:

$$\chi|_{\delta_R=0} = i\frac{f\omega_{eg}}{2}\frac{2\gamma_m}{\Omega_c^2+\gamma_e\gamma_m}, \tag{3.1a}$$

$$\left.\frac{\partial\chi}{\partial\omega}\right|_{\delta_R=0} = \frac{f\omega_{eg}}{2}\frac{4(\Omega_c^2-\gamma_m^2)}{(\Omega_c^2+\gamma_e\gamma_m)^2}, \tag{3.1b}$$

$$\left.\frac{\partial^2\chi}{\partial\omega^2}\right|_{\delta_R=0} = i\frac{f\omega_{eg}}{2}\frac{16(\gamma_e\Omega_c^2+2\gamma_m\Omega_c^2-\gamma_m^3)}{(\Omega_c^2+\gamma_e\gamma_m)^3}. \tag{3.1c}$$

Here we have ordered the terms in brackets depending on the relative strength for the typical values of atomic systems under investigation here, $(\Omega_c \approx \gamma_e \gg \gamma_m)$.

The slope of the band gives the group velocity of a travelling wavepacket:

$$\begin{aligned} v_{gr} &= \left.\frac{d\omega}{dk}\right|_{\delta_R=0} = \\ &= c\left(\sqrt{\epsilon(\omega_{eg})}+\frac{\omega_{eg}}{2\sqrt{\epsilon(\omega_{eg})}}\left.\frac{\partial\chi}{\partial\omega}\right|_{\delta_R=0}\right)^{-1} = \\ &= \frac{c}{1+\dfrac{f\omega_{eg}^2}{\Omega_c^2}}. \end{aligned} \tag{3.2}$$

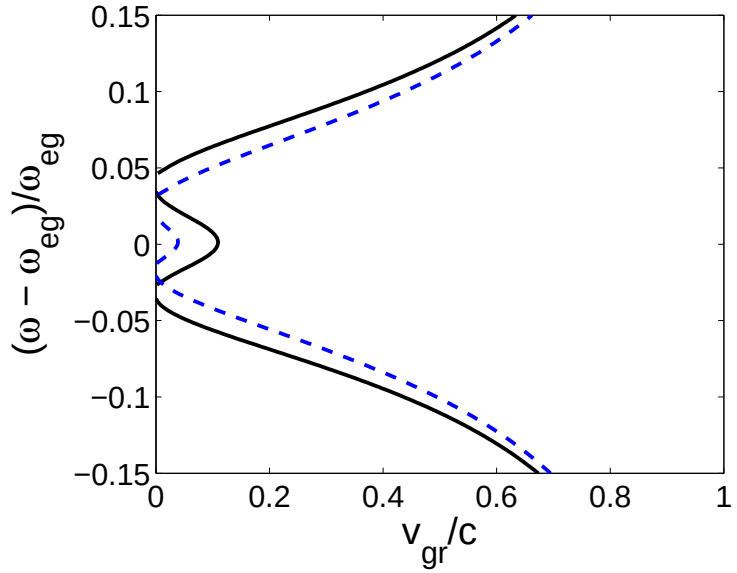

FIGURE 3.2: Group velocity near Raman resonance in an EIT atomic medium. Parameters and colours as in Fig. 3.1.

It is the ratio between the intensity of the control field and the Rabi splitting that tunes the propagation speed in the atomic medium. As far as we lower the control field the DP mini-band is squeezed and the DP slows down as it is depicted in Fig. 3.1 and Fig. 3.2.

It is also important to estimate the absorption experienced by the radiation during the propagation: this is given by the imaginary part of the susceptibility. We see from the expression (3.1a) that at Raman resonance the absorption is determined by the dephasing parameter γ_m: as it comes from non-radiative processes, it is in general orders of magnitude smaller than the usual atomic linewidth; for this reason, it can be neglected. By using the Taylor expansion of $K(\omega)$, it is then the second order derivative to give the leading order in the absorption process:

$$\begin{aligned}\frac{\gamma(\omega)}{v_{gr}} &= \frac{1}{2}\,\mathrm{Im}\left[\frac{\partial^2 k}{\partial\omega^2}\right]\Bigg|_{\delta_R=0}(\omega-\omega_{eg})^2 = \\ &= \frac{1}{c}\frac{\omega_{eg}}{4\sqrt{\epsilon(\omega_{eg})}}\frac{\partial^2\chi}{\partial\omega^2}\Bigg|_{\delta_R=0}(\omega-\omega_{eg})^2 = \\ &= i2\gamma_e\frac{f\,\omega_{eg}^2}{\Omega_c^4}(\omega-\omega_{eg})^2. \end{aligned} \tag{3.3}$$

Here we have exploited the linearity of the DP band near Raman reso-

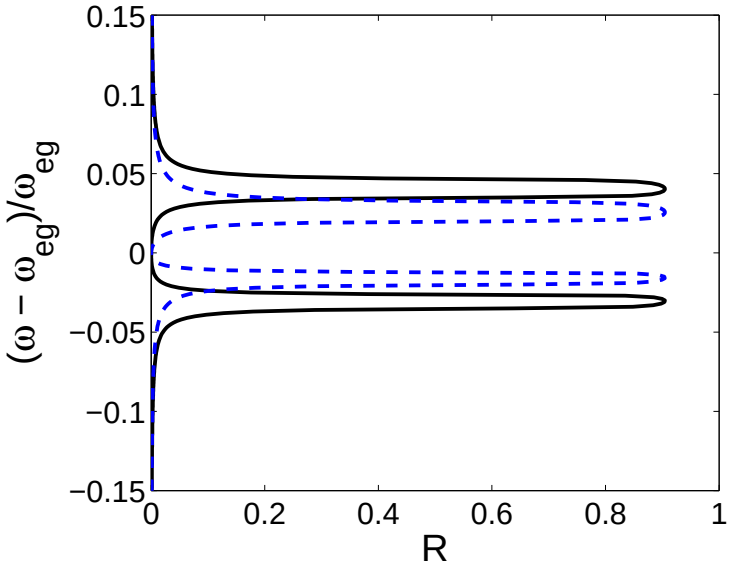

FIGURE 3.3: Reflectivity spectrum for an EIT atomic medium near resonance. Parameters and colours as in Fig. 3.1.

nance, $\Delta\omega = v_{gr}\,\Delta K$, and the formula

$$\frac{\partial^2 k}{\partial \omega^2} = \frac{1}{c}\left[\frac{\partial \chi}{\partial \omega}\frac{1}{\sqrt{\epsilon(\omega)}}\left(1 - \frac{\omega}{4\epsilon(\omega)}\frac{\partial \chi}{\partial \omega}\right) + \frac{\omega}{2}\frac{1}{\sqrt{\epsilon(\omega)}}\frac{\partial^2 \chi}{\partial \omega^2}\right]. \tag{3.4}$$

The expression (3.3) shows the parabolic behavior in the absorption spectrum near Raman resonance with the resulting dip whose amplitude is fixed by the dressing frequency.

3.1.1 Reflectivity dip

A crucial feature of EIT is the vanishing reflectivity experienced by an incoming wave at Raman resonance. The robustness of this behavior is guaranteed by the fact that the vacuum light line crosses the DP branch regardless of the particular values chosen for the system parameters, as it is reported in Fig. 3.3.

To show this good impedance matching, we derive the reflectivity at the interface between a homogeneous medium under EIT condition and vacuum by using the simple model for reflectivity at the interface between media with different refractive indices (2.30). The index of refraction for the atomic medium in the vicinity of Raman resonance, $\omega = \omega_{eg} + \delta\omega$, is

obtained from the dispersion law:

$$n(\omega) = \frac{c\,K}{\omega} = \frac{\omega_{eg} + (c/v_{gr})\delta\omega}{\omega_{eg} + \delta\omega}, \tag{3.5}$$

where we use the linear form of the dispersion near Raman resonance and we have $c/v_{gr} \gg 1 \gg (\delta\omega/\omega_{eg})(c/v_{gr})$. We put this result into the formula (2.30) and we get the reflectivity at the boundary of the EIT medium:

$$R = \left(\frac{\delta\omega(1 - c/v_{gr})}{2\omega_{eg} + \delta\omega(1 + c/v_{gr})}\right)^2; \tag{3.6}$$

here we eliminate the term proportional to (v_{gr}/c) in the numerator and the terms in δK in the denominator. We then obtain the expression for the parabolic dip

$$R(\omega) \approx \frac{(\omega - \omega_{eg})^2}{4\omega_{eg}^2}\left(\frac{c}{v_{gr}}\right)^2. \tag{3.7}$$

The width of the dip is fixed by the group velocity and it is then proportional to the control field intensity, Ω_c^2. The coupling of light is not allowed over the whole DP band, but only in the region near Raman resonance as you can see in Fig. 3.3.

3.2 Scattering on defects

As we have seen above, the linear susceptibility gives a static description of a polariton that propagates through a homogeneous system. The model is valid either for a monochromatic wave or a wavepacket: in fact as long as the radiation-matter interaction is constant in time, the modes at different energies do not interact and they can be treated separately.

Within a static picture, it is of great interest the investigation of the scattering in the presence of *defects*. In fact, the optical response of a system offers the possibility to infer some information about its internal structure. Here we present a simple approach to the scattering problem. We consider a 1D geometry for the propagation of the polariton: in this case the scattering is given by the reflectivity from the defect. The reflectivity on a vacuum slab embedded in a homogeneous EIT medium is given by an oscillatory function depending on the length of the defect with an envelope which is related to the reflectivity on a single interface[1] (2.32).

Furthermore, if we consider an atomic gas trapped in an optical lattice in the MI phase, it is important from both a theoretical and an experimental point of view to have tools to test the regularity of the structure [69,

[1] See the discussion in Chapter 2.

70]. The EIT dispersion offer the possibility to test the response of the medium also in the resonance region where the two-level system has a bad impedance matching. In the following we will study the lattice case both near resonance and round the Bragg frequency in the purely excitonic regime. In the first case we expect a result similar to the bulk system while in the latter case we look for the localization of light in the defect due to the periodicity. We note that, near the Bragg frequency, the difference between the two-level and three-level atoms is not important because we are far from resonance. We use the TM algorithm that offers a numerically easy and safe way to calculate the reflectivity spectra for different geometries. We first neglect the absorption by following the approach of Chapter 2 and then we introduce γ_e in order to determine the robustness of the different effects: in fact, in the case of three-level atoms spontaneous emission from the excited state is no more quenched and the Hopfield argument [40] is not valid in general.

3.2.1 Vacuum defect

In Fig. 3.5 and Fig. 3.7, we show the reflectivity spectra for a set of vacuum defects with varying length embedded both in an infinite system and in between two finite slabs.

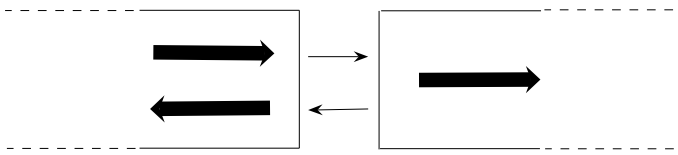

(a)

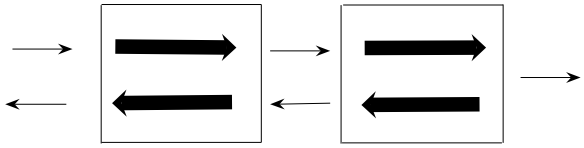

(b)

FIGURE 3.4: Vacuum defect embedded in atomic EIT lattices. Panel (a): semi-infinite atomic lattices. Panel (b): finite slabs of atomic media. The big arrows indicate polariton modes, while the thin ones represent plane waves.

In the first case (black lines), we divide the space in three parts as in Fig. 3.4(a): two semi-infinite regions of EIT atomic medium separated by a defect of length l; in the first atomic part, we consider two counterpropagating polariton modes (incident and reflected); two plane waves travelling in opposite directions are used to built the electric field in the vacuum defect while a single transmitted polariton is propagating in the second semi-infinite atomic layer. Frequency matching conditions are imposed at the interfaces. As usual, the structure of the polariton modes comes from the diagonalization of the TM of the elementary cell and the reflection and transmission coefficients are calculated by imposing boundary conditions at the two interfaces.

In the latter case (red lines), the five regions depicted in Fig. 3.4(b) of space have to be considered: an initial and a final part of vacuum separated by the atomic system which is composed by two finite layers, each of which with $N/2$ cells, and the defect in between them. The spectra for this geometry are calculated from the TM of the whole atomic system $M_{tot} = M_{N/2} M_l M_{N/2}$,

$$R_N = \left| \frac{m_{tot,(1,2)}}{m_{tot,(2,2)}} \right|^2 . \tag{3.8}$$

The spectra in Fig. 3.5 and Fig. 3.7 recall the cases studied in the previous chapter. The main differences between the semi-infinite geometry and the finite slabs in fact are the same: the spectra for the finite systems show Fabry-Perot interference fringes due to the reflection of the polariton modes at the interfaces of the slabs and there is a factor 4 which multiplies the spectrum of the infinite case to recover the peaks of the finite geometry where the reflectivity is small. Furthermore, propagation is forbidden at gap frequencies for the semi-infinite media, while it depends on the number of cells, $N/2$, in the finite systems: here we consider the long lattice limit.

Resonance region

In the region near resonance shown in Fig. 3.5, we observe a dependence of the reflectivity on the length of the defect which can be analyzed for the infinite structure. If the defect is not present ($l = 0$), a polariton mode can propagate through the system without any reflection for frequencies corresponding to the photonic bands; in the gaps, the propagation is forbidden and we fix $R = 1$ in the figures for simplicity. As long as we introduce a defect, there is some reflection due to the mismatch of the electric field between plane waves and polariton modes. This mismatch is related to the relative phase accumulated by the plane waves in the propagation through

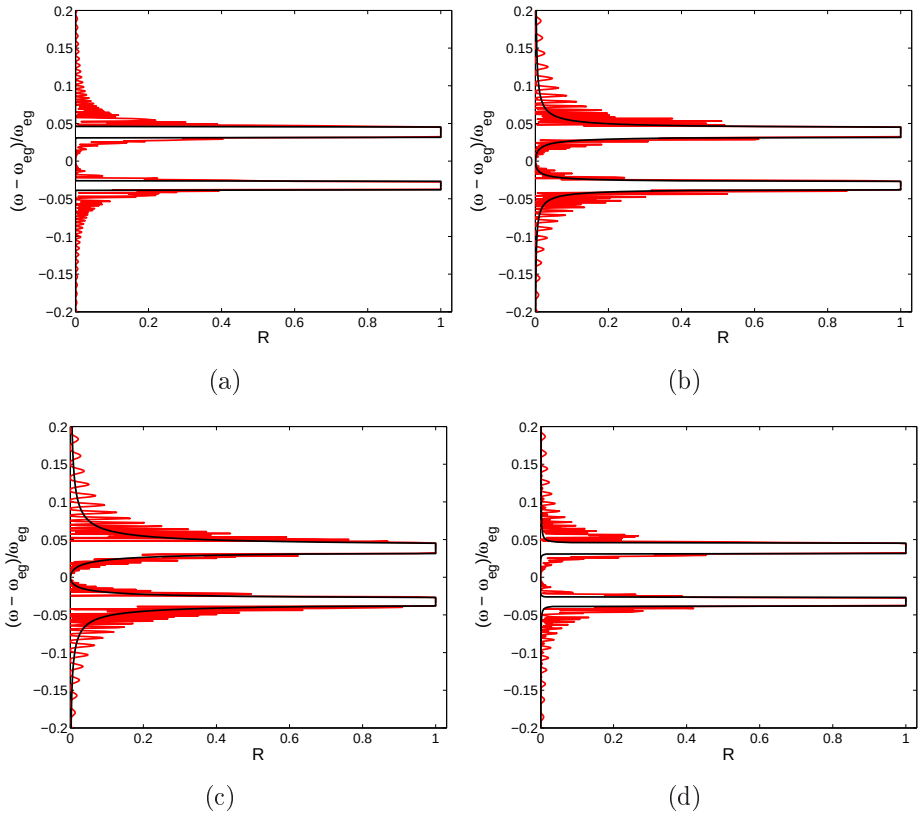

FIGURE 3.5: Polariton scattering on a vacuum defect: reflectivity spectra for an infinite system (solid black lines) and a couple of finite slabs (solid red lines). The length of the defect (in units of the inverse of the resonant wavelength $2\pi/k_{eg}$) is: $l = 0$ (a), $l = 0.1$ (b), $l = 0.2$ (c), $l = 0.5$ (d). Parameters of the system: $f = 0.04$, $\Omega_c = 0.07\omega_{eg}$. The finite slabs contain $N/2 = 100$ cells.

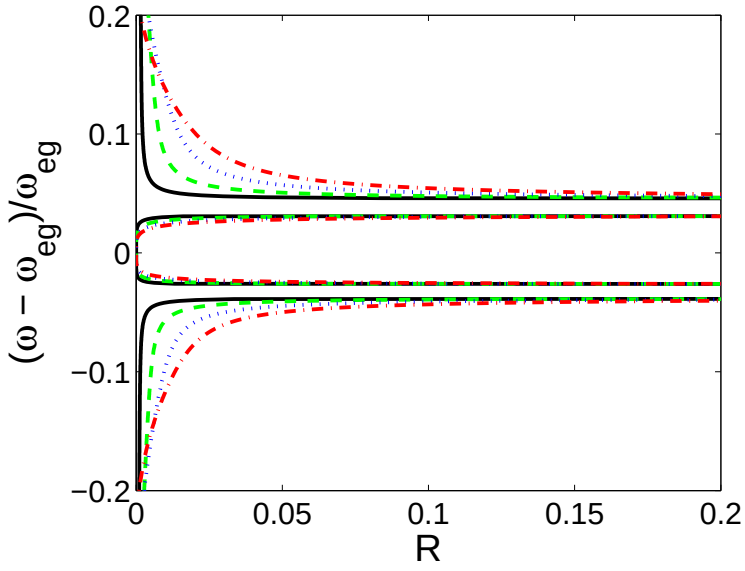

FIGURE 3.6: Comparison between *minimum reflectivity* defects, corresponding to values in the set of l_m [see condition (3.10)]: $m = 1$ (solid black line), $m = 2$ (dashed green line), $m = 3$ (dotted blue line), $m = 4$ (dot-dashed red line). Parameters as in Fig. 3.5.

the defect

$$\phi_l(\omega) = e^{2\,i(\omega/c)l}. \tag{3.9}$$

Exactly at Raman resonance the EIT dispersion crosses the vacuum light line and the atomic medium is transparent to the polariton propagation: the reflectivity dip guarantees the perfect coupling from the atomic gas to vacuum and vice versa, as we stated above. As far as we move away from Raman resonance, reflectivity increases till the gaps. When the defect reaches the length

$$l_m = m(\pi/k_{eg}) \tag{3.10}$$

with m integer, the phase displacement vanishes at Raman resonance and it is in general small along the DP mini-band because $\omega \approx \omega_{eg}$: the reflectivity is small along the whole spectrum. Nevertheless, it is not exactly zero away from Raman resonance and there is an increase proportional to m, as it is shown in Fig. 3.6 in particular in the regions near the gaps.

Bragg frequency

Near the Bragg frequency, we observe the formation of localized modes for frequencies inside the gaps for the finite structure: this feature is clearly visible in the comparison between the two different geometries in Fig. 3.7.

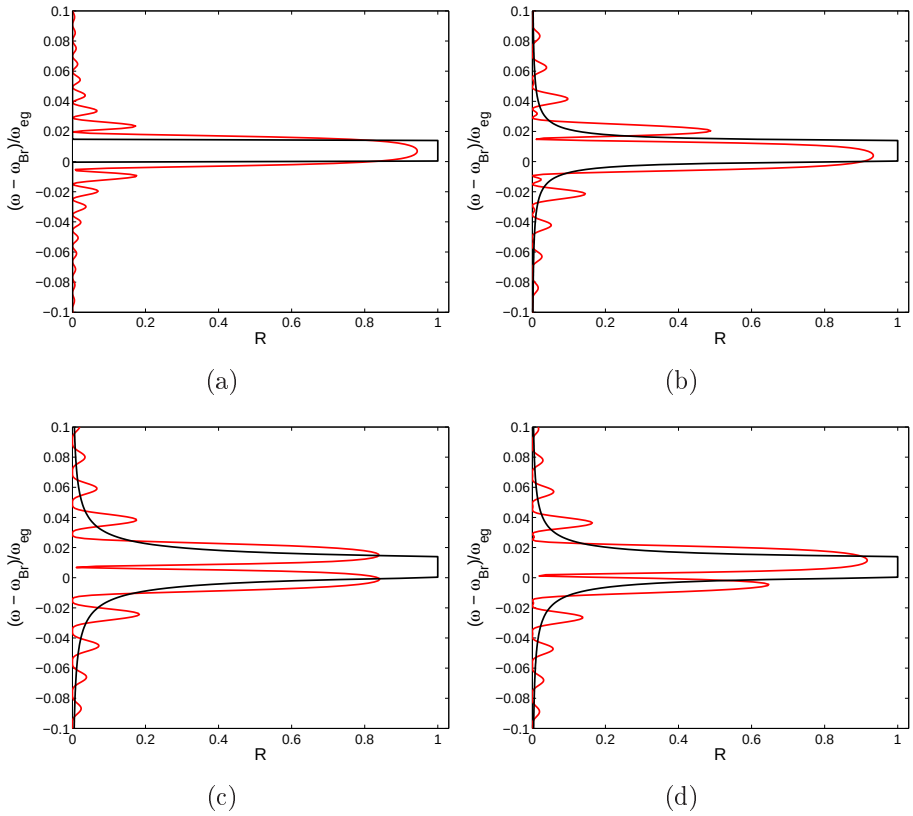

FIGURE 3.7: Polariton scattering on a vacuum defect near Bragg frequency: reflectivity spectra for an infinite system (solid black lines) and a couple of finite slabs (solid red lines). In the finite case, we observe the appearance of localized modes for frequencies inside the gap of the semi-infinite geometry. The lengths of the defects, expressed in units of the lattice constant a, are: $l = 0$ (a), $l = 0.2$ (b), $l = 0.5$ (c), $l = 0.7$ (d). Coupling strengths of the system as in Fig. 3.5. The finite slabs contain $N/2 = 150$ cells.

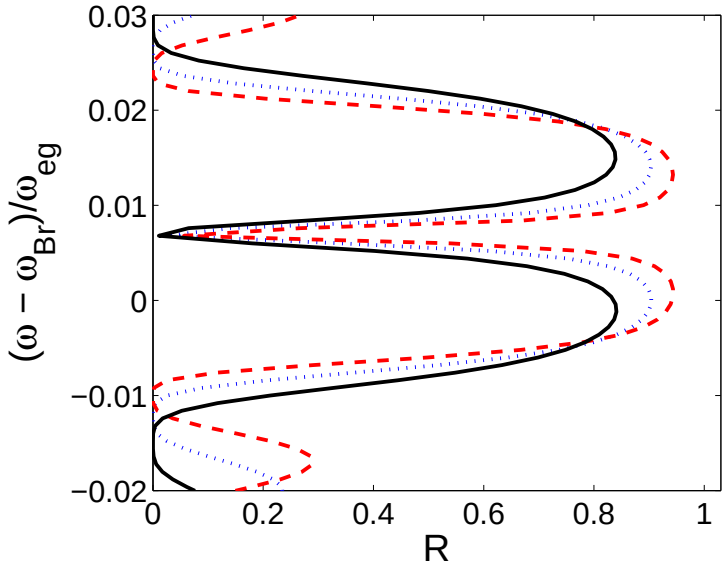

FIGURE 3.8: Compression of the width of the localized mode resonance by increasing the number of cells in the atomic lattices: $N/2 = 150$ (solid black line), $N/2 = 175$ (dotted blue line), $N/2 = 200$ (dashed red line). The defect is long $l = 0.5\,a$.

In this case, the defect becomes a sort of cavity embedded in between the two lattices that act as mirrors. Because the system is finite, some light can tunnel through the structure and a stationary state for the electric field is established: it is peaked corresponding to the defect and it vanishes exponentially in the atomic parts. The phase displacement between the two plane waves in the defect is now given by

$$\phi_l^{Bragg} = e^{2i(\pi/a)l}. \tag{3.11}$$

By varying the length of the defect $l \in [0, a]$, the frequency of the localized mode shift from the upper bound to the lower bound of the Bragg gap: it is in the center when $\phi_l^{Bragg} = -1$. Because we are considering the slab case, the reflectivity of the mirrors depends on the number of cells of each lattice (2.24): by varying the lengths of the slabs $L = (N/2)a$ we change the width of the resonance as it is shown in Fig. 3.8.

3.2.2 Atomic defect

It is also of interest to consider the case of an atomic impurity embedded in the three-level atomic lattice; we built up a toy model that describes a sort of *photon blockade* process as it was suggested in the investigation of the non-linear interaction in a four-level atomic gas [71].

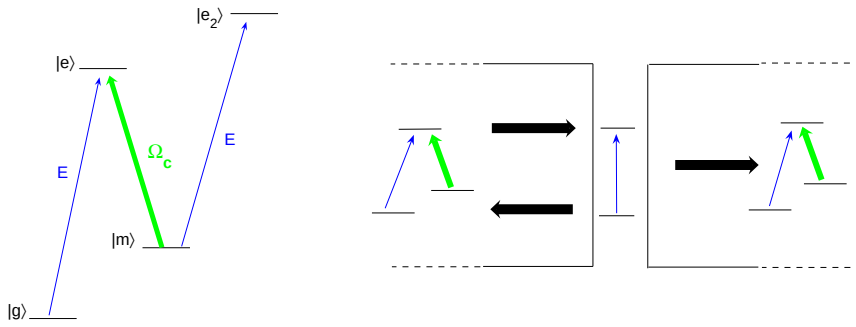

(a) (b)

FIGURE 3.9: The four-level configuration (Panel a) which is studied with to the toy model based on the two-level defect (Panel b): the dressed atom has an allowed transition $|m\rangle \leftrightarrow |e_2\rangle$ that is near resonant with the probe electric field. This transition is mimicked by using the two-level atom in the semi-infinite geometry.

The atomic configuration we want to mimic is depicted in Fig. 3.9: in addition to the three-level Λ configuration, the metastable state is coupled to a second excited state $|e_2\rangle$ and this transition is near resonant with the $|g\rangle \leftrightarrow |e\rangle$ one. The idea is that we have a sequence of travelling photons: a photon brings one of the three-level atoms into the $|m\rangle$ state and then the next photon sees the two-level transition to the $|e_2\rangle$ state. To reproduce this situation, we simply substitute the TM of the vacuum defect with the one containing the phase shift induced by a two-level atom (2.17) described by its resonant frequency ω_d and oscillator strength f_d which is in general different from f because of the different dipole moment. In the reflectivity spectrum, a peak appears corresponding to the resonant frequency as we have seen in the previous chapter for the single atom case (2.25). By tuning the atomic parameters, it is possible to shift and to change the width of the reflection peak within the mini-band, as it is shown in Fig. 3.10. The two-level impurity acts as a wall that abruptly blocks the flow through the otherwise transparent medium.

3.2.3 Effect of absorption

To estimate the effect of absorption we introduce $\gamma_e \neq 0$ in the expressions of the susceptibility derived in Chapter 1. In this case, only the finite slabs geometry makes sense because in the semi-infinite case polaritons are completely absorbed regardless of the extinction length.

Near the Bragg frequency there are no changes in the reflectivity spectrum

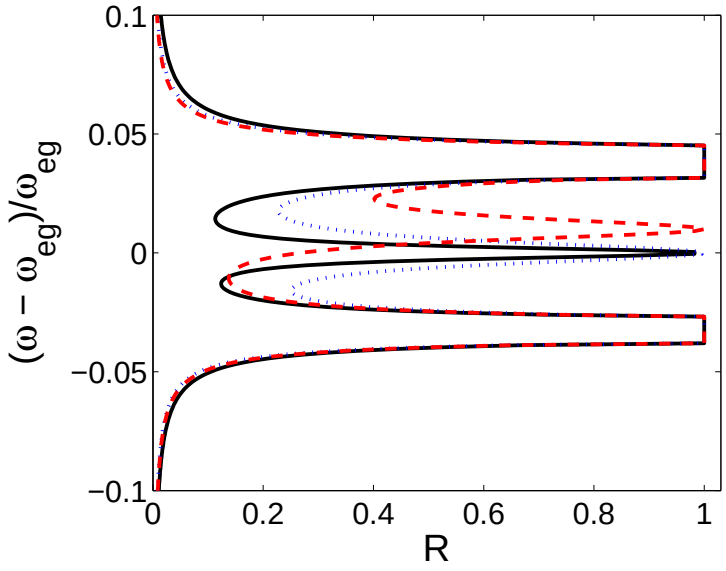

FIGURE 3.10: Polariton scattering on an atomic two-level defect embedded in an infinite lattice of three-level atoms. Oscillator strengths for the atomic lattice as in Fig. 3.5. Atomic parameters for the impurity: $f_d = 0.3f$, $\omega_d = \omega_{eg}$ (solid black line); $f_d = 0.6f$, $\omega_d = \omega_{eg}$ (dotted blue line); $f_d = 0.6f$, $\omega_d = (1.01)\,\omega_{eg}$ (red dashed line).

for the number of cells studied above: this is due to the fact that we discuss the purely excitonic regime and then Bragg frequency is far off-resonant and absorption is vanishingly small.

It is instead strong the effect in the resonance region: the reflectivity peaks corresponding to the gaps for the infinite structure are reduced depending on the value of γ_e. Furthermore, the Fabry-Perot like fringes disappear because the multiple reflections at the interfaces of the structure are forbidden because of absorption. The comparison between the spectra with different values of γ_e is in Fig. 3.11.

For the atomic defect, it is crucial to check the behavior of the impurity peak: its form strongly depends on the detuning between ω_d and ω_{eg}; in fact the reflection is peaked at ω_d while corresponding to Raman resonance we have the absorption dip characteristic of EIT. In Fig. 3.12(a) we see that if $\omega_d = \omega_{eg}$ the central peak is unchanged regardless the value of γ_e, while in the detuned case of Fig. 3.12(b), the impurity reflection is strongly reduced in an asymmetric way. Furthermore, as long as we raise γ_e, we squeeze the absorption dip and the tails of the peak are damped.

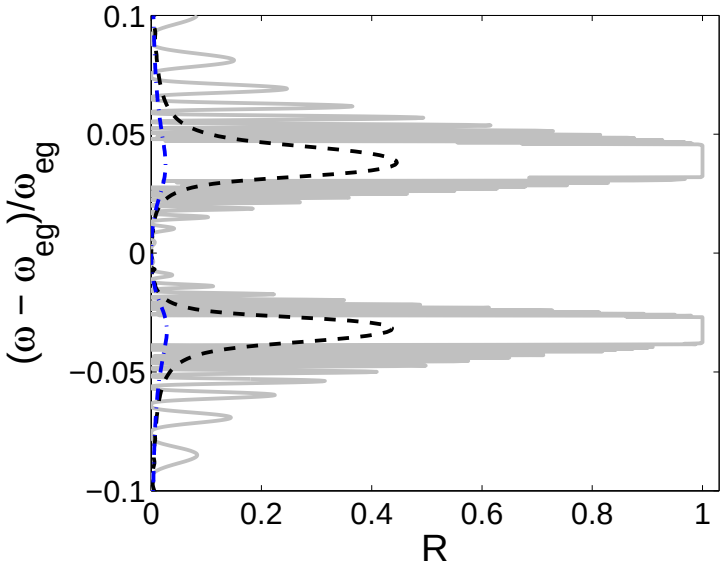

FIGURE 3.11: Effect of absorption on the reflection from defects. Case of a vacuum defect for a slab geometry, spectrum near resonance frequency, parameters as in Fig. 3.5; different values of the excited state linewidth: $\gamma_e = 0$ (solid grey line), $\gamma_e = 0.01\,\omega_{eg}$ (dashed black line), $\gamma_e = 0.07\,\omega_{eg}$ (dot-dashed blue line).

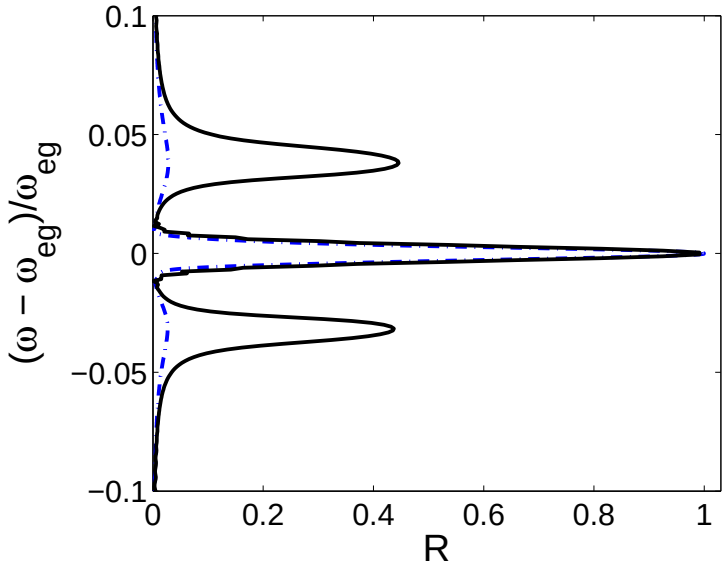

(a)

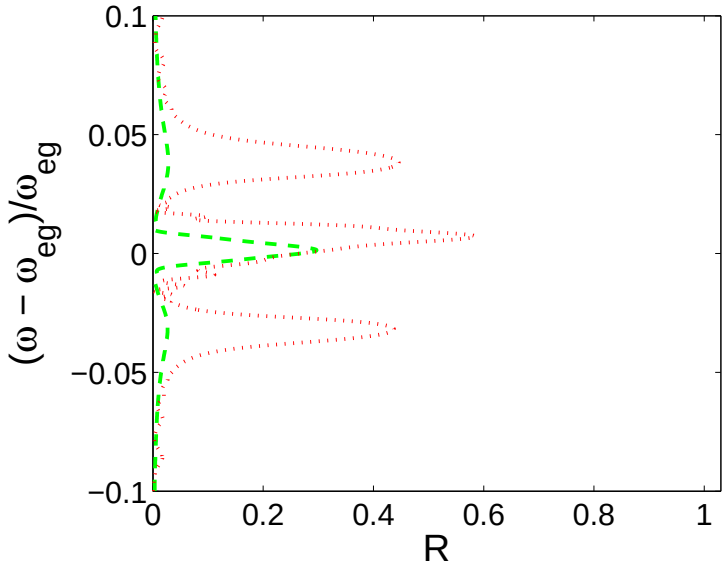

(b)

FIGURE 3.12: Effect of absorption of the reflection from defects. Atomic defect for a slab geometry, spectrum near resonance frequency; atomic parameters for the lattice as in Fig. 3.5. The oscillator strength for the atomic impurity is $f_d = 0.6\, f$. (a) Resonance cases ($\omega_d = \omega_{eg}$): $\gamma_e = 0.01\,\omega_{eg}$ (solid black line), $\gamma_e = 0.07\,\omega_{eg}$ (dot-dashed blue line). (c) Detuned cases ($\omega_d = 1.01\,\omega_{eg}$): $\gamma_e = 0.01\,\omega_{eg}$ (dotted red line), $\gamma_e = 0.07\,\omega_{eg}$ (dashed green line).

Part II

Light manipulation

Dynamic EIT

The control of light pulse propagation in matter is a key element of optical devices for fundamental science as well as for technological applications. In many cases, this is made difficult by the presence of competing effects like dispersion and absorption. Furthermore, the available time for manipulation is limited by the very high propagation speed of light in conventional materials.

As we have seen in Part I, by dressing the matter excitations with coherent external fields, a resonant probe laser pulse can be made to propagate across an otherwise strongly absorbing medium at an ultraslow group velocity and without being distorted. This is the *Electromagnetically Induced Transparency* (EIT). The incoming light is coupled to a *Dark Polariton* (DP) which shows vanishing absorption and dispersion [25–27, 29] and whose group velocity can be controlled via the intensity of the control field [28].

The dynamical modulation of the control field while the pulse is propagating opens up a wide variety of possibilities for light manipulation in the spirit of the so-called *Dynamic Photonic Structures* (DPS) [33]. For example, by completely switching off the control field, the probe light can be halted and stored as an atomic (spin-like) excitation, and later retrieved after a macroscopic time: such light storage techniques [29, 72–75] are considered as a crucial tool for all-optical information technologies. A periodic dynamical modulation of a spatially homogeneous control field can lead to intriguing phenomena such as frequency triggering in time of the EIT band [76]. A non-adiabatic variation of the control field has been proposed as a tool to compensate the pulse broadening at the exit of a delay line [77, 78] or after retrieval of a previously stored light wavepacket [79]. Extremely fast modulations of the control field have been anticipated to produce a substantial dynamical Casimir emission [80].

Light trapping schemes have been proposed which exploit a spatially modulated medium: the creation of a control field grating as well as the use of

atoms trapped in regular periodic structures allow the creation of tunable stop bands within the EIT window [58, 59, 81, 82]. Mutual interactions of moving spin coherence gratings is also an efficient way to stop two-color light and to perform wavelength conversion and it has been recently experimentally realized [83, 84].

A combined spatial and temporal modulation of the control field is discussed in [85–87] where the simultaneous propagation of both control and probe pulses is considered: a ramp of the control field in an otherwise homogeneous medium induces different propagation velocities in the different parts of the probe pulse, which then results in a controllable reshaping of its profile.

Dilute ultracold gases are among the most promising media for EIT applications. Both slow light and light storage have been experimentally realized in this systems [30, 31]. The first experimental realization of EIT in a *Mott Insulator* (MI) has been recently reported for light storage purposes [32]. Unfortunately, the typical size of atomic samples is often small as compared to the duration and waist of the probe pulse, which imposes strict bounds on the efficiency of storage techniques. Most of the theoretical works were so far focused on the case of a homogeneous atomic medium with some boundary condition.

In Part II, we present a model that is able to include the spatial inhomogeneity of a system and therefore to describe the propagation dynamics at the interface between vacuum and the EIT medium. Effects of dynamic modulation in homogeneous systems are described. By taking advantage of the interfaces of the medium, we show how it is possible to manipulate the wavepacket shape by means of a dynamical modulation of the control field intensity.

The multi-layer structure offers the possibility to spatially engineer the radiation-matter interaction by exploiting the advanced trapping techniques of ultracold atoms, while waveguide technology supports the creation of vacuum dispersion regions of tunable length. In the usual pulsed scheme in homogeneous system [85, 86] the manipulation scheme is limited to a single interface, while in this case we can figure out a wide range of different structures involving several interfaces and several layers with different group velocities. As an example, the lossless switching from a single pulse to a train of separated pulses can be addressed. Furthermore, the reduced optical depth of each layer allow for a more efficient modulation [75].

CHAPTER 4

Pulse propagation through inhomogeneous and dynamic structures

The description of radiation-matter interaction based on the susceptibility, that we have used in Part I, refers to a stationary situation. If we want to model the propagation of a light pulse through a dynamic system, we need to consider the full evolution in time of the electric field coupled to the atomic polarizations. The *Optical Bloch Equations* (OBE) seen in Chapter 1 which describe the atomic dynamics have to be plugged into the Maxwell's formalism: the resulting set of partial differential equations gives a complete semi-classical picture [35]. In particular, we focus our attention on the *Dark Polariton* (DP) branch near resonance for an atomic medium under *Electromagnetically Induced Transparency* (EIT) conditions: this system shows the crucial properties of transparency and slow propagation of light needed in view of applications for the manipulation of the light signal.

In Section 1, we discuss a peculiar approach to the *Maxwell-Bloch* (MB) formalism which allows the simultaneous description of both a spatial modulation and a time dependence of the atomic parameters and control beam intensity. The inhomogeneity of the system requires a careful reformulation of the *Slowly Varying Envelope Approximation* (SVEA) [34] in order to safely keep the terms responsible for the reflection at interfaces.

In Section 2, we compare the dispersion obtained from our specific MB equations with the conventional EIT case discussed in Chapter 3: this

comparison is also useful in clarifying the mixed nature of polaritons. For the reflection at interfaces in the stationary situation, we recover the Fresnel law plus some corrections which are in general small and do not introduce spurious effects.

In Section 3, we discuss the propagation through a multi-layer structure composed by vacuum regions and EIT blocks which can be made dynamic. We analyse the simple cases of a homogeneous medium and a sharp interface between different layers.

Starting from the observation that the scattering of a DP pulse on a sharp interface, provided the pulse fits in the EIT dip, usually causes only small reflection in both the static and dynamic cases we derive, in Section 4, a single effective equation for the propagation of the electric field. This equation takes into account the effect of the atomic medium through the polariton group velocity and the relative absorption coefficient. It is useful to investigate ultraslow light regimes were the MB formalism becomes numerically too demanding to be solved.

4.1 Maxwell-Bloch formalism

We restrict our attention to a 1D geometry at normal incidence for the probe field. As the different polarizations of e.m. field are in this case decoupled, the vector nature of Maxwell's equations disappears and one is left with a scalar problem for each component [39]:

$$\left(\frac{\partial^2}{\partial x^2} - \frac{1}{c^2}\frac{\partial^2}{\partial t^2}\right) E(x,t) = \mu_0 \frac{\partial^2}{\partial t^2} P(x,t). \tag{4.1}$$

Here $P(x,t)$ is the polarization of the atomic medium (1.2). The constants c and μ_0 are, respectively, the velocity of light in vacuum and its magnetic permeability.

We consider a laser probe pulse of the form $E(x,t) = (\mathcal{E}(x,t)e^{-i\omega_0 t} + c.c.)$, where ω_0 is the carrier frequency and the pulse envelope $\mathcal{E}$ is assumed to vary on a time scale much slower than ω_0. Under this approximation, we can perform a *modified Slowly Varying Envelope Approximation* (mSVEA) and neglect the second order time-derivatives of the envelope. Differently from the conventional SVEA discussed in textbooks, e.g. [34], all the derivatives of the field with respect to the spatial coordinates are retained: this feature is in fact crucial as we intend to investigate configurations involving abrupt jumps in the spatial distribution of atoms $n(x)$. For this reason we have not separated out the spatial part of the envelope from the carrier. The same form $P(x,t) = (\mathcal{P}(z,t)e^{-i\omega_0 t} + c.c.)$ is assumed for the atomic polarization. This leads to the following rewriting

of Maxwell's equation (4.1):

$$\left(\frac{\partial^2}{\partial x^2}+\frac{\omega_0}{c^2}\left(\omega_0+2i\frac{\partial}{\partial t}\right)\right)\mathcal{E}=-\mu_0\omega_0^2\mathcal{P}. \tag{4.2}$$

Here we have neglected the first order derivative in time of the polarization envelope which is proportional to second-order time derivative of the electric field [68].

The presence of three-level atoms is taken into account by plugging the optical polarization (1.2) arising from the OBE (1.23) into the Maxwell's equation (4.2). The resulting set of MB equations is then given by

$$\frac{1}{\omega_0}\frac{\partial\mathcal{E}}{\partial t} = \frac{i}{2}\frac{1}{k_0^2}\left(\frac{\partial^2}{\partial x^2}+k_0^2\right)\mathcal{E}+\frac{i}{2}\frac{nd_{eg}}{\epsilon_0}\tilde{\rho}_{eg}, \tag{4.3a}$$

$$\frac{\partial\tilde{\rho}_{eg}}{\partial t} = -\left(\frac{\gamma_e}{2}+i\delta_e\right)\tilde{\rho}_{eg}+i\frac{d_{eg}\mathcal{E}}{\hbar}-i\frac{\Omega_c}{2}\tilde{\rho}_{mg}, \tag{4.3b}$$

$$\frac{\partial\tilde{\rho}_{mg}}{\partial t} = -\left(\frac{\gamma_m}{2}+i\delta_R\right)\tilde{\rho}_{mg}-i\frac{\Omega_c}{2}\tilde{\rho}_{eg}. \tag{4.3c}$$

After choosing an appropriate normalization, the MB equations can be cast in the more symmetric form

$$\frac{\partial\mathcal{E}}{\partial t} = \frac{i}{2}\left(\frac{\partial^2}{\partial x^2}+1\right)\mathcal{E}+i\frac{\sqrt{f\omega_{eg}}}{2}\tilde{\rho}_{eg}, \tag{4.4a}$$

$$\frac{\partial\tilde{\rho}_{eg}}{\partial t} = -\left(\frac{\gamma_e}{2}+i\delta_e\right)\tilde{\rho}_{eg}+i\frac{\sqrt{f\omega_{eg}}}{2}\mathcal{E}-i\frac{\Omega_c}{2}\tilde{\rho}_{mg}, \tag{4.4b}$$

$$\frac{\partial\tilde{\rho}_{mg}}{\partial t} = -\left(\frac{\gamma_m}{2}+i\delta_R\right)\tilde{\rho}_{mg}-i\frac{\Omega_c}{2}\tilde{\rho}_{eg}. \tag{4.4c}$$

In particular, we choose the probe frequency ω_0 as the unit for frequency, and the same with $k_0=(\omega_0/c)$ for the wavevector[1]. The electric field is measured in terms of

$$\mathcal{E}_0=\sqrt{\frac{n\hbar\omega_0}{2\epsilon_0}}. \tag{4.5}$$

The physical meaning of this choice is related to the energy density in the system: the energy density associated to the atoms is

$$W_{at}=n\hbar\omega_0|\tilde{\rho}_{eg}|^2, \tag{4.6}$$

where we use the fact that the probe frequency is near resonance, $\omega_0\approx\omega_{eg}$; while the energy in the e.m. field is [88]

$$W_{em}=2\epsilon_0\mathcal{E}_0^2|\mathcal{E}|^2. \tag{4.7}$$

$\mathcal{E}_0$ is then the electric field associated to an excitation which is exactly shared between atoms in the excited state and photons: ($|\mathcal{E}|^2=|\tilde{\rho}_{eg}|^2=1, W_{at}=W_{em}$). The strength of the light-matter coupling is quantified by the adimensional oscillator strength f defined in (1.19).

[1] This means that we have made the following substitutions: $\omega_0 t\leftrightarrow t$, $k_0 z\leftrightarrow z$, $\gamma_e/\omega_0\leftrightarrow\gamma_e$, etc.

4.1.1 Features and limitations of mSVEA

Before proceeding, it is important to assess the features and limitations of the mSVEA approach that we introduced in the previous subsection. This approximation leads in fact to equations (4.2) and (4.4) that differ from the standard formalism used for EIT-related problems and offer important advantages for the specific systems under consideration here.

In the absence of atoms the mSVEA Maxwell's equation (4.2) with $\mathcal{P} = 0$ gives the following approximate dispersion for the free e.m. field[2]:

$$\Omega(k) = \frac{c^2 k^2 + \omega_0^2}{2\omega_0}. \tag{4.8}$$

On one hand, this dispersion is able to simultaneously describe both the forward ($k > 0$) and the backward ($k < 0$) propagating photons. This will be useful to handle reflectivity problems without the need for a coupled mode theory. On the other hand, the deviation from the linear dispersion of light is responsible for a spurious wavepacket broadening. However, this effect start to be important over propagation lengths that are much longer that the ones under investigation here.

At the interface with a generic semi-infinite medium of linear susceptibility $\chi(\Omega)$, the reflectivity of a monochromatic wave at normal incidence can be straightforwardly calculated from (4.2) as

$$R(\Omega) = \left| \frac{1 - k'/k}{1 + k'/k} \right|^2 \tag{4.9}$$

where the mSVEA wavevectors in vacuum and in the medium are respectively

$$k = \frac{\omega_0}{c} \sqrt{1 + 2\frac{\Omega - \omega_0}{\omega_0}} \tag{4.10}$$

$$k' = \frac{\omega_0}{c} \sqrt{1 + \chi(\Omega) + 2\frac{\Omega - \omega_0}{\omega_0}}. \tag{4.11}$$

Provided the frequency Ω is close to the carrier ω_0, the approximate reflectivity (4.9) is accurate up to corrections of the order $(\Omega - \omega_0)/\omega_0$. This condition is well satisfied in an EIT medium in the frequency region around resonance as the light propagation is dominated by the frequency dispersion of the susceptibility $\chi(\Omega)$.

[2]In deriving the formula (4.8), we remember that the equation (4.2) gives the dispersion for the envelope which is shifted by $(-\omega_0)$ with respect the dispersion of the electric field

It is important to note that at the level of the mSVEA approximation one is allowed to replace the k^2 term in (4.8) with a generic function $F(k)$ that satisfies the conditions:

$$\Omega(\pm k_0) = c|k_0|, \tag{4.12}$$

$$\left.\frac{d\Omega}{dk}\right|_{\pm k_0} = \pm c. \tag{4.13}$$

This feature is of great interest when one is to numerically solve the set of equations (4.4).

In fact, we solve the set of MB equations by means of a Finite Difference Time Domain (FDTD) algorithm with a 4th order Runge-Kutta scheme to propagate the fields in time. Spatial derivatives of the fields are evaluated in momentum space using a Discrete Fast Fourier Transform. The crucial issue limiting the speed of the numerical calculation is the time step of the FDTD evolution: its maximum value is set by the width of the frequency band considered in the problem. A proper choice of $F(k)$ with suitable upper and lower bounds allows to restrict this bandwidth without affecting the physics.

In particular, we have chosen an Erf-shaped[3] function which gives the dispersion

$$\Omega(k) = ck_0 \left(1 + \frac{\mathrm{Erf}(\sqrt{\pi}|k - k_0|)}{2k_0}\right). \tag{4.14}$$

The bandwidth is chosen wide enough not to introduce spurious physics in the frequency region of interest close to ω_0. The choice of a linear $F(k)$ at ω_0 suppresses the spurious dispersion of the wavepacket that would be otherwise introduced by the mSVEA. We have checked that the results do not depend on the specific choice of $F(k)$ and remain the same if, e.g., a linear form or the original quadratic form of $F(k)$ are taken which are of course computationally much more time-consuming.

4.2 Homogeneous system: Polariton picture

The MB formalism (4.4) shows how the electric field and the atomic polarizations interact via the laser fields. If we consider a homogeneous atomic medium, this interaction gives rise to mixed eigenmodes for the systems: these states are exactly the *polaritons* [26, 27, 29, 40].

[3]Here we use the following definition for the Erf function: $\mathrm{Erf}(x) = \frac{2}{\sqrt{\pi}} \int_0^x e^{-y^2} dy$.

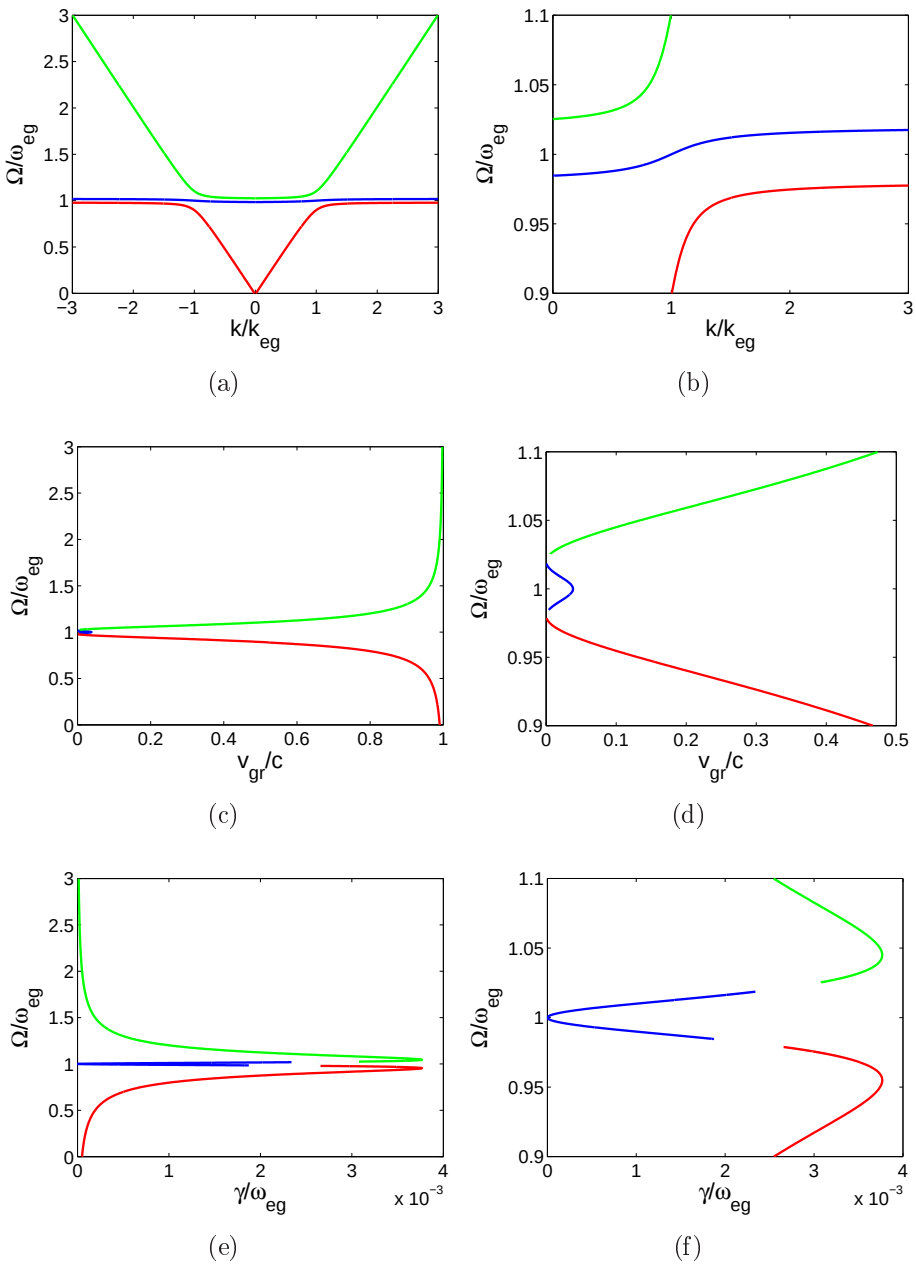

FIGURE 4.1: Polariton dispersion resulting from the diagonalization of the MB formalism (4.4), (4.15). We consider a resonant dressing and the probe carrier is at Raman resonance ($\delta_e = \delta_R = 0$). Parameters of the system: oscillator strength $f = 0.04$, control Rabi frequency $\Omega_c = 0.07\,\omega_{eg}$, excited state linewidth $\gamma_e = 0.01\,\omega_{eg}$. Panel (a): Band diagram for both positive and negative wavevector; panel (c): Group velocity of the polariton wavepacket (positive branch); panel (e): Effective linewidth for the polaritons. Panels (b), (d) and (f) contain the zoom near the positive DP branch respectively for (a), (c) and (e).

4.2.1 Polariton dispersion

In the following we consider the particular case of a resonant dressing and probe carrier, $\omega_0 = \omega_{eg}$, which corresponds to the Raman resonance condition. From the secular equation for the matrix

$$\begin{pmatrix} F(k) & \sqrt{f}\omega_{eg}/2 & 0 \\ \sqrt{f}\omega_{eg}/2 & -i\gamma_e/2 & \Omega_c/2 \\ 0 & \Omega_c/2 & -i\gamma_m/2 \end{pmatrix}, \tag{4.15}$$

which is equivalent to the system (4.4) multiplied by ω_{eg}, we obtain the dispersion for the model we have built up. We use the resonant frequency as the origin for the frequency axis: $\Omega = \omega - \omega_{eg}$. By considering a linear form for the dispersion of light in vacuum, $F(k) = c|k| - \omega_{eg}$, we have

$$\begin{aligned} &(c|k| - \omega_{eg} - \Omega)\left[\left(-\Omega - i\frac{\gamma_e}{2}\right)\left(-\Omega - i\frac{\gamma_m}{2}\right) - \frac{\Omega_c^2}{4}\right] + \\ &-\frac{\sqrt{f}\omega_{eg}}{2}\left(\frac{\sqrt{f}\omega_{eg}}{2}(-\Omega - i\gamma_m)\right) = 0, \\ &c|k| = \omega_{eg} + \Omega + \frac{f\omega_{eg}^2}{4}\left[-\Omega - i\frac{\gamma_e}{2} - \frac{\Omega_c^2}{4(-\Omega - i\gamma_m/2)}\right]^{-1}. \end{aligned} \tag{4.16}$$

This dispersion corresponds to the linearization near the resonant frequency of the general law (2.19) we used in the previous chapter:

$$ck = \left(\omega_{eg} + \Omega + \frac{1}{2}\chi(\Omega)\omega_{eg}\right). \tag{4.17}$$

If we expand the dispersion near Raman resonance

$$\Omega(k) = \frac{\partial\Omega}{\partial k}(k - k_{eg}) + \frac{1}{2}\frac{\partial^2\Omega}{\partial k^2}(k - k_{eg})^2, \tag{4.18}$$

and we use the relations

$$\frac{\partial\Omega}{\partial k} = \left(\frac{\partial k}{\partial\Omega}\right)^{-1}, \tag{4.19}$$

$$\frac{\partial^2\Omega}{\partial k^2} = -v_{gr}^3\frac{\partial^2 k}{\partial\Omega^2}, \tag{4.20}$$

we can derive the expressions for the group velocity (3.2) and the polariton lifetime (3.3) for the DP near Raman resonance:

$$\frac{v_{gr}}{c} = \left[1 + \frac{f\,\omega_{eg}^2}{\Omega_c^2}\right]^{-1}, \tag{4.21}$$

$$\begin{aligned} \gamma(k) &= \frac{\gamma_e}{2}\frac{4f\omega_{eg}^2}{\Omega_c^4}\frac{1}{c}v_{gr}^3(k-1)^2 = \\ &= \frac{\gamma_e}{2}\frac{4\Omega_c^2}{f^2\omega_{eg}^4}c^2(k-1)^2. \end{aligned} \tag{4.22}$$

In Fig. 4.1, we see the polariton branches resulting from the (4.16): in the present work, we are interested in the central mini-band where the group velocity of light and the absorption rate are small [see Fig. 4.1(b), Fig. 4.1(d), Fig. 4.1(f)].

4.2.2 Polariton structure

The diagonalization of the matrix (4.15) gives also the structure of the polaritons in terms of electric field and atomic polarizations. To calculate the components of the eigenvector, we rewrite the matrix by subtracting from the diagonal terms the dispersion $F(k)$ and we also neglect the atomic linewidths which are small as compared to resonance frequency:

$$\begin{pmatrix} 0 & \sqrt{f}\omega_{eg}/2 & 0 \\ \sqrt{f}\omega_{eg}/2 & \omega_{eg} - c|k| & \Omega_c/2 \\ 0 & \Omega_c/2 & \omega_{eg} - c|k| \end{pmatrix}. \tag{4.23}$$

The explicit form of the polaritons is given by [24]

$$u_{LP} = \sin\theta\cos\phi\,\mathcal{E} - \sin\phi\,\rho_{eg} + \cos\theta\cos\phi\,\rho_{mg}, \tag{4.24a}$$
$$u_{DP} = \cos\theta\,\mathcal{E} - \sin\theta\,\rho_{mg}, \tag{4.24b}$$
$$u_{UP} = \sin\theta\sin\phi\,\mathcal{E} + \cos\phi\,\rho_{eg} + \cos\theta\sin\phi\,\rho_{mg}. \tag{4.24c}$$

Here we have defined the angles

$$\tan(\theta) = \frac{\sqrt{f}\omega_{eg}}{\Omega_c}, \tag{4.25a}$$
$$\tan(2\phi) = \frac{\sqrt{f\omega_{eg}^2 + \Omega_c^2}}{2(\omega_{eg} - c|k|)}. \tag{4.25b}$$

Furthermore, for each polariton state at a wave vector k, the group velocity and the lifetime are related to the relative weights of the radiation and matter excitation components:

$$v_{gr}(k) = c\,\frac{|\mathcal{E}(k)|^2}{|\mathcal{E}(k)|^2 + |\tilde{\rho}_{eg}(k)|^2 + |\tilde{\rho}_{mg}(k)|^2}, \tag{4.26}$$
$$\gamma(k) = \gamma_e\,\frac{|\tilde{\rho}_{eg}(k)|^2}{|\mathcal{E}(k)|^2 + |\tilde{\rho}_{eg}(k)|^2 + |\tilde{\rho}_{mg}(k)|^2}. \tag{4.27}$$

4.3 Multi-layer system: the EIT chain

We consider a pulse of light launched into a layered geometry consisting of several atomic EIT media separated by empty regions of space. We

assume the atoms in the different EIT layers to have the same Raman frequency. The probe pulse carrier is taken exactly on Raman resonance and the pulse bandwidth is assumed to fit within the EIT frequency window. The propagation of the pulse across the system can be simulated using the MB formalism (4.4) with spatially dependent $f(x)$ and $\Omega_c(x)$. A pictorial view of the layered medium, the *EIT chain*, is shown in Fig. 4.2. In the following, we distinguish two situations: the *static* case in which the radiation-matter parameters remain constant during the propagation and the *dynamic* scheme which is characterized by a time perturbation of some quantity. In particular, we address the variation in time of the dressing field amplitude Ω_c.

We point out that in all the figures representing the propagation of the polariton, we will report only the electric field component which is the quantity we inject in the atomic system and we measure at the end of the process. It is clear that the electric field and the polariton are the same thing in vacuum, while there are the atomic polarization component in matter.
The shaded parts in the figures correspond to atomic media while the white ones are the vacuum regions. The pulses move from left to right, apart the cases of reflected peaks, and the dashed lines represent the initial pulses. In all the examples shown in the following, we have used standard values for the some parameters: oscillator strength $f = 0.04$ and excited state linewidth $\gamma_e = 10^{-3}\,\omega_0$. The pulses are gaussian-shaped with temporal length $\omega_0\,\sigma_t = 400$.

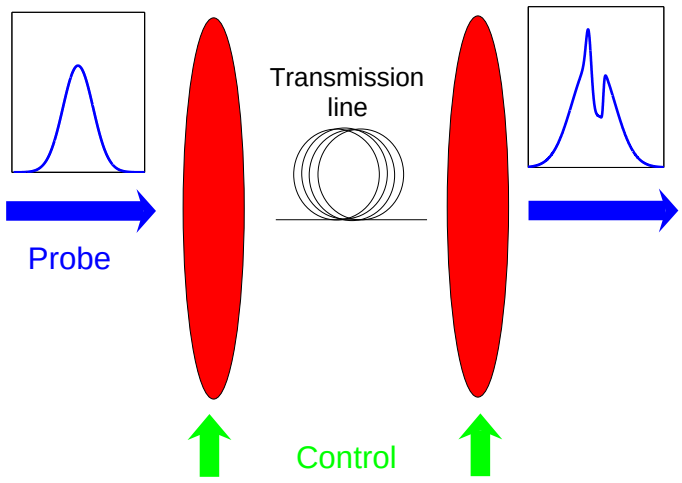

FIGURE 4.2: Pictorial scheme of a double-layer EIT chain. The direction of the control beam is chosen orthogonal to the probe simply for clarity and in general it depends on the specific setup.

4.3.1 Static case

In a static situation, the pulse propagates across the whole structure with only a negligible reflection at the interfaces as it is shown in Fig. 4.3 for the case of a vacuum defect in between two atomic EIT layers. The propagation time is equal to the sum of the thickness of each layer divided by the relative group velocity. As usual, the continuity of the electric field is preserved by the boundary conditions at the interfaces. As a consequence of the spatial dependence in the propagation speed, the shape of the wavepacket is modified while going from one layer to another, which gives rise to discontinuities in the derivative of the pulse envelope at the interfaces: the spatial width of a pulse entering an EIT layer is in fact shrunk by (v_{gr}/c) as a consequence of the reduced group velocity (see Fig. 4.4). The reversed process takes place when it leaves the layer.

We can describe the same process also in terms of the polariton picture. In the presence of an interface, the different wavevector components of the polariton wavepacket are mixed by the spatial inhomogeneity of the system. On the other hand, as long as the system is static, energy conservation imposes a matching condition between the wavevectors across the interface. If we consider the region around Raman resonance, the dispersion is linear both in vacuum and in the EIT layer, yet with different slopes. For a given frequency width of the wavepacket, the wavevector spread, i.e. the inverse spatial width of the pulse, is then increased by the ratio c/v_{gr} when entering a EIT medium, which recovers the intuitive result stated above.
An important distinction has therefore to be carefully made in the notation: the width of the wavepacket in the EIT layer will be denoted by $\bar{\sigma}_x = (\sigma_t\, v_{gr})$ while in vacuum it will be denoted by $\sigma_x = (\sigma_t\, c)$.

By using the lifetime of the DP (4.22), we define two quantities that are useful to describe the propagation of a wavepacket through a homogeneous EIT layer of length L. In fact, the intensity of the DP field decays in time as

$$I_{DP}(\Omega) \propto e^{-2\gamma(\Omega)t} = e^{-L/\ell_{abs}}. \tag{4.28}$$

From this relation, we obtain the absorption length

$$\ell_{abs} = \frac{v_{gr}}{2\gamma(\Omega)}. \tag{4.29}$$

In the case of a DP pulse we can estimate the range over which it can propagate undistorted. By using the relations for the frequency and wavevector spreads $\Delta\Omega = 1/\sigma_t$ and $\Delta k = 1/\bar{\sigma}_x$, we have:

$$\ell_{abs}(\Delta\Omega) = \left(\frac{v_{gr}}{c}\frac{f\omega_{eg}^2}{4\gamma_e}\sigma_t\right)\bar{\sigma}_x, \tag{4.30}$$

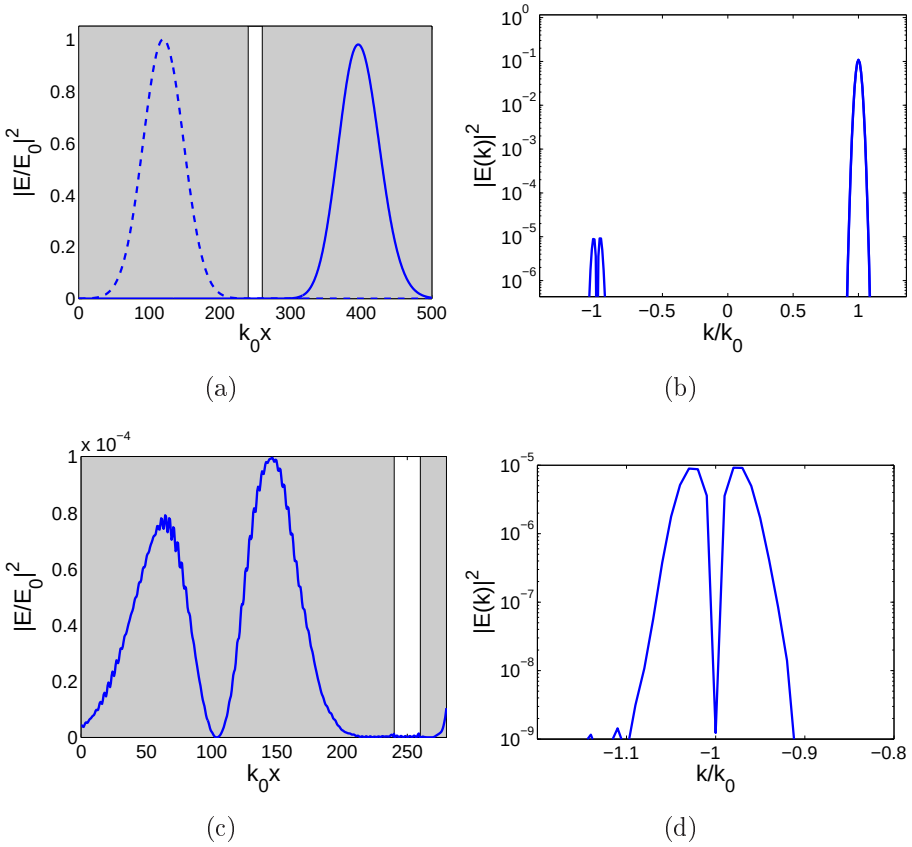

FIGURE 4.3: A DP crossing a vacuum defect in between two atomic layers. The group velocity in the atomic medium is $v_{gr} = 0.11c$. Solid lines represent the electric field at the end of propagation. (a) Real space representation. (b) Wavevector space, reflection round $k/k_0 = -1$ with reflectivity dip; in the main peak the dashed initial pulse is covered by the solid line. Panels (c) and (d) show the details of the reflected peak in both real and momentum space. By varying the length of the defect the result change quantitatively but the reflected peak is always negligible as compared to the transmitted one.

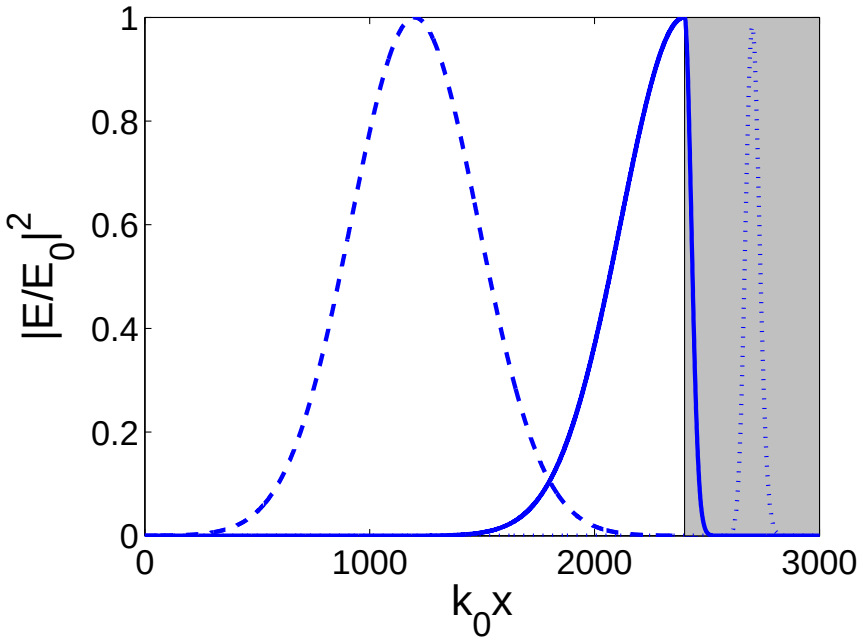

FIGURE 4.4: Propagation across a static interface. Solid line: pulse shape while being spatially compressed in entering into a medium with $v_{gr} = 0.11\ c$. Dotted line: pulse shape once completely entered.

For a pulse going through an atomic samples, we obtain a gaussian transmittivity window in frequency:

$$T(\omega) = e^{-\Omega^2/\Delta\omega_{Tr}^2}. \tag{4.31}$$

where the width of the window is

$$\Delta\omega_{Tr} = \frac{1}{2}\sqrt{\frac{c}{L}}\frac{\Omega_c^2}{\sqrt{f\omega_{eg}^2\gamma_e}}, \tag{4.32}$$

Provided the pulse fits the EIT reflectivity (3.7) and absorption (4.32) dip in each layer and provided the start and end layers consist of the same medium, the pulse duration and shape remain unchanged at the end of the propagation process. In more pictorial terms, the Raman point on the DP branch allows for a good impedance matching between the different regions of space: it acts as the link along the EIT chain.

4.3.2 Dynamic case

As shown in (4.21) and (4.26), the variation of the dressing laser intensity that affects the group velocity also tunes the electric field amplitude of the

probe pulse: the more photonic the polariton, the faster it is. The modulation of this external parameter offers a straightforward way to dynamically act on the EIT chain.

The combined change of group velocity and electric field suggests a variety of possible geometries depending on the desired application; for example, if we are thinking to a tunable delay line [89], we will be more interested in modifying the group velocity without affecting the shape. Instead, we will consider the spatial dependence of the control field in order to reshape the pulse [90] to go beyond the limiting dimensions and profiles of wavepackets obtained with standard techniques.

For this reason, while discussing the effect of control field modulation, two cases will be distinguished: the *homogeneous layer*, when the pulse is completely contained in a single EIT slice during the whole time-modulation sequence, and the *interface*, when the modulation takes place while the pulse is instead overlapping two neighboring layers. The latter process is always feasible, while the former depends on the ratio between the length of the pulse in the medium and the thickness of the involved EIT layers. All the possible geometries related to the EIT chain can be derived from these two basic situations as it will be shown in the next chapter. For the examples of dynamic modulation shown here, the ramp time is fixed at $\omega_0 \tau = 100$.

Homogeneous Layer

When the whole pulse fits into the EIT medium, the dynamics is easily understood within the polariton picture discussed above and it is characterized by the wavevector conservation. A time-dependent perturbation with ramp time τ of the dressing field induces an evolution in the polariton wavefunction and group velocity by changing the weights of radiation and matter components [26, 27, 29] as it is clear from (4.24). For each value of k, this evolution results in a finite transition rate from the DP to the UP and LP: we will discuss in the next chapter this process in detail. In general, the matrix element of the coupling goes as the time derivative of the perturbation and can be neglected as long as the process is adiabatic, i.e. slow as compared to the inverse of the splitting between the different bands [91–94]. Then we expect that provided

$$\sqrt{f}\omega_{eg}\tau \gg 1, \tag{4.33}$$

a polariton injected on the DP branch will spend all its lifetime on this branch. In particular, the dynamical modulation of the frequency spectrum ensures that if the pulse fulfills the EIT condition at the entrance time, then it will fulfill it at all later times [33].

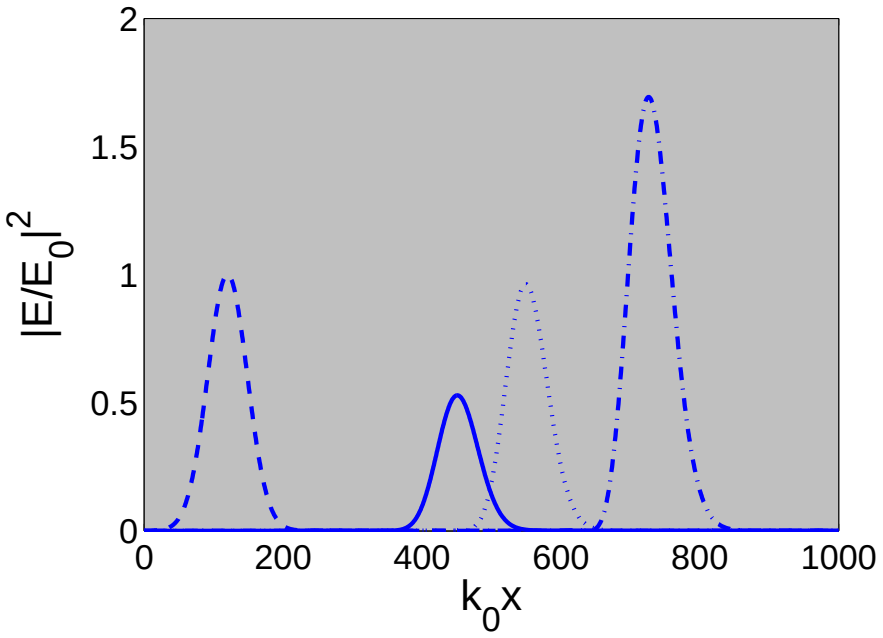

FIGURE 4.5: Wavepacket propagation in a dynamic homogeneous EIT layer. Dotted line: propagation without modulation. Solid line: result of a slow down ramp $v_{gr}^f = v_{gr}^i/2$. Dot-dashed line: result of a speed up ramp $v_{gr}^f = 1.8\ v_{gr}^i$.

We consider a generic variation in the group velocity from the initial value v_{gr}^i to the final one v_{gr}^f. The resulting pulse shape does not depend on the functional form of the velocity variation. The spatial shape of the pulse is fixed by the initial distribution in the wavevector space (Δk) and is not modified. The peak electric field intensity is instead multiplied by (v_{gr}^f/v_{gr}^i) according to (4.26). In the case in which the group velocity modulation is brought back to the initial value ($v_{gr}^f = v_{gr}^i$), the pulse emerges with an unchanged profile: as a result, the layer can be considered as a very compact, yet programmable delay line. Examples of modulations are illustrated in Fig. 4.5.

Interface

A dynamical modulation taking place while the pulse overlaps an interface provides a simple way of reshaping the pulse: only the part of the pulse which is located inside the EIT layer is in fact affected by the modulation of the dressing field. In contrast to the the spatially homogeneous case considered above, the shape of the emerging pulse now strongly depends on the details of the modulation ramp even in the adiabatic limit. This crucial fact is illustrated in Fig. 4.6: the group velocity of a EIT medium

is reduced while a pulse is exiting into vacuum.

The results can be understood by isolating three portions of the pulse: the first part is already in vacuum when the modulation begins, while the last part is still in the EIT medium when the modulation is completed. The first part is therefore not affected by the modulation, while the electric field amplitude of the third part is homogeneously lowered. When this part of the pulse eventually exits into vacuum, its spatial length is stretched out even more than the first part by a factor v_{gr}^i/v_{gr}^f. As clearly visible in the figure, this results into a strongly asymmetric pulse shape.

Finally, the modification of the central part of the pulse depends in a non-trivial way on the details of the ramp. For a fast [but still adiabatic as compared to the interband splitting, according to (4.33)] modulation, the first and third parts of the pulse are connected by a sharp jump in the electric field amplitude. For slower ramps, this jump is replaced by a smooth crossover. Details about this process in more complicated structures and applications to realistic experimental situations will be discussed in the next chapter.

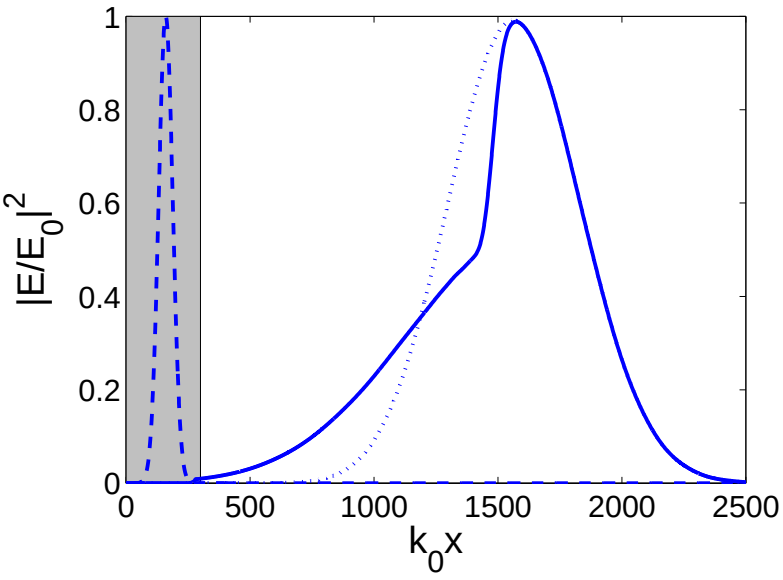

FIGURE 4.6: A DP pulse exiting from a EIT medium into vacuum, $v_{gr}^i = 0.11\,c$. Dotted line: propagation without modulation. Solid line: result of a slow down ramp $v_{gr}^f = v_{gr}^i/2$.

4.4 Polariton flow: effective description

The MB formalism (4.4) gives a complete picture of the pulse propagation which is able to take into account inter-band transitions[4] as well as reflection at the interfaces. In fact, as we see in Fig. 4.1(a), we consider the three polariton branches for both positive and negative wavevectors. As the solution of the three coupled equations is time- and memory-consuming, it quickly becomes unfeasible for growing values of the velocity mismatch between the different media.

For this reason, an effective approach able to investigate the ultraslow light regime can be of great interest. Starting from the dispersion of the DP branch, we have written a single equation for the electric field intensity. The crucial feature of this effective model is that it is able to include the effect of both absorption and spatial inhomogeneity of the structure. With the derivation of this equation, we have a complete formalism to analyze the propagation of a DP pulse through inhomogeneous and dynamic structures: the MB equations capture the essential physics in relation to specific geometry and modulation of the parameters while the effective equation allows to test the effect of the developed techniques using realistic values.

4.4.1 Continuity equation

From the MB formalism, we have seen that the dynamic modulation of the pulse does not result into an increased reflection as compared to the static case and transmittivity is very good as long as the pulse fits in the EIT transmission window. The features that were observed in the solution of the MB equations in the absence of absorption suggest that the system can be described by means of a continuity equation for the polariton flow both in the homogeneous system case and in presence of interfaces.

In terms of the polariton density $n_p(x,t)$, the continuity equation reads

$$\frac{\partial}{\partial t} n_p(x,t) + \frac{\partial}{\partial x} \left(n_p(x,t) v_{gr}(x,t) \right) = 0. \tag{4.34}$$

Physically, this equation means that the total number of polaritons is conserved. It is useful to rewrite this equation in terms of the electric field intensity $I = |\mathcal{E}|^2$ corresponding to the polariton flux $n_p v_{gr}$ [see (4.26)] instead of the polariton density.

For static inhomogeneous geometries with abrupt changes in the polariton velocity, the polariton density shows in fact discontinuities while the

[4] For a detailed discussion see next chapter.

electric field remains everywhere continuous, even at the interfaces. In the static situation ($v_{gr}(x,t) = v_{gr}^0(x)$), the initial local polariton flux (i.e. electric field in each point) remains constant and propagates following the velocity field $v_{gr}^0(x)$.

Taking into account (4.26), Eq.(4.34) then becomes

$$\frac{\partial I}{\partial t} + v_{gr}\frac{\partial I}{\partial x} = -\frac{I}{v_{gr}}\frac{\partial v_{gr}}{\partial t}. \tag{4.35}$$

The LHS of the equation contains the propagation terms for the static situation. The general solution is a mixed translation and dilation of the starting pulse $I^0(x)$ according to the trajectories in space-time which are solution of the Cauchy problem: $(\dot{\xi} = v_{gr}(\xi), \xi(t) = x)$ [26, 29, 85]. The specific solution clearly depends on the geometry. The RHS of (4.35) is instead responsible for the amplitude variation in the dynamic case.

4.4.2 Analytic solutions for the interface geometry

We consider a semi-infinite geometry with the left half-space made of a homogeneous EIT medium and the right half-space of vacuum; the velocity grid is defined by

$$v_{gr}(x,t) = v(t)\theta(-x) + c\theta(x), \tag{4.36}$$

where we take into account the possibility of a time perturbation of the group velocity in the EIT medium. We consider a positive velocity $v(t) > 0$, so that the electric field moves from left to right. If we assume an initial electric field intensity distribution $I^0(x)$, the analytic solution of (4.35) in this geometry is

$$I(x,t) = \begin{cases} I^0\left(x - \mathcal{I}_0^t\right)\dfrac{v(t)}{v(0)}, & x < 0 \\ I^0\left(-\mathcal{I}_0^{t-x/c}\right)\dfrac{v(t-x/c)}{v(0)}, & 0 < x < ct \\ I^0\left(x - ct\right), & x > ct \end{cases} \tag{4.37}$$

Here we have defined

$$\mathcal{I}_a^b = \int_a^b v(t')dt'. \tag{4.38}$$

This expression allows to study both the homogeneous case and the interface geometry and both the dynamic and the static case. In fact, depending on the initial distribution of the electric field and the time at which we look the solution we can address the different situations. Because the electric field moves from left to right, the three different parts that compose the solution are divided in a simple way: the first part contains the points

which are still in the atomic medium at the observation time, the second part takes the points which cross the interface during the process while in the third part there are the points which started in vacuum. In Fig. 4.7 we compare the solutions of MB formalism (4.4) with those of the continuity equation (4.39) in the case of a static and a dynamic interface. The agreement is very good.

4.4.3 Effect of losses

Even if the carrier frequency ω_0 sits exactly on Raman resonance, finite time duration of the wavepacket requires including absorption for the tails of the wavevector spectrum [86,95]. This leads to a finite and momentum-dependent decay rate for the polaritons according to (4.27). Taking inspiration from the approximated form (4.22) of the decay rate [68], a simple diffusion term can be used to model the broadening coming from losses. The propagation equation (4.35) for the intensity I then becomes

$$\frac{\partial I}{\partial t} + v_{gr}\frac{\partial I}{\partial x} = -\frac{I}{v_{gr}}\frac{\partial v_{gr}}{\partial t} + \frac{\partial}{\partial x}\mathcal{D}\frac{\partial I}{\partial x}, \tag{4.39}$$

where

$$\mathcal{D} = i\left(\frac{d^2\omega}{dk^2}\right)_{\delta_R=0} = v_{gr}\,\frac{4\gamma_e}{f}\frac{c}{\omega_{eg}^2} \tag{4.40}$$

is the diffusion coefficient. We will see the crucial contribution of this term in the next chapter. It is worth noticing that this equation is only useful as an effective model: in fact to actually take into account losses it is crucial to use the complete equation for the dark polariton field instead of its intensity [29].

We solve equation (4.39) by means of a Runge-Kutta algorithm in the time domain exploiting a spatial grid shaped on the group velocity of each layer: in this way, the numerical solution of the propagation is much faster than the one of the three MB coupled equations. In particular, it is able to explore regimes where $v_{gr}/c \ll 1$.

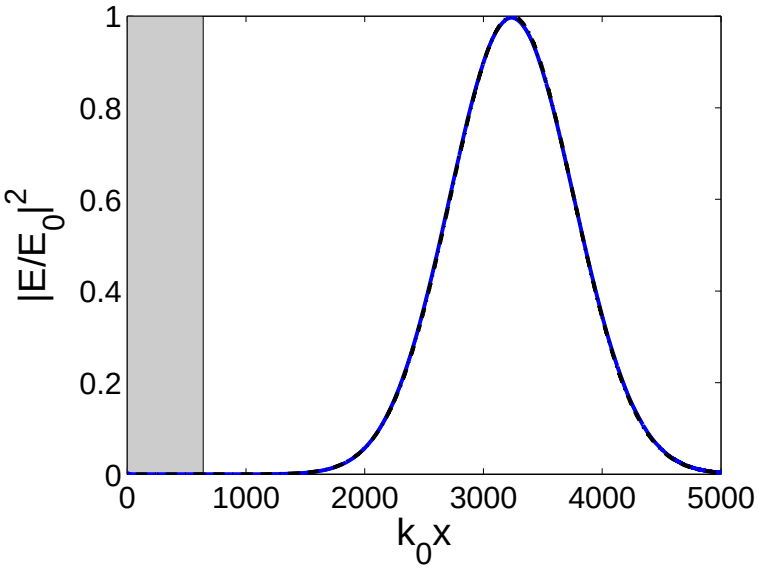

(a)

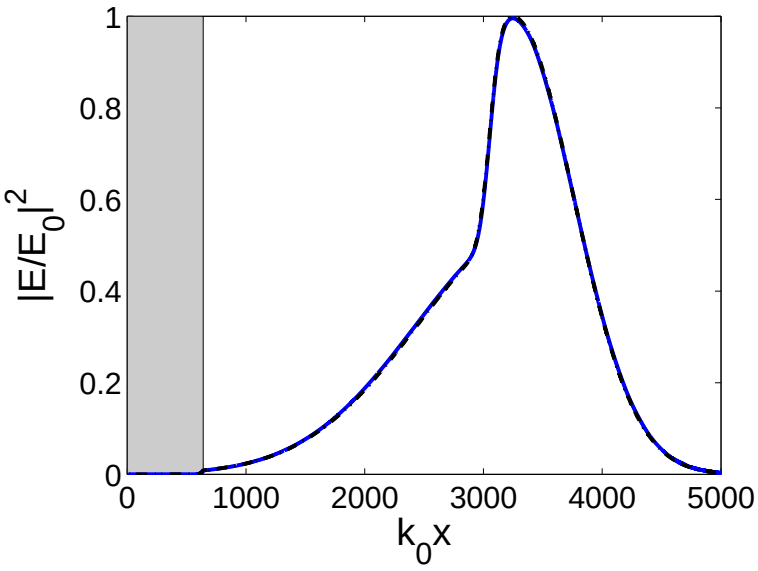

(b)

FIGURE 4.7: Comparison between the numerical solutions of MB equations (solid, blue line) and the analytical result of the continuity equation (4.35) for the polariton flow (dash-dotted, black line) for the interface geometry both in the static and dynamic case. The parameters are the same as the cases analyzed above.

CHAPTER 5

EIT-based Dynamic Photonic Structures with atoms

The outstanding properties of coherent optical media supporting *Electromagnetically Induced Transparency* (EIT) seen in Chapters 3 and 4 suggest that such kind of systems are an efficient environment to perform dynamic modulations of light pulses. *Dynamic photonic structures* (DPS) [33] are attracting an increasing interest in view of optical information processing, and ultracold samples offers a sort of protected environment where the different techniques can be tested. The present Chapter is devoted to study the effects and the engineering possibility of a dynamic manipulation of a slowly propagating polariton in ultracold atomic EIT samples.

In Section 1, we test the application of adiabatic transition theory [91] to the *Maxwell-Bloch* (MB) formalism developed in the previous chapter in analogy with the evolution of the Schrödinger's equation. The goal is the study of the time-dependent coupling rate induced between the *Dark Polariton* (DP) and the other bands (LP and UP). We find interesting results at Raman resonance about the general behavior of this coupling depending whether the shape of the time-dependent modulation of the control field is analytic or not. In particular, we show that for an Erf-shaped perturbation an intermediate regime is found before the expected exponential decay of the asymptotic coupling with the interaction time takes place. On the other hand a sinusoidal modulation of the control field induces quite a cumbersome oscillating behavior in the coupling. In both cases adiabatic transition theory well applies also for short interaction times.

In Section 2, we propose a *Photon Energy Lifter* scheme [37] for a homogeneous EIT ultracold gas. The idea is to adiabatically raise the resonant atomic frequency after the injection of a DP inside the system. The excitation is then stuck to the Raman resonance and then the change in the atomic frequency eventually results in a wavelength conversion of the extracted pulse. Experimental issues are discussed by comparing the properties of different cold samples routinely obtained in laboratory.

Section 3 contains a detailed discussions about the results of a modulation of the control field amplitude in the multi-layer EIT chain introduced in the Chapter 4. The reshaping of the electric field in the linear optical regime can be regarded as a quantum wavepacket manipulation since Maxwell's equations are recovered from the quantum mechanical treatment of light in the limit of low intensity. The use of inhomogeneous geometries offers an original contribution in the growing field of DPS. Realistic values for the atomic samples are used within calculations carried out with the effective equation (4.39).

5.1 Inter-band coupling

We consider a homogeneous EIT medium and a polariton wavepacket which is propagating across it. We want to study the effect of a variation in time of the dressing amplitude Ω_c that is performed in a homogeneous way. The advantage of such a configuration is that the different k-component of the signal do not mix during the process and then the problem can be solved for the plane wave case.

We observe that the set of MB equations with the mSVEA (4.4) has the same structure as a Schrödinger's equation for a three-component wavefunction ψ which is expanded in terms of the basis $(\mathcal{E}, \tilde{\rho}_{em}, \tilde{\rho}_{eg})$. If we neglect absorption, the Hamiltonian for the evolution of the system is represented by the matrix (4.23), which at Raman resonance reads

$$H(t) = \begin{pmatrix} 0 & 0 & \sqrt{f}\omega_{eg}/2 \\ \sqrt{f}\omega_{eg}/2 & 0 & -\Omega_c(t)/2 \\ 0 & -\Omega_c(t)/2 & 0 \end{pmatrix}. \tag{5.1}$$

It is useful to rewrite the Schrödinger's equation in the polariton basis (UP, DP, LP),

$$i\frac{\partial}{\partial t}\tilde{\psi}(t) = \left(\tilde{H}(t) + i\dot{\mathcal{R}}\mathcal{R}^{-1}(t)\right)\tilde{\psi}(t), \tag{5.2}$$

where $\mathcal{R}(t)$ is the matrix which turns the radiation-matter picture into the polariton one: $\tilde{\psi}(t) = \mathcal{R}(t)\psi(t)$. By looking at (4.24), we immediately

see that

$$\mathcal{R}(t) = \begin{pmatrix} \sin\theta\cos\phi & -\sin\phi & \cos\theta\cos\phi \\ \cos\theta & 0 & -\sin\theta \\ \sin\theta\sin\phi & \cos\phi & \cos\theta\sin\phi \end{pmatrix}. \tag{5.3}$$

The operator $\tilde{H} = \mathcal{R}H\mathcal{R}^{-1}$ is the Hamiltonian (5.1) which is diagonal in the polariton basis while the other term, $\dot{\mathcal{R}}\mathcal{R}^{-1}$, derives from the rotation in the Hilbert space of the instantaneous eigenstates (i.e. the polaritons).

5.1.1 Adiabatic Transition Theory

We consider a smooth perturbation of the Hamiltonian: if the system is initially prepared in an eigenstate, it will follow the evolution in time of the relative eigenvector performing a so called *adiabatic transition* [91]. Furthermore because the eigenstates of the Hamiltonian evolve in time we expect a finite coupling rate among them. The adiabatic following is driven by the first term on the RHS of equation (5.2) while the second term couples the different instantaneous eigenstates. If we define a characteristic time scale τ for the variation of the Hamiltonian and $\Delta\omega$ is the energy gap between a specific couple of instantaneous eigenstates, the intuitive condition for the adiabaticity with respect to the chosen transition is $\tau\Delta\omega \gg 1$. An exponential decay with the increase of τ in a two-level system is in general expected [96].

If the system is, at the starting time t_0, in the eigenstate $|l_1\rangle(t_0)$ of the Hamiltonian $\tilde{H}(t_0)$, it turns out that the first order in perturbation theory for the amplitude of transition between the evolved eigenstate $|l_1\rangle(T)$ and another instantaneous eigenstate $|l_2\rangle(T)$ of $\tilde{H}(T)$ is [91]

$$p_{l_1\to l_2}(T) = \left| \int_{t_0}^{T} dt\, \alpha_{l_1 l_2}(t)\, exp\left(i \int_{t_0}^{t} \omega_{l_2 l_1}(t')dt' \right) \right|^2, \tag{5.4}$$

where

$$\alpha_{l_1 l_2}(t) = {}_t\langle l_2| \left(\frac{d}{dt} |l_1\rangle_t \right) \tag{5.5}$$

is the projection of the evolution of $|l_1\rangle(t)$ on $|l_2\rangle(t)$, while $\omega_{l_1 l_2}$ is the frequency of the transition between the states. The α terms are exactly the elements of the coupling matrix $\dot{\mathcal{R}}\mathcal{R}^{-1}(t)$. If we assume constant values for $\alpha_{l_1 l_2}(t)$ and $\omega_{l_1 l_2}(t)$ corresponding to respectively the maximum and minimum of the two quantities and we substitute them into the integral (5.4), the fact that the coupling has to be small gives an adiabatic criterion that goes beyond the intuitive condition (4.33) stated in Chapter 4:

$$\left| \frac{\alpha_{l_1 l_2}^{max}}{\omega_{l_2 l_1}^{min}} \right| \ll 1. \tag{5.6}$$

In the case of the atomic Hamiltonian (5.1), by using the expression (5.3) and the definitions (4.24), (4.25) we obtain the matrix for the change of basis:

$$\mathcal{R} = \frac{1}{\sqrt{2}} \begin{pmatrix} \sin\theta & -1 & \cos\theta \\ \sqrt{2}\cos\theta & 0 & -\sqrt{2}\sin\theta \\ \sin\theta & 1 & \cos\theta \end{pmatrix}, \tag{5.7}$$

where we have exploited $\phi = \pi/4$. Because of the unitarity of $\mathcal{R}$, it is easy to write its inverse $\mathcal{R}^{-1}$ and then we have the coupling matrix:

$$\dot{\mathcal{R}}\mathcal{R}^{-1} = \begin{pmatrix} 0 & (1/\sqrt{2})\dot{\theta} & 0 \\ -(1/\sqrt{2})\dot{\theta} & 0 & -(1/\sqrt{2})\dot{\theta} \\ 0 & (1/\sqrt{2})\dot{\theta} & 0 \end{pmatrix}. \tag{5.8}$$

It depends only on the ratio between the Rabi splitting and the control field intensity:

$$\dot{\theta} = \left(1 + \frac{f\,\omega_{eg}^2}{\Omega_c^2}\right)^{-1} \left(-\frac{\sqrt{f}\,\omega_{eg}}{\Omega_c^2}\right) \frac{d\Omega_c}{dt} = -\frac{\sqrt{f}\,\omega_{eg}}{f\,\omega_{eg}^2 + \Omega_c^2} \frac{d\Omega_c}{dt}. \tag{5.9}$$

Consequently the integral (5.4) becomes

$$p_{\pm}(T) = \left| \frac{1}{\sqrt{2}} \int_{t_0}^{T} dt \frac{\sqrt{f}\,\omega_{eg}}{\Omega^2(t)} \frac{d\Omega_c(t)}{dt} exp\left(\pm i \int_{t_0}^{t} \frac{\Omega(t')}{2} dt'\right) \right|^2 \tag{5.10}$$

where $p_{\pm}(T) = p_{DP \to UP,LP}$ and $\Omega^2(t) = f\,\omega_{eg}^2 + \Omega_c^2(t)$. In the slow light case $\sqrt{f}\omega_{eg} \gg \Omega_c$, the condition for adiabaticity (5.6) requires

$$\frac{1}{f\,\omega_{eg}^2} \left| \frac{d\Omega_c(t)}{dt} \right| \ll 1. \tag{5.11}$$

It is important to check the validity of this calculation of the effective coupling within the MB formalism. In fact, it provides a good expression to estimate the loss of signal in the specific dynamic structures we are dealing with, due to inter-band coupling.

Two specific cases of adiabatic perturbations are to be considered in the following: the first one is an Erf-shaped variation of the dressing field intensity while in the other case we have a sinusoidal tuning. These curves are representative of two different classes; in fact, the main difference among them is the behavior of the derivatives: the first function is analytic, while the latter one has discontinuities in the second order derivatives at the boundaries of the variation. In the next subsections, it is illustrated a comparison between the results coming from the numerical simulation of the MB equations, with analytical results of the integral (5.10) for different cases. The simulations are carried out for polariton plane waves sitting

at Raman resonance. We investigate the asymptotic coupling p^{∞} which is the transition rate for large T and the behavior of the peak p^{max}. For both of them, we calculate the dependence on the time scale of the perturbation τ for different values of the oscillator strength f. In general, we consider $\sqrt{f}\omega_{eg} \gg \Omega_c$.

5.1.2 Analytic Perturbation: Erf shape

We first consider a variation in time of Ω_c which has the form:

$$\Omega_c(t) = \Omega_{c,0} - \delta\Omega_c \left[1 + \mathrm{Erf}\left(\frac{t}{\tau}\right)\right], \tag{5.12a}$$

$$\frac{d\Omega_c(t)}{dt} = -\frac{\delta\Omega_c}{\tau}\frac{2}{\sqrt{\pi}}e^{-(t/\tau)^2}. \tag{5.12b}$$

For the specific case, it is clear that $t_0 \to -\infty$.

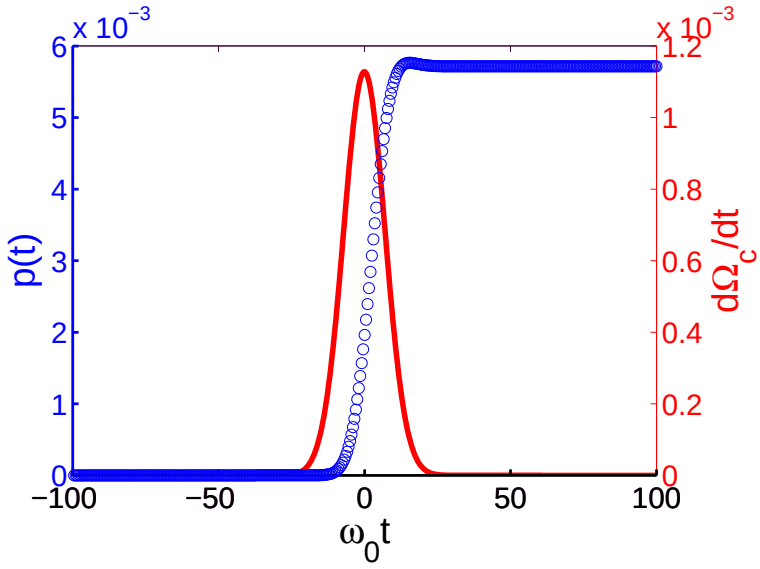

FIGURE 5.1: Example of result from the simulation of MB equations performed by using a plane wave input: derivative of the ramp for $\Omega_c(t)$ (solid red line) and relative evolution of the coupling outside the DP (blue dots) are shown. An Erf-shaped ramp of Ω_c is considered.

By applying the condition (5.6) to the present situation, for the process to be adiabatic it must hold

$$\left| 2\sqrt{\frac{2}{\pi}}\frac{\delta\Omega_c}{\sqrt{f}\,\omega_{eg}}\frac{1}{\sqrt{f}\,\omega_{eg}\tau} \right| \ll 1. \tag{5.13}$$

It is interesting to note that while the last fraction on the LHS expresses the intuitive condition on the ratio between the rate of change and the energy spacing, the complete formula also contains another fraction which is much smaller than 1 in the regime under investigation here and it extends the validity of the adiabaticity approximation for smaller τ. By using the coupling integral (5.10) and the expressions for the specific case (5.12), we first introduce the rough approximation $\Omega(t) \to \sqrt{f}\omega_{eg}$ which leaves in the integrand a gaussian function and an oscillating term:

$$p(T) \approx \left| \sqrt{\frac{2}{\pi}} \frac{\delta\Omega_c}{\sqrt{f}\omega_{eg}\tau} \int_{-\infty}^{T} dt e^{-(t/\tau)^2} e^{i\sqrt{f}\omega_{eg}t/2} \right|^2 . \tag{5.14}$$

By using the general result [97]

$$\int_0^{+\infty} dt\, e^{-(at^2+2bt+c)} = \frac{1}{2}\sqrt{\frac{\pi}{a}} e^{\frac{b^2-ac}{a}} \mathrm{Erfc}\left(\frac{b}{\sqrt{a}}\right), \tag{5.15}$$

we obtain

$$p(T) \approx \left| -\frac{\delta\Omega_c}{\sqrt{2f}\omega_{eg}} e^{-(f\,\omega_{eg}^2\tau^2/16)} \mathrm{Erfc}\left(-\frac{T}{\tau} + i\frac{\sqrt{f}\,\omega_{eg}\tau}{4}\right) e^{i\beta(T,f,\tau)} \right|^2 . \tag{5.16}$$

where β is a real function, and thus the last term becomes unity after taking the absolute value.

Asymptotic Coupling

The expression (5.16) is qualitatively in agreement with the results coming from the simulations [see e.g. Fig. 5.1]. For fixed τ and f, the function $\mathrm{Erfc}(z) = 1 - \mathrm{Erf}(z)$ of the complex variable z vanishes for

$$\mathrm{Re}\,[z] \propto -T \to \infty, \tag{5.17}$$

while it goes to the constant value 2 in the opposite limit:

$$\mathrm{Re}\,[z] \propto -T \to -\infty. \tag{5.18}$$

This behavior corresponds with the asymptotic values for the coupling: for $T \to -\infty$ it vanishes because it is the beginning of the process, while for $T \to +\infty$ the transition rate becomes stationary because $d\Omega_c/dt \to 0$.

The formula (5.16) suggests a gaussian decay for the asymptotic coupling p^∞ depending on τ. As shown in Fig. 5.2, this approximation holds only for small τ while for larger values of the time scale of the perturbation the decay is smoother. It is interesting within the present analysis to discriminate between an exponential and a gaussian decay. By using numerical

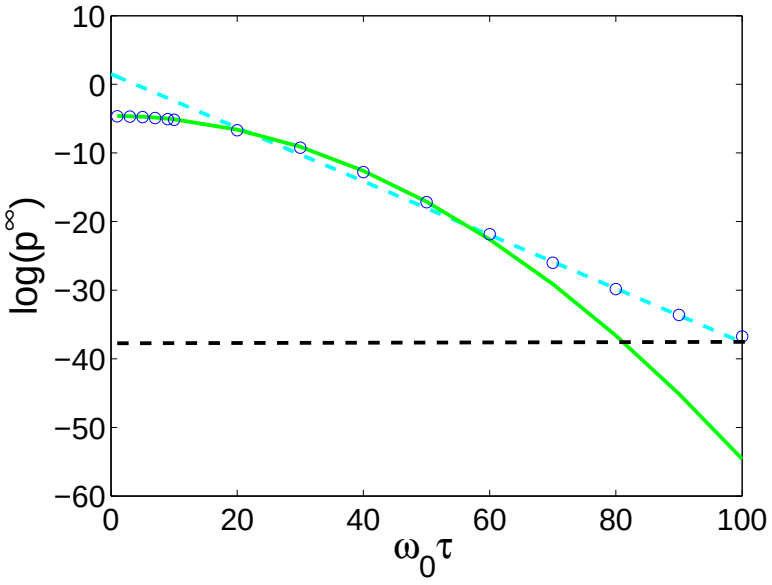

(a)

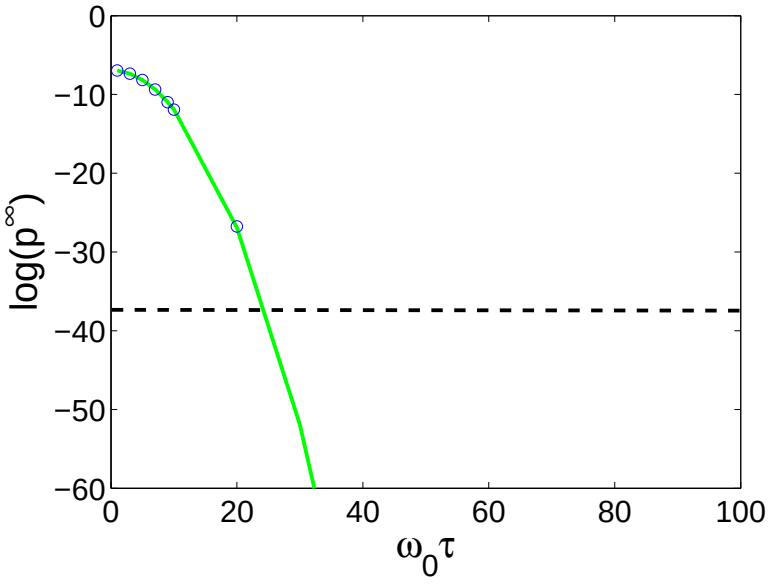

(b)

FIGURE 5.2: Behavior of the asymptotic coupling p^{∞} depending on τ for different values of the oscillator strength f: (a) $f = 0.04$, (b) $f = 0.4$. The control Rabi frequency is fixed as $\Omega_{c,0}/\omega_{eg} = 0.04$ with a variation $\delta\Omega_c/\omega_{eg} = 0.01$. Comparison between the data coming from the MB simulation (blue dots) and the gaussian decay extracted from (5.16) (green curve). $\log p^{\infty}$ is plotted and the dashed line indicates the limiting precision of the simulations. In panel (a) is clearly visible the crossover between a gaussian and an exponential decay; this latter is fitted (cyan dashed line) and the exponent is approximately $\sqrt{f}\omega_{eg}\tau$.

evaluations of the complete coupling integral (5.10) it turns out that a good approximation consists in replacing $\sqrt{\Omega(t)} \to \sqrt{f}\omega_{eg}$ in the exponent of the oscillating term while retaining the whole $\Omega(t)$ in the fractional term.

For $T \to \infty$, the integral corresponds to the Fourier Transform of a product: the Gaussian derivative of the perturbation times the inverse of $\Omega^2(t)$. To further simplify the expression, we expand the denominator of the fractional term and we separate the different orders: up to first order in Ω_c^2/f, the integrand is

$$\begin{aligned} I(t) \;\approx\; & \sqrt{\frac{2}{\pi}}\frac{1}{\tau}\frac{\delta\Omega_c}{\sqrt{f}\,\omega_{eg}}\left(1-\frac{(\Omega_{c,0}-\delta\Omega_c)^2}{f\,\omega_{eg}^2}+\right. \\ & +2\frac{\delta\Omega_c\,(\Omega_{c,0}-\delta\Omega_c)}{2f\,\omega_{eg}^2}\mathrm{Erf}\left(\frac{t}{\tau}\right)+ \\ & \left.-\frac{\delta\Omega_c^2}{f\,\omega_{eg}^2}\mathrm{Erf}^2\left(\frac{t}{\tau}\right)+O\left(\frac{\Omega_c^4}{f^2\,\omega_{eg}^4}\right)\right)e^{-(t/\tau)^2}e^{i\sqrt{f}\,\omega_{eg}t/2}. \quad (5.19) \end{aligned}$$

The first and second terms are constant and give only a negligible correction to the constant coefficient in front of the gaussian decay already present in (5.16).

The other terms are more complicated: the presence of the gaussian function allows to solve the corresponding integrals as scalar products in a gaussian metric. It is then necessary to expand the functions in terms of Hermite Polynomials [97], which are the basis of the gaussian metric.

By using this method, the Fourier transform of the third term in bracket [second line of (5.19)] multiplied for the gaussian function results

$$\begin{aligned} & A\int_{-\infty}^{\infty}\mathrm{Erf}\left(\frac{t}{\tau}\right)\sin\left(\frac{\sqrt{f}}{2}\omega_{eg}t\right)e^{-(t/\tau)^2}dt = \\ & \qquad = A\sqrt{\pi}(-i)\mathrm{Erf}\left(i\frac{\sqrt{f}\,\omega_{eg}\tau}{4\sqrt{2}}\right)e^{-(f\,\omega_{eg}^2\tau^2/16)}. \quad (5.20) \end{aligned}$$

where A contains the coefficients in front of the functions to be integrated. The asymptotic expansion of this expression for large values of τ is given by

$$A\;2\sqrt{2}\frac{2}{\sqrt{f}\tau}e^{-(f\,\omega_{eg}^2\tau^2/32)}\left(1+\frac{16}{f\,\omega_{eg}^2\tau^2}+\frac{768}{f^2\,\omega_{eg}^4\tau^4}+.....\right) \quad (5.21)$$

The results (5.16) and (5.21) show that at the lowest orders the decay of the coupling with τ has a gaussian shape, but with an exponent which changes from term to term. In Fig. 5.3 it is shown also the contribution coming from the Erf^2 term in (5.19). In Fig. 5.2(a), a fit is depicted which

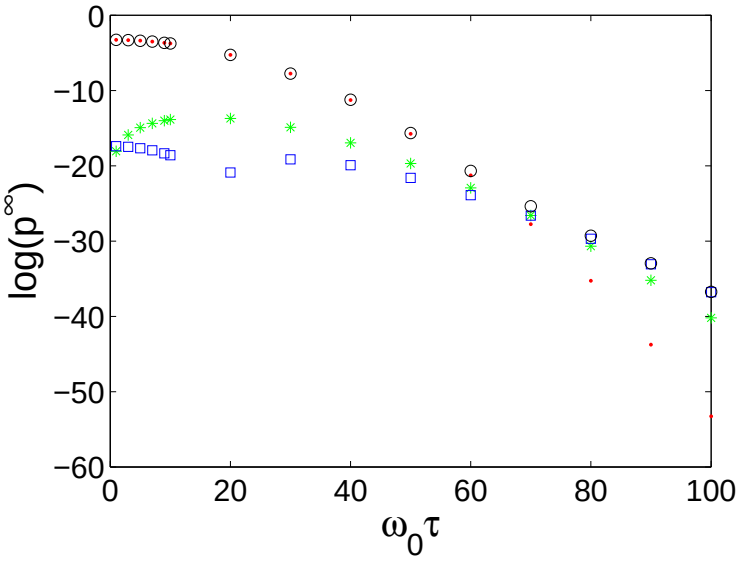

FIGURE 5.3: Effect of the different terms in the first-order approximation of the integrand (5.19) for the asymptotic coupling p^{∞}: complete integrand (black circles), terms with simple gaussian decay (red dots), Erf term (green stars), Erf^2 term (blue squares). Values as in Fig. 5.2(a).

suggests the fact that an exponential decay may be the result of the sum of this several gaussian terms: it is interesting to note the crossover between the two regimes. In the case shown in Fig. 5.2(b) the region of exponential decay is not reached within the accuracy of the simulations while the gaussian regime is clearly visible.

Coupling peak

By looking at (5.16), we observe that the modulus of $\mathrm{Erfc}(z)$ has a peak in the region $\mathrm{Re}\,[z] \approx 0$. The exact position of the peak depends on the value of τ: for $\tau \to 0^+$ and $\tau \to +\infty$, it moves towards $T = 0$. Thus, for large values of τ, it can be approximated by

$$p(0) = \left(\sqrt{\frac{2}{\pi}}\frac{\delta\Omega_c}{\sqrt{f}\omega_{eg}}\right)^2 \left| e^{-(f\,\omega_{eg}^2\tau^2/16)} \left(\frac{\sqrt{\pi}}{2} - \int_0^{i\frac{\sqrt{f}\,\omega_{eg}\tau}{4}} dz\; e^{-z^2}\right)\right|^2 =$$

$$\overset{\tau\to\infty}{\approx} \left(\sqrt{\frac{2}{\pi}}\frac{\delta\Omega_c}{\sqrt{f}\,\omega_{eg}}\right)^2 \left(\frac{\pi}{4}\; e^{-(f\,\omega_{eg}^2\tau^2/16)} + \frac{4}{f\,\omega_{eg}^2\tau^2}\right) \approx p^{max}. \quad (5.22)$$

where the second term comes from the asymptotic expansion of the Dawson's integral [97] and it gives the leading order in the decay. In Fig. 5.4

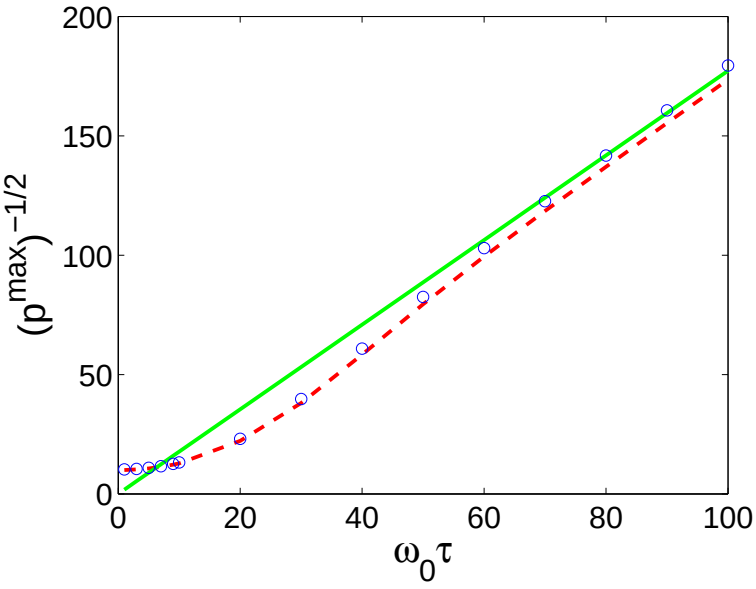

(a)

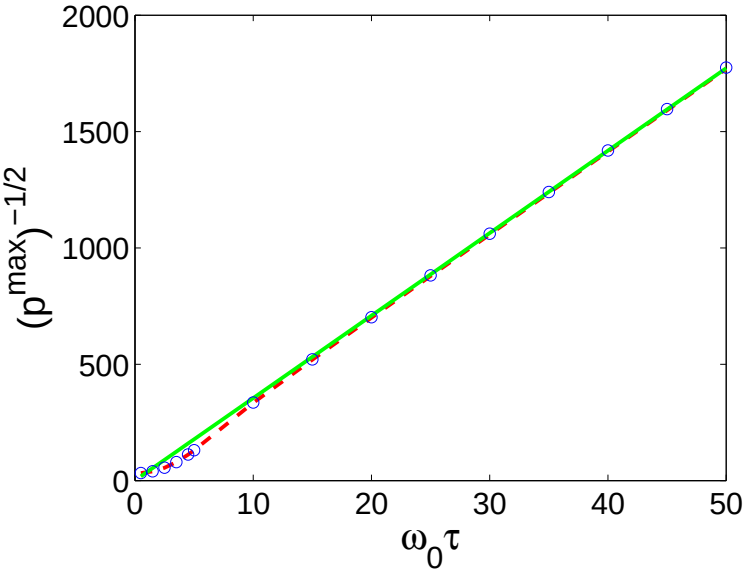

(b)

FIGURE 5.4: Behavior of the coupling peak p^{max} depending on τ for different values of f. Comparison between the data coming from the MB simulation (blue dots), the numerical evaluation of the maximum of the expression (5.16) (red dashed line) and the analytical expansion for large τ (5.22) (green solid line). The relation is linearized by plotting $1/\sqrt{p^{max}}$. Same values as in Fig. 5.2.

there is the comparison between this analytic evaluation and the data coming from the simulation which shows a good agreement.

5.1.3 Non-analytic Perturbation: Sin^2 shape

After the investigation of an analytic form for the perturbation, we analyse the case of a ramp which has a discontinuity in the second derivative:

$$\Omega_c(t) = \begin{cases} \Omega_{c,0} & t < 0 \\ \Omega_{c,0} + \delta\Omega_c \sin^2\left(t\frac{\pi}{8\tau}\right) & 0 < t < 4\tau \\ \Omega_{c,0} + \delta\Omega_c & t > 4\tau \end{cases} \tag{5.23a}$$

$$\frac{d\Omega_c(t)}{dt} = \begin{cases} 0 & t < 0 \\ \frac{\pi}{8\tau}\delta\Omega_c \sin\left(t\frac{\pi}{4\tau}\right) & 0 < t < 4\tau \\ 0 & t > 4\tau \end{cases} \tag{5.23b}$$

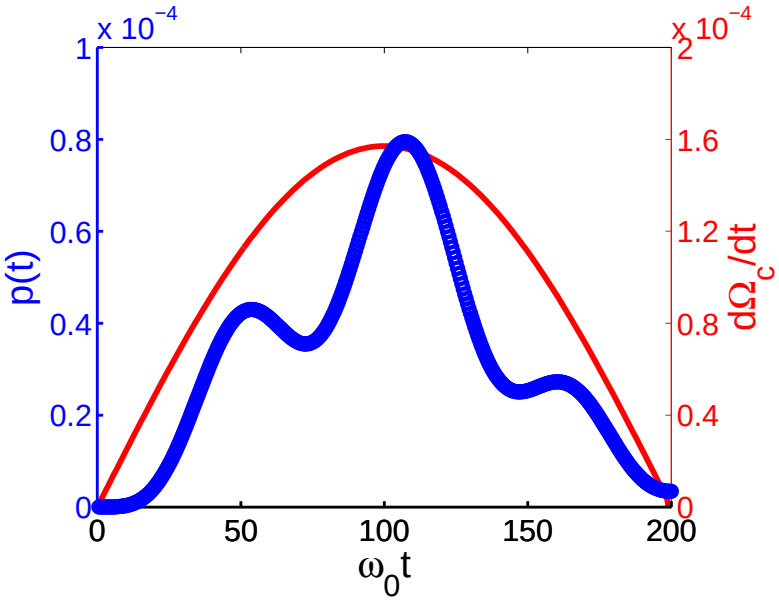

FIGURE 5.5: Example of result from the simulation of MB equations performed by using a plane wave input: derivative of the ramp for $\Omega_c(t)$ (red solid line) and relative evolution of the coupling outside the DP (blue dots) are shown. A sinusoidal ramp of Ω_c is considered.

The adiabaticity condition (5.6) takes the form

$$\left| \frac{\pi}{4\sqrt{2}} \frac{\delta\Omega_c}{\sqrt{f}\,\omega_{eg}} \frac{1}{\sqrt{f}\,\omega_{eg}\tau} \right| \ll 1, \tag{5.24}$$

which differs from (5.13) just for a numerical coefficient. Performing the approximation $\Omega(t) \to \sqrt{f}\omega_{eg}$ as before, the integral (5.10) is analytically

solved

$$p(T) = \left(\frac{\pi}{2\sqrt{2}}\frac{\delta\Omega_c}{\sqrt{f}\,\omega_{eg}\tau}\frac{1}{f\,\omega_{eg}^2 - [\pi/(2\tau)]^2}\right)^2 \cdot$$
$$\cdot\left\{\left(\frac{\pi}{4\tau}\right)^2\left[1+\cos^2\left(\frac{\pi}{4\tau}T\right) - 2\cos\left(\frac{\pi}{4\tau}T\right)\cos\left(\frac{\sqrt{f}}{2}\omega_{eg}T\right)\right] + \right.$$
$$\left. -\frac{\pi}{4\tau}\,\sqrt{f}\,\omega_{eg}\,\sin\left(\frac{\pi}{4\tau}T\right)\,\sin\left(\frac{\sqrt{f}}{2}\omega_{eg}T\right) + \frac{f\,\omega_{eg}^2}{4}\sin^2\left(\frac{\pi}{4\tau}T\right)\right\} \quad (5.25)$$

Asymptotic coupling

By the replacement $T = 4\tau$, the integral (5.25) shows an oscillatory behavior with and algebraic decay:

$$p^{\infty} = \left(\frac{\sqrt{2}}{8}\frac{\delta\Omega_c}{\sqrt{f}\,\omega_{eg}}\frac{(\pi/\tau)^2}{f\,\omega_{eg}^2 - [\pi/(2\tau)]^2}\right)^2 4\,\cos^2\left(\sqrt{f}\,\omega_{eg}\tau\right), \quad (5.26)$$

that is proportional to $1/\tau^4$.

The drastic change in the decay of the asymptotic coupling with respect to the Erf case is directly related with the jump in the second order derivative of $\Omega_c(t)$ at the boundaries of the sinusoidal ramp which is clear from Fig. 5.5. The asymptotic coupling p^{∞} is the square modulus of the Fourier Transform evaluated at $\omega = \sqrt{f}\omega_{eg}/2$ of a function which is in a good approximation the derivative of the perturbation. The function (5.23b) has a jump in its own first derivative. The paradigm of a function which has a jump is the Heavyside step function: its Fourier Transform shows a $1/\omega$ decay. It is also a straightforward property of the Fourier Transform that, given a function g and its derivative g': $\mathcal{F}(g') \propto i\omega\mathcal{F}(g)$. By applying a dimensional argument, it is then clear that

$$p^{\infty} \propto 1/(\sqrt{f}\omega_{eg}\tau)^4. \quad (5.27)$$

In Fig. 5.6, the analytical result (5.26) is compared to the values obtained with the MB simulations. The agreement is very good for both the oscillatory and decay behavior.

Coupling peak

For $\tau \to \infty$, the coupling peak p^{max} is located at $T = 2\tau$ which corresponds with the maximum rate of variation of the perturbation and it decays as

$$p^{max} \approx \left(\frac{\pi\sqrt{2}}{8}\frac{\delta\Omega_c}{\sqrt{f}\,\omega_{eg}}\right)^2\left(\frac{2}{\sqrt{f}\,\omega_{eg}\tau}\right)^2, \quad (5.28)$$

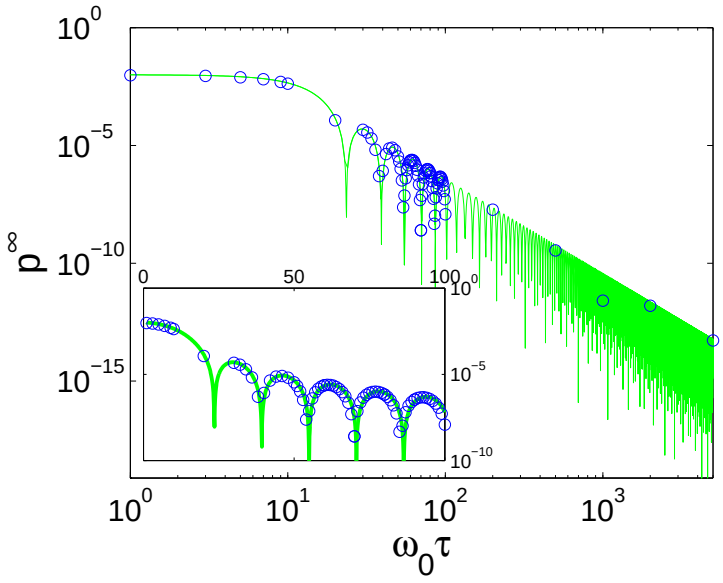

(a)

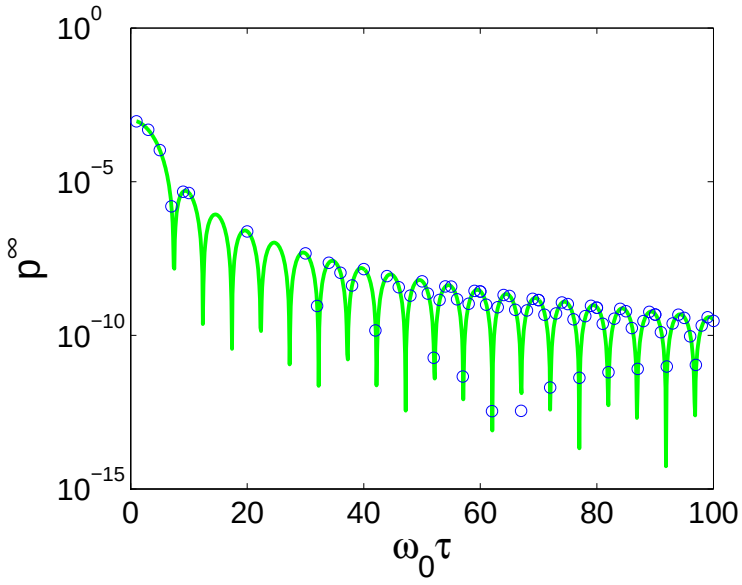

(b)

FIGURE 5.6: Behavior of the asymptotic coupling p^∞ depending on τ for different values of the oscillator strength f: (a) $f = 0.04$, (b) $f = 0.4$. The control Rabi frequency is fixed as $\Omega_{c,0}/\omega_{eg} = 0.04$ with a variation $\delta\Omega_c/\omega_{eg} = 0.01$. Comparison between the data coming from the MB simulation (blue dots) and the analytical expression (5.26) (green line).

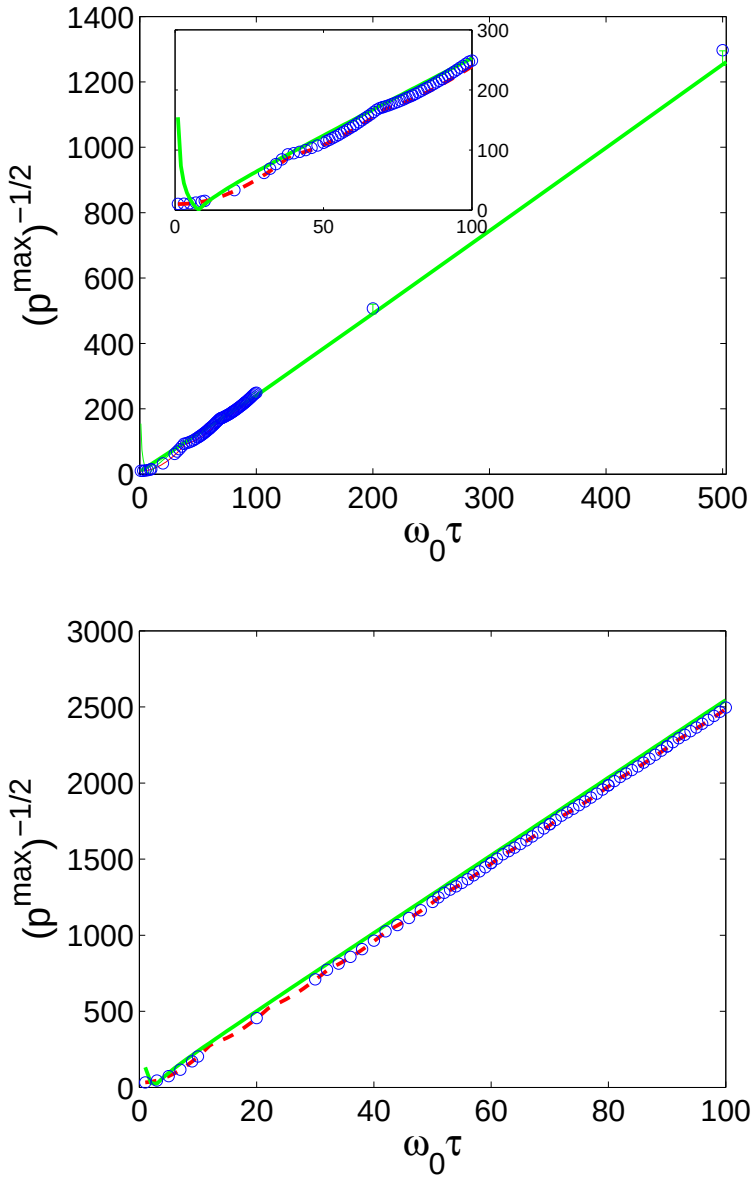

FIGURE 5.7: Behavior of the coupling peak p^{max} depending on τ for different values of f. Comparison between the data coming from the MB simulation (blue circles), the $1/\tau^2$ dependence for large τ (green solid curve) and the numerical evaluation of the peak of (5.25) (red dashed line). Values as in Fig. 5.6. In Panel (a), the error bars for long τ values derive from the oscillatory behavior of the coupling.

which has the same dependence as for the Erf perturbation.

By looking at the condition (5.6) and its applications to the cases under investigation [(5.13) and (5.24)], it is evident the origin of the general behavior found in (5.22) and (5.28): the coupling peak corresponds to the maximum rate of change of the perturbation, i.e. the steepest part of the ramp. The fact that τ is the time scale of the perturbation means exactly that the derivative of $\Omega_c(t)$ has a $1/\tau$ dependence which goes squared into the coupling peak value.

Adiabatic transition theory appears as a very useful tool to investigate the inter-band coupling within MB dynamic formalism. Although this treatment neglect the role of absorption and the multi-level nature of the system [92,93], a very good agreement is shown between analytical results and simulations. In particular the cross-over between a gaussian and an exponential decay of the asymptotic coupling in the analytic perturbation case is found which goes beyond standard results. Furthermore, non-analytical perturbations show an algebraic decay as a result of discontinuities in the temporal derivatives. The understanding of the Fourier Transform mechanism at the basis of the integral (5.4) suggest the possibility to quench the inter-band coupling also at fast modulation rate by using an *ad hoc* tailored perturbation of the control beam.

5.2 Photon Energy Lifter

Obtaining a coherent and widely tunable frequency conversion of an optical signal is a central task in optical telecommunications [98]. Several techniques have been developed during the years to perform this operation, but most of them suffer from significant limitations in their application range, or are disturbed by spurious effects.

The basic idea of the photon energy lifter consists in the adiabatic shift of the polaritonic band on which a photon is injected. If the shift is operated in a spatially homogeneous way then because of wavevector conservation the energy of the propagating excitation is simultaneously lifted: when the polariton leaves the sample, it is reconverted to a photon with a different colors.

This was originally proposed for solid-state photonic structures [37] and experimentally demonstrated by ultrafast tuning of a solid-state microcavity [99], but it is interesting to explore the potential of cold atom systems to this purpose: the very long optical coherence time of ultracold samples [32, 100] and the easy tunability by external electric or magnetic fields makes them very promising for this kind of applications. Recently, similar frequency-matching effects were observed experimentally in hot

atomic vapor [101].

5.2.1 Proposed scheme

As a specific example, we shall consider in what follows a system of Rubidium (^{87}Rb) atoms. The optical properties are varied by means of an external magnetic field (taken as perpendicular to the probe propagation axis) which shifts the atomic levels via the Zeeman effect [102].

We concentrate on the D_2 transition at a frequency $\omega_{eg} = 2\pi\, 384\,\mathrm{THz}$ [103]. As we are interested in substantial shifts, we focus our attention in the high field regime ($B > 5 \times 10^3\,\mathrm{G}$) where the atomic nucleus is decoupled from the electronic degrees of freedom, and the energy shift mostly comes from the electronic total angular momentum only: $\Delta E = \mu_B g_J J_z B_z$, where μ_B is the Bohr magneton, g_J is the Landé factor of the considered level and J_z is the z component of the total angular momentum of the electron. We use the $|J = 1/2, J_z = \mp 1/2\rangle$ sublevels of the $5^2S_{1/2}$ electronic ground state as respectively ground $|g\rangle$ and metastable $|m\rangle$ states, and the $|J = 3/2, J_z = 1/2\rangle$ sublevel of the $5^2P_{3/2}$ electronic excited state as excited $|e\rangle$ state. The corresponding Landé factors are $g_{J=1/2} = 2$ and $g_{J=3/2} = 4/3$. The nucleus is not affected by the optical process and maintains the same polarization it had in the initial state: in the absolute atomic ground state, the nuclear spin is e.g. polarized antiparallel to the electron spin of the $|J = 1/2, J_z = -1/2\rangle$ state.

A linear polarization is used for the dressing light beam that couples the $|m\rangle$ and the $|e\rangle$ states, and a circular (σ_+) one is used to probe the polariton dispersion on the $|g\rangle \to |e\rangle$ transition. Using tabulated values for the electric dipole moment of the D_2 transition and assuming an atomic density $n \approx 10^{14}\,\mathrm{cm}^{-3}$, the radiation-matter coupling (1.19) for the system under consideration is of the order of $\sqrt{f} \approx 10^{-4}$.

To maximize the available time to perform the lifter operation, it is useful to have a very slow group velocity, which in turns requires a small dressing amplitude. In the following, we shall choose $\Omega_c/\omega_{eg} = 10^{-7}$. This value $\Omega_c \approx 2\pi\, 38\,\mathrm{MHz}$ corresponds to 5 times the radiative linewidth of the D line of Rb atoms.

The dressing frequency is chosen in a way to have $\delta_c = 0$ at the initial value B_{in} of the magnetic field: the corresponding polariton dispersion is the one shown in Fig. 5.8(a). The light pulse is injected into the system in proximity of the resonant point $k = k_{eg}$, where the interface reflectivity goes to zero, and injection is most effective [see the circle in Fig. 5.8(c)]: the width of this dip results from (3.7) to be of the order of $2 \times 10^{-8}\omega_{eg}$ and the group velocity (3.2) is $v_{gr}/c \approx 7 \times 10^{-8}$, i.e. $v_{gr} \approx 20\,\mathrm{m/s}$.

The magnetic field variation is performed while the light pulse to be shifted is completely contained in the lattice and it is propagating through an effectively bulk system. As the magnetic field is varied in a spatially homogeneous way, the Bloch wave vector is conserved during the process. If the field variation is slow enough as compared to the frequency difference of neighbouring bands, the polaritons will adiabatically follow the band and their frequency at the end of the process will be accordingly shifted [see the circle in Fig. 5.8(b)].

As an example, we propose to tune the magnetic field from 1 up to 2 T: this results in the metastable and excited states being shifted by respectively $(\delta_m - \delta_g)/\omega_{eg} = 7.3 \times 10^{-5}$ and $(\delta_e - \delta_g)/\omega_{eg} = 6.1 \times 10^{-5}$ with respect to the ground state. For light initially injected in proximity of ω_{eg}, the shift of the photon frequency results approximately equal to δ_m, which amounts to the quite sizeable value 14 GHz/T. As the lifter operation is based on an adiabatic shift of the polariton dispersion, it completely preserves the pulse shape and the coherence properties of the incident wavepacket, both at classical and at quantum level.

5.2.2 Experimental issues

To verify the actual feasibility of such a promising experiment, it is important to mention the main practical difficulties that may arise in a real experiment, and discuss how these can be overcome.

1. We have verified that the transmittivity of the lattice interfaces is close to 1 for both the injection and the extraction process [Fig. 5.8(c) and Fig. 5.8(d)]. The pulse is injected into the lattice at a frequency corresponding to the EIT reflectivity dip around Raman resonance. The extraction takes place in close proximity of the Raman resonance where reflectivity is again very low. This, in spite of the fact we are very close to a gap: thanks to the now significant detuning δ_c, the metastable state is in fact weakly coupled to light, and the corresponding crossing point is displaced slightly away from the light line.

2. In order to have a reasonably long time to vary the magnetic field, we have verified that the group velocity of the polariton states involved in the lifter operation is slow. Light initially propagates on the EIT slow light branch, which is deformed during the lifter operation. At the end, the wavepacket is found on the very flat region below the gap where the group velocity is low [Fig. 5.8(e) and Fig. 5.8(f)].

3. The wavepacket has to be shorter than the sample length, still its frequency spectrum has to fit in the reflectivity dip at both injection

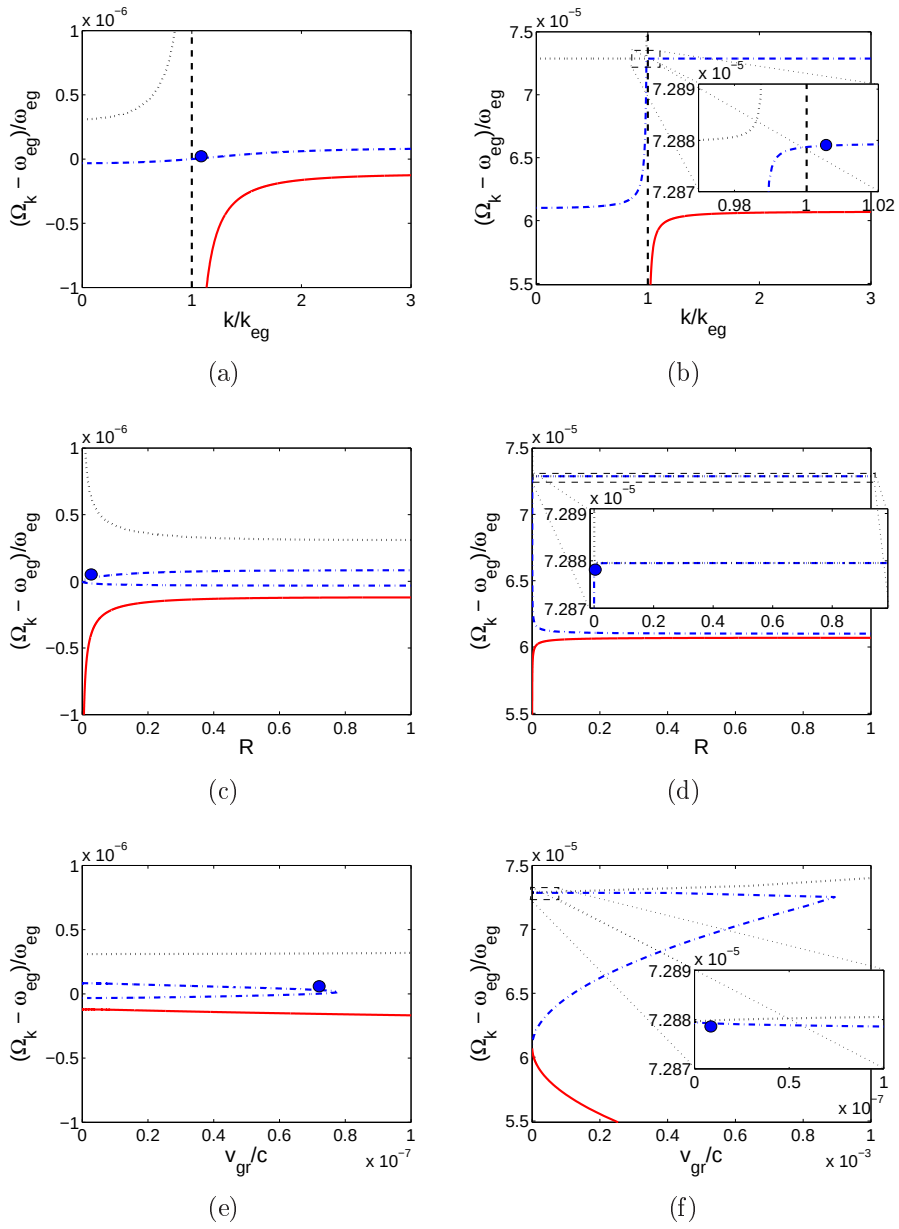

FIGURE 5.8: Polariton properties in a 1D homogeneous gas of three-level atoms. Dispersion (a,d), reflectivity (b,e), group velocity (c,f) in the region around resonance. Red, solid line is LP; blue, dot-dashed line is DP; black, dotted line is UP; black, dashed line is photon dispersion in vacuum. Parameters for a homogeneous cold Rb gas with density $n = 10^{14}\,\mathrm{cm}^{-3}$, oscillator strength $\sqrt{f} \approx 4 \times 10^{-4}$ and dressing amplitude $\Omega_c/\omega_{eg} = 10^{-7}$. Panels (a,b,c): $\omega \approx \tilde{\omega}_m = \omega_{eg}$, $\delta_c = 0$ (initial state of the photon lifter). Panels (d,e,f): $\delta_c/\omega_{eg} = 1.2 \times 10^{-5}$ (final state of the lifter). In the different panels, the blue circles indicate the position of the wavepacket to be "lifted".

and extraction. A sample of length L is able to accommodate pulses with at most $\Delta k \gtrsim 1/(L)$. From Fig. 5.8(a), this corresponds to a lower bound on the frequency width of the incoming wavepacket $\Delta\omega_{in} = \Delta k\, v_{gr}^{in} > 2.5 \times 10^{-10}\, \omega_{eg}$. One can easily see in Fig. 5.8(c) that this frequency spread still fits within the injection window where reflectivity is low. The same can be verified in Fig. 5.8(b) and Fig. 5.8(d) for the extraction process.

4. In order for the pulse shape not to be affected, dispersion of the group velocity should be small for the wavevector window Δk under examination. Initially, this is not a problem, as we are working close to the center of the EIT branch where the group velocity has a weak dispersion. The situation can be more critical on extraction, because of the strong squeezing of the polariton band in the region just below the gap. The importance of this effect can be reduced by choosing pulses initially tuned just above the Raman resonance.

5. The main problem in using a BEC is related to the coherence time fixed by the dephasing mechanism between the ground and the metastable states. In cold gases γ_m is typically of the order of tens of KHz [30,90,104] in particular due to atomic collisions although it is strongly system dependent. For carefully prepared system atomic coherence up to 1 ms were observed [31] and this is promising in view of lifter applications. A good candidate for longer coherence time is the MI phase of ultracold atoms in optical lattice: in the first realization of EIT in a MI of Rb atoms [32] a coherence time of 240 ms has been reported. In this system, the inhomogeneous broadening of the lineshape is suppressed because of the ordered arrangement of atoms and the many-body excitation spectrum is gapped. However the MI is usually much smaller ($10 - 30\,\mu$m) than a BEC cloud and this is a crucial disadvantage for the lifting process. The use of a thermal gas created in a Dark Magneto-Optical Trap (DMOT) [105] seems to show EIT features similar in group velocity and system length to a BEC, still it requires a simpler setup.

5.2.3 Perspectives

One major constraint that still exists on the experimental parameters concerns the speed at which the magnetic field has to be actually varied. As this has to be done while the wavepacket is inside the atomic cloud, a very slow group velocity and a long system are required. Using values for state-of-the-art cold atomic samples (either BEC or DMOT) namely $L = 200\,\mu$m, and $v_{gr} = 20$ m/s, one obtains that one disposes of a time of

approximately 10 μs to perform the magnetic field variation. This means that a variation of $\Delta B = 1\,\mathrm{T}$ requires a very large rate of $1\,kG/\mu\mathrm{s}$.

As this can pose serious difficulties in an actual experiment, it is worth briefly exploring alternative strategies. An interesting possibility is to further reduce the dressing amplitude Ω_c. As the polariton group velocity is proportional to the square of the dressing amplitude, the value $\Omega_c = 10^{-8}\omega_{eg}$ similar to the one used in slow light experiment [30] already leads to a group velocity of the order of 20 cm/s which corresponds to an available time of 1 ms. In the high-field regime considered here, a photon frequency shift of 1 GHz then requires a magnetic field variation of 500 G in 1 ms, a rate routinely used in cold atom experiments.

This calculations indicates that the possibility to design such an experiment with conventional techniques is realistic; in particular, such a demonstration can gain a lot from an increase in the dimensions of actual MI samples.

5.3 Photon Wavepacket Manipulation

The easy tunability of the properties of the dressing field together with the slow propagation of the DP allow for an efficient dynamic modulation of the signal. A dynamic EIT chain can then be the paradigm for a new class of inhomogeneous DPS: in this case both a space and time modulation of the wavepacket can in fact be performed. The basic ingredient of the dynamic EIT chain is the defect geometry.

5.3.1 Dynamic modulation on a vacuum defect

The physics of a defect geometry can be understood in terms of the homogeneous system and interface cases seen in the previous chapter. Two regions of a homogeneous EIT medium are separated by a thin layer of vacuum. The thickness L_d of the defect region is taken to be small as compared to the effective length of the pulse in this layer σ_x.

The case is shown in Fig. 5.9 and Fig. 5.10. The temporal shape of the modulation of Ω_c is shown in the inset: $v_{gr}^{\pm}$ are the maximum and minimum values of the group velocity, determined by the maximum and minimum values $\Omega_c^{\pm}$ of the control field amplitude. τ_s is the interval between the two ramps, i.e. the *storage* time. For a given pulse width $\bar{\sigma}_x$ in the EIT medium, the pulse width in vacuum is $\sigma_x = \bar{\sigma}_x(c/v_{gr}^{\pm})$. As we have assumed $\sigma_x \gg L_d$, the slope of the pulse in the vacuum is very small, so the pulse amplitude can be considered as almost homogeneous. The modulation takes place

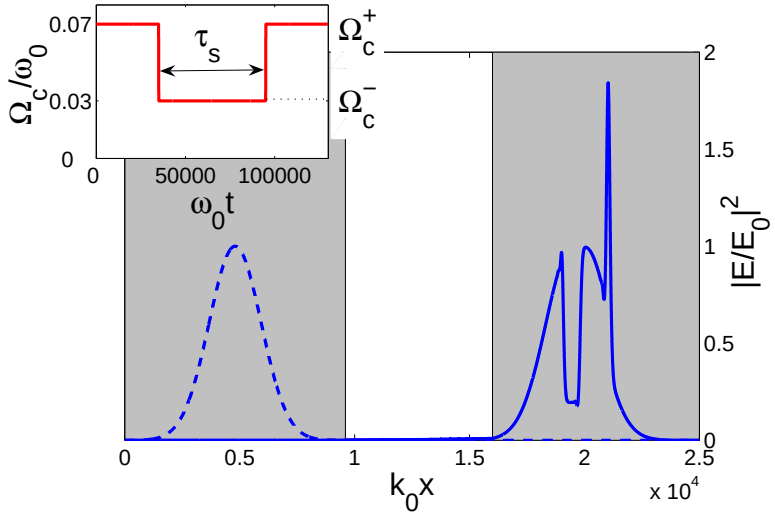

FIGURE 5.9: Modulation of a wavepacket using a vacuum defect. In the EIT medium, the group velocity is decreased from $v_{gr}^+ = 0.11\,c$ to $v_{gr}^- = 0.02\,c$ and then increased back to v_{gr}^+ as shown in the inset. Pulse at the beginning (dashed line) and at the end of the process (solid line). Inset: temporal dependence of Ω_c. Parameters of the system: excited state linewidth $\gamma_e = 10^{-3}\omega_0$, pulse length $k_0\bar{\sigma}_x = 1600$, defect thickness $k_0 L_d = 6400$.

in three stages: the slow down ramp, the storage time and the speed up ramp. When Ω_c is decreased, the pulse intensity in the atomic medium is correspondingly reduced by a factor v_{gr}^-/v_{gr}^+ while the amplitude of the central part remains unchanged as it is sitting in vacuum [Fig. 5.10(a)]. Later on during the storage time, when this part of the pulse enters the EIT medium again, it results spatially compressed to a narrower width $L_d(v_{gr}^-/c)$ [Fig. 5.10(b)]. The part of the pulse that crosses the defect during the storage time does not experience any modulation: in Fig. 5.10(b), this part lies just behind the narrow peak and is $(\tau_s v_{gr}^- - L_d(v_{gr}^-/c))$ long. The final ramp which restores the group velocity to its initial value v_{gr}^+ is responsible for an increase of the electric field amplitude in the EIT medium. Correspondingly to the vacuum layer, a hole is imprinted in the pulse profile [Fig. 5.10(c)]. Once entered back into the EIT medium, its width becomes $L_d(v_{gr}^+/c)$. This modulation in a vacuum defect geometry is then a simple example of the wavepacket reshaping. Note that the resulting dynamics is very different from the homogeneous case where the second ramp would simply compensate the first one.

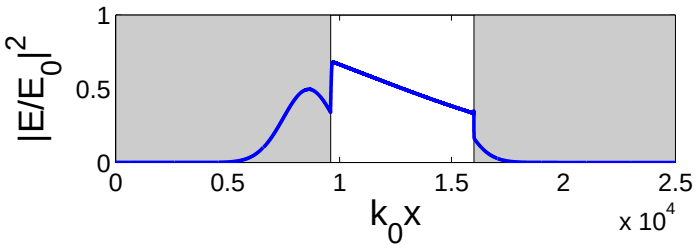

(a)

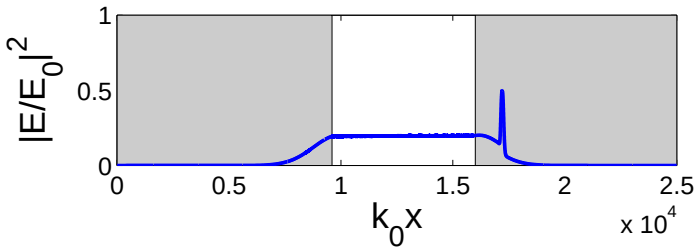

(b)

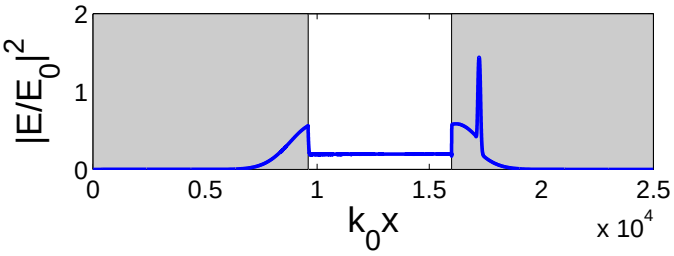

(c)

FIGURE 5.10: Modulation of a wavepacket using a vacuum defect. Three snapshots during the propagation time. (a) Slow down ramp; (b) propagation through the defect during the storage time: formation of the peak; (c) speed up ramp: setting the hole. Parameters in Fig. 5.9.

5.3.2 Comparison between Maxwell-Bloch and the effective equation

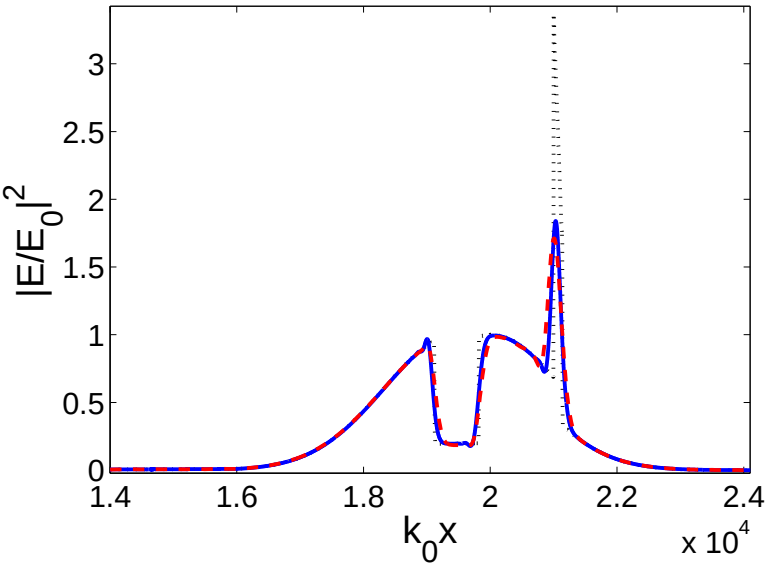

FIGURE 5.11: Comparison between the solutions of the wavepacket propagation using different methods: MB formalism (solid, blue line); continuity equation for the polariton flow (dotted, black line); effective equation with absorption term (dashed, red line). Parameters as in Fig. 5.9.

We compare the MB result with the solution of the effective equation. The continuity equation model (4.35) can be applied to the defect geometry of Fig. 5.9, by defining

$$v_{gr}(x,t) = v(t)\left(\theta(-x) + \theta(x - L_d)\right) + c\theta(x)\theta(L_d - x), \tag{5.29}$$

where the beginning of the defect is located at $x_d = 0$. For times longer than $t = (L_d/c)$, the solution for the electric field intensity is

$$I(x,t) = \begin{cases} I^0\left(x - \mathcal{I}_0^t\right)\dfrac{v(t)}{v(0)} & x < 0 \\ I^0\left(-\mathcal{I}_0^{t-x/c}\right)\dfrac{v(t-x/c)}{v(0)} & 0 < x < L_d \\ I^0\left(-\mathcal{I}_0^{t_0}\right)\dfrac{v(t_0)}{v(0)}\dfrac{v(t)}{v(t_d)} & L_d < x < L_d + \mathcal{I}_{L_d/c}^t \\ I^0\left(L_d - ct_d\right)\dfrac{v(t)}{v(t_d)} & L_d + \mathcal{I}_{L_d/c}^t < x < L_d + \mathcal{I}_0^t \\ I^0\left(x - \mathcal{I}_0^t\right)\dfrac{v(t)}{v(0)} & x > L_d + \mathcal{I}_0^t \end{cases} \tag{5.30}$$

Here $t_d(x)$ and $t_0(x)$ are the instants of time at which the point of the wavepacket which is located at x at the time t has passed through $x = L_d$ and $x = 0$, respectively. They can be found by the conditions:

$$x = L_d + \mathcal{I}_{t_d}^t, \tag{5.31a}$$

$$t_0 = t_d - L_d/c. \tag{5.31b}$$

where we have defined

$$\mathcal{I}_a^b = \int_a^b v(t')dt'. \tag{5.32}$$

This analytic solution gives the black dash-dotted curve in Fig. 5.11. By adding also the absorption term, the effective model captures all the features with a good agreement. In particular, it perfectly reproduces the height of the peak that was instead overestimated by the simple continuity equation (4.35). This is a strong confirmation that the effect of a small absorption on the propagation can be modeled by a diffusive term: it is very important in order to investigate to what extent it is possible to tailor sharp structures on the wavepacket.

5.3.3 Manipulation Schemes in Cold Gases

The EIT chain can be implemented experimentally by using clouds of ultracold atoms as the EIT media. Optical fibers can be used to fix the optical distance between the EIT layers [90]: because of compression entering the atomic regions, the distances in vacuum have to be not negligible with respect to the length of the pulse σ_x; for a $1\,\mu$s-long wavepacket, the spatial width in vacuum is in fact 300 m.

By using data from [30, 31, 103], we estimate realistic value for the parameters describing the system. As a typical example, we consider a cloud of Sodium (Na) atoms of density $n = 8 \cdot 10^{13}\,\mathrm{cm}^{-3}$. For the optical transition, we use the D_2 line. As the ground state, we can use the $|g\rangle = |3S_{1/2}, F = 1, m_F = -1\rangle$ sublevel; for the metastable state, we can use $|m\rangle = |3S_{1/2}, F = 2, m_F = -2\rangle$, and for the excited state we can use $|e\rangle = |3P_{3/2}, F = 2, m_F = -2\rangle$. In this way, the resonance frequency is $\omega_{eg} = 2\pi$ 508THZ, the electric dipole moment is $d_{eg} = 1.5\ 10^{-29}$C m, the linewidth is $\gamma_e = 2\pi\ 10\,\mathrm{MHz}$ and the oscillator strength is $f = 6\ 10^{-9}$. For a control field of Rabi frequency $\Omega_c = 2\pi\ 17\,\mathrm{MHz}$, a group velocity $v_{gr} = 10^{-7}\,c$ is obtained and an absorption coefficient $\mathcal{D} = 6\ 10^{-7}\,\omega_{eg}/k_{eg}^2$. The parameters of the recent experiment [32] are not much different. From now on, physical units are used in the figures.

We have used the effective equation (4.39) to simulate several simple geometries. We concentrate our attention on a pair of different configurations: the single and the double layer structures.

Single Layer

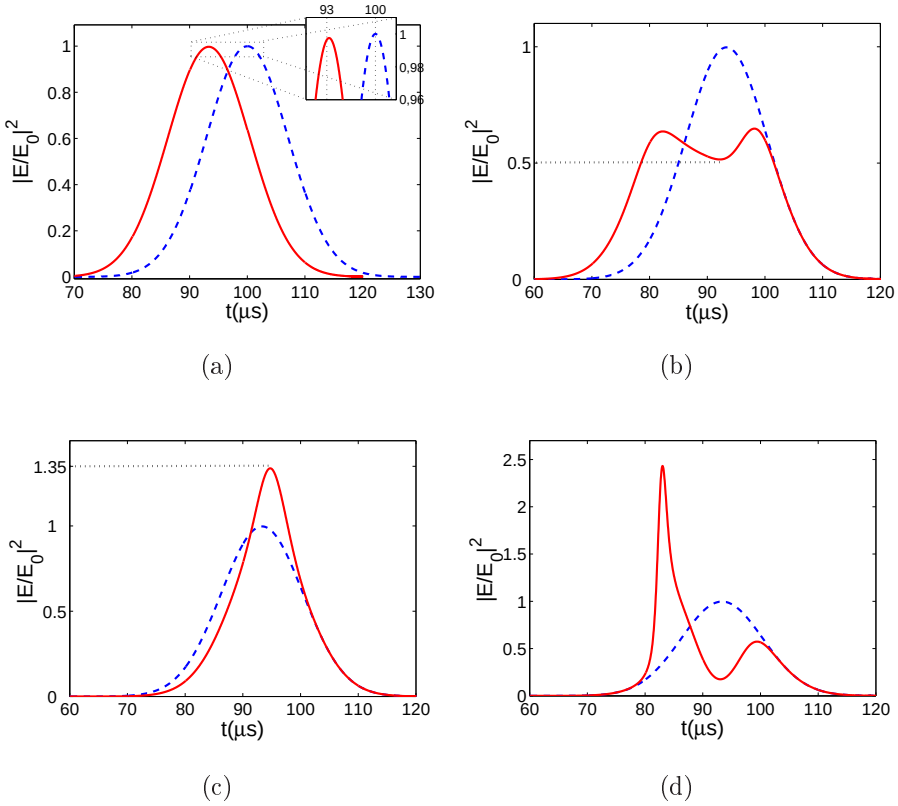

FIGURE 5.12: Propagation of a light pulse across a single EIT layer: $L = 200\,\mu$m, $v_{gr} = 10^{-7}\,c$, $\mathcal{D} = 6\ 10^{-7}(\omega_{eg}/k_{eg}^2)$. Gaussian pulse: $\sigma_t = 10\mu$s, $\ell_{abs} \approx 500\bar{\sigma}_x = 15 \cdot 10^4\,\mu$m. All curves have been obtained using the model of (4.39). Panel (a) Static case: delay between a pulse propagating in vacuum (dashed blue) and one crossing the EIT layer (solid red). Panels (b,c,d) Dynamic cases. (b) Effect of a slow down ramp for the dressing field: $\Delta v = -0.5\ v_{gr}$, $\tau = 3.5\,\mu$s; (c) Effect of a speed up ramp: $\Delta v = +0.5\ v_{gr}$, $\tau = 3.5\,\mu$s; (d) Effect of a double ramp [as e.g. in Fig. 5.9]: $v_{gr}^{+}/v_{gr}^{-} = 10$, $\tau = 3.5\,\mu$s and storage time $\tau_s = 8\,\mu$s. The blue dashed lines in (b,c,d) refer to the static case.

We first consider a single EIT layer which has length $L = 200\,\mu$m. We inject a gaussian pulse with temporal width in vacuum: $\sigma_t = \sigma_x/c = 10\,\mu$s. Thanks to the small size of the sample with respect the pulse absorption is negligible, as it can be seen from the explicit expression of the absorption length (4.30).

The simplest quantity to measure is the time delay accumulated along the propagation for different values of L: if the layer is characterized by a group velocity v_{gr}, then the delay with respect the vacuum ($v_{gr} = c$) case

is

$$T = \frac{L}{v_{gr}} \frac{c - v_{gr}}{c} \xrightarrow{v_{gr}/c \to 0} \frac{L}{v_{gr}}. \tag{5.33}$$

For a sufficiently slow group velocity, very small variations in the atomic layer thickness can be detected from the delay time. Simulated images are shown in Fig. 5.12(a). Of course, this measurement requires a good temporal resolution of the detector as well as some knowledge of the system parameters, in particular of v_{gr}.

The simplest example of dynamical modulation consists of a single-ramp modulation of Ω_c. As discussed above, the effect of the modulation depends on several parameters: a crucial quantity is the ratio $R = L/\bar{\sigma}_x$ between the layer thickness and the pulse length. Here, we focus our attention on the $R < 1$ case; the dressing field is modulated when the peak of the probe is near the center of the layer. Only the small part of the pulse contained in the layer then feels the modulation. As the layer is thin, the crossing time can be faster than the ramp time, which means that different parts of the pulse experience different portions of the ramp. Assuming the ramp time to be longer than the crossing time, the effect of the modulation on each given slice of the pulse can then be estimated as

$$|\mathcal{E}^f|^2(T) = |\mathcal{E}^i|^2 \frac{v_{gr}^i + \Delta v_{gr}(T)}{v_{gr}^i}, \tag{5.34}$$

where T is the time at which the slice exits the layer and the initial values refer to the entrance of the slice in the EIT medium. If we approximate the ramp as linear, the variation in the electric field is then given by $(\Delta v/v_{gr}^i)(T/\tau)$, where Δv is the amplitude of the group velocity ramp. The plots of Fig. 5.12(b) and Fig. 5.12(c) show the resulting pulse in the case of positive and negative values of Δv, respectively: one can see that the modulation is most apparent in the $\Delta v < 0$ case where the crossing time is longer.

The last case we treat is the double ramp, that is illustrated in Fig. 5.12(d): the pulse is slowed down and then accelerated back to the initial group velocity. In the $R < 1$ case under consideration here, the part of the pulse which is modulated during the slow-down ramp exits from the layer before the restoring ramp has begun. This latter ramp is then responsible for the creation of the peak in the trailing part of the pulse. The resulting shape is very similar to the case shown in Fig. 5.9, yet time-reversed.

Double Layer

The EIT monolayer can be used as the building block for more complex geometries. As an example, the case of wavepacket manipulation in a double

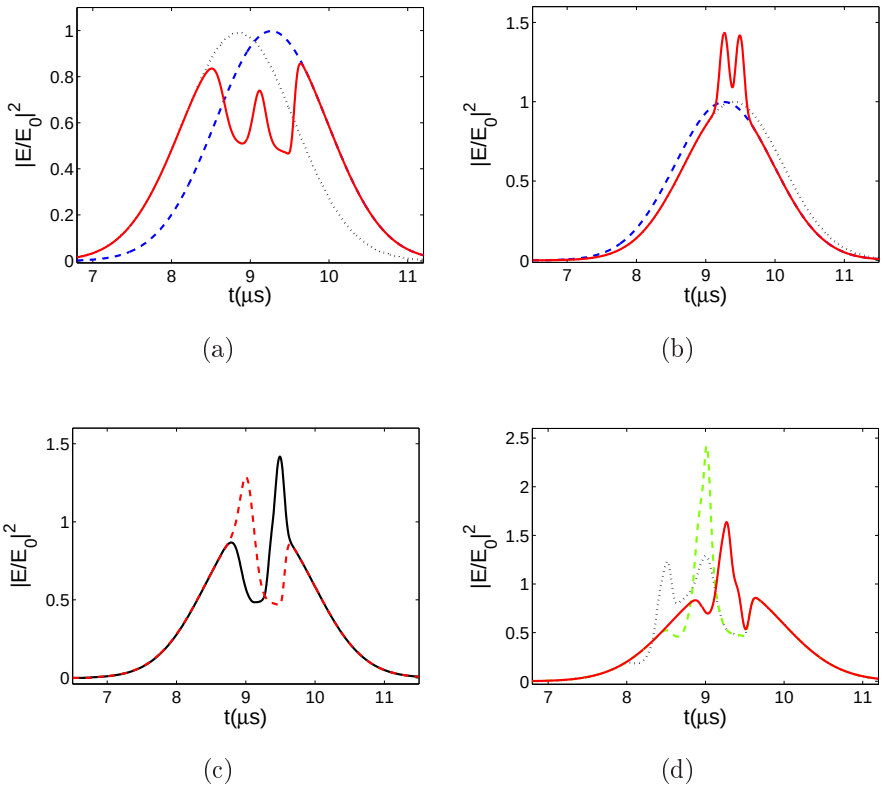

FIGURE 5.13: Propagation of a light pulse across a EIT double-layer structure: $L = 30\,\mu$m (each layer), interlayer distance $\Delta L = 3\ 10^7\,\mu$m, $v_{gr} = 5\ 10^{-7}\,c$, $\mathcal{D} = 3\ 10^{-6}\,\omega_{eg}/k_{eg}^2$. Gaussian pulse: $\sigma_t = 1\,\mu$s, $\ell_{abs} \approx 400\,\bar{\sigma}_x = 6 \cdot 10^4 \mu$m. All curves have been obtained using (4.39). (a) Slow down ramp in both layers: $\Delta v = -0.5\ v_{gr}$, $\tau = 50\,$ns. (b) Speed up ramp in both layers: $\Delta v = +0.5\ v_{gr}$, $\tau = 50\,$ns. In (a,b) blue dashed lines correspond to the propagation without modulation at the initial group velocities while the same for black dotted lines with the final values of group velocity. (c) Single ramps with opposite signs in the different layers: $\Delta v = \pm 0.5\ v_{gr}$, $\tau = 50\,$ns (red dashed and black solid curves are symmetric under a sign exchange between the two layers). (d) Double ramp with opposite signs in the different layers for different storage times $\tau_s = 0.1\,\mu$s (red solid), $0.5\,\mu$s (green dashed), $1\,\mu$s (black dotted).

layer geometry is illustrated in Fig. 5.13. As in the previous discussions, we restrict our attention to the short layer regime: in the specific case considered here, the gaussian pulse has a duration $\sigma_t = 1\,\mu$s, corresponding to a $\bar{\sigma}_x = 150\,\mu$m much longer than the single EIT layer $L = 30\,\mu$m and a $\sigma_x = 300\,$m much longer than the vacuum interlayer distance $\Delta L = 30\,$m.

The use of the same single ramp for the dressing field on both layers allows the creation of several similar structures on the same pulse. These structures are separated by a delay depending on the distance between the layers. This is shown in Fig. 5.13(a) and Fig. 5.13(b). By choosing a fast enough slow-down ramp, the peak that appears between the different layers can be shaped down to the absorption length. This fact is extremely interesting in view of creating strongly localized polariton, whose dynamics has been predicted to show peculiar features [106]. The result of a pair of ramps with opposite signs in the different layers is illustrated in Fig. 5.13(c). By exchanging the signs of the ramps, a specular modulation can be obtained.

The last case we present consists of a double ramp with opposite signs in the two layers. In this case, an interesting enhancement of the central peak is visible as a consequence of the double layer structure. This result is easily understood by noting that the part of the pulse which is modulated in the first layer by the first ramp gets modulated in the same way when crossing the second layer during the second ramp. In this way, it can reach higher values as compared to the single layer case previously considered. This mechanism starts being effective as soon as the storage time is longer than the interlayer delay time, $\tau_s > (\Delta L/c)$. The efficiency is maximum when the storage time exactly equals the time required for the signal to cross the whole double layer structure, $\tau_s = (\Delta L/c) + 2(L/v_{gr})$. For longer storage times τ_s, the enhancement is no longer effective. The resulting pulse are shown in Fig. 5.13(d) for different values of the storage time τ_s. In all the cases, the initial and final part of the pulse are unaffected by the modulation.

5.4 The EIT slab: light storage

The case of a EIT layer in vacuum is presently of great experimental interest for light storage purposes [29, 72–75]. The idea is very simple: by switching off the control field Ω_c while the wavepacket is inside the EIT medium, the DP is fully mapped into a metastable coherence ρ_{mg}. As this has a vanishing group velocity and long lifetime, it can remain stored in the atoms for macroscopically long times. When the control field Ω_c is switched on again, the wavepacket is retrieved.

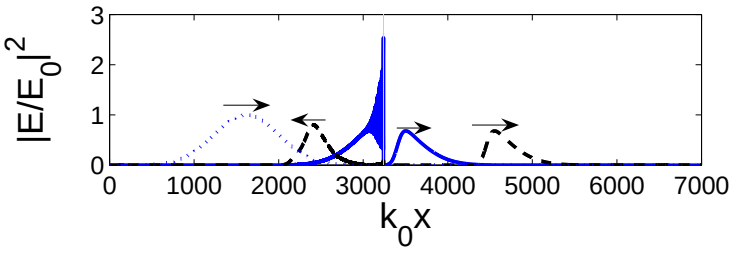

(a)

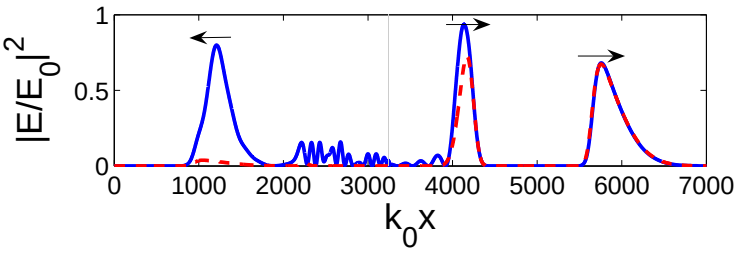

(b)

FIGURE 5.14: Light Storage in an EIT layer. Ω_c is modulated in time from $\Omega_c^+ = 0.07\omega_0$ to $\Omega_c^- = 0$ with the same shape shown in the inset of Fig. 5.9. The storage time is $\omega_0\tau_s = 1350$. The initial group velocity in the EIT layer is $v_{gr} = 0.11\ c$. The pulse has a gaussian shape with $k_0\sigma_x = 540$ in vacuum and the atomic layer has a length $k_0 L_d = 10$. Snapshots during the process in the absence of losses $\gamma_e = \gamma_m = 0$: (a) Initial pulse (blue dotted line), pulse splitted immediately after the stopping ramp (solid blue line) and counterpropagating wavepackets during the storage time (dashed black line). (b) Emerging wavepackets after the retrieval ramp in the absence of absorption (solid blue line) and in the presence of losses, $\gamma_e = 0.07\omega_0$ (dashed red line). The arrows indicate the direction of propagation of each pulse.

The main limitations to the efficiency of a light storage process originate from spontaneous emission processes from the excited state (a finite ρ_{eg} component is always present for any pulse of finite duration), leakages due to the finite optical depth of sample as the usually considered systems are shorter than the effective length of the pulse, and ground-state decoherence $\gamma_m > 0$ [29, 75]. Even though this last effect sets the ultimate limit to the performances of light storage experiments, for the parameters considered in the present work it is negligible as compared to the other processes.

A situation similar to the experimental realization in [32] is simulated in Fig. 5.14: because of numerical limitations in the solution of the MB equations, we have been forced to consider a EIT medium with a much bigger v_{gr}/c. Apart from this, all other parameters were rescaled in a way to get the correct physics of the system. During the storage time, Ω_c is made to vanish with the same temporal profile as shown in the inset in Fig. 5.9.

As in the previous case, the process consists of three stages. During the stopping ramp [Fig. 5.14(a)], the signal is cut in three parts: the front part, which has already crossed the defect, is not affected by the modulation. The central slice that is contained in the EIT layer is stored as an atomic polarization and its electric field vanishes. When the back part of the pulse hits the medium, this is no longer transparent and the pulse is reflected: as the width of the reflectivity dip is proportional to the group velocity v_{gr}, reflectivity is in fact substantial in the light storage configuration $v_{gr} = 0$ [19, 29, 66].

When the retrieval ramp is applied, the excitations stored in the EIT layer recover their electric field components and propagate out of the atomic medium. The retrieval efficiency (defined as the ratio of this pulse to the initial pulse) is 15% for this simulation, which qualitatively agrees with the estimation in [32]. The three emerging wavepackets are clearly visible in [Fig. 5.14(b)]. For this system the main problems are the leackages due to small thickness of the atomic sample which is much smaller than the waists of the laser beams.

To conclude this section, it is important to assess the role of dissipative effects in the light storage process. The pulse profiles in the presence of spontaneous emission from the excited state are shown as red dashed curves in Fig. 5.14(b). The first part of the pulse is not affected by absorption because the length of the sample is small as compared with the absorption length. The retrieved pulse is only partially reduced by spontaneous emission processes. The reflected pulse is instead completely modified: when Ω_c is turned down, localized excitations are created near the interface. When $\Omega_c = 0$, the metastable state is in fact decoupled from light; matter excitations in the flat part of LP and UP bands are very sensitive to losses.

For these reason, the reflected wavepacket quickly disappears as soon as losses are included.

Also in the absence of absorption, the reflection process can strongly depend on the structure of interfaces and provide reflected pulses with dramatically different shapes. This features can be of great interest when one considers a Mott Insulator of 2-level atoms where absorption can be suppressed as a consequence of the ordered lattice structure [15]. In this case, information on the interface structure can be inferred from the reflection properties.

chapter 6

Conclusion and perspectives

In the present thesis, we have investigated the linear optical response of ultracold atomic gases in different configurations. Light-atom strong coupling, slow light behavior and dynamic structures are the main keywords of this work.

In Part I, we have addressed the use of light as a probe for the structure of an atomic Mott Insulator (MI). We have considered stationary situations where the calculations have been carried out by using Transfer Matrix technique in a 1D geometry. The system is of great interest because the strong localization of atoms at the lattice site positions induces a suppression of absorption processes: this is promising in view of the observation of strong light-atoms coupling. In particular, we have found visible signatures of the interplay between the light-matter mixing and the diffraction due to the periodic arrangement of atoms in both the band diagram and the reflectivity spectra.

The high reflectivity shown by the two-level atomic system prevents the propagation of resonant light inside such a sample. The coherent dressing of three-level atoms which results into Electromagnetically Induced Transparency (EIT) create a frequency window for light propagation in the form of the so called Dark Polariton (DP). We have studied the scattering of slow DP on defects as a non-destructive probe of the microscopic structure of the atomic MI. These features are robust with respect to absoprtion within the EIT window.

Further results in this direction are expected from a full 3D treatment by means of Scattering Matrix. In this case technical problems related to the description of the optical response of atoms have to be addressed [15, 18].

The solution of the complete scattering problem from a defect in a MI represents a big issue from both a theoretical and experimental point of view [69, 70]. The development of the Scattering Matrix code for atomic systems is also of interest for the study of light scattering from several randomly placed atoms which is at the basis of current investigations of Coherent Backscattering from atomic samples [107].
Another possible development is related to the toy-model of an atomic two-level impurity in a three-level system as the starting point for a complete investigation of non-linear interactions at the single photon level.

In Part II, we have studied the propagation in time of a DP pulse injected into a generic inhomogeneous and dynamic structure composed of vacuum regions and EIT layers. We have built up a complete 1D Maxwell-Bloch (MB) formalism, adapted to the presence of sharp interfaces through the application of a modified Slowly Varying Envelope Approximation (mSVEA). By using this formalism we have simulated both static and dynamic situations both in homogeneous geometries and at interfaces. Light storage configurations have been computed as well.

We have shown a good agreement between the results of MB formalism and the prediction of Adiabatic Transition theory for the inter-band coupling due to a dynamic modulation of the control field intensity. We have found a sharp deviation from the expected exponential decay of the asymptotic coupling for fast ramps. A more detailed study may be in order to find specific form of the perturbation which suppress the coupling for fast modulations and to extend to our case the study of absorption [92].

Withtin the MB formalism, we have simulated realistic configuration where the inhomogeneity of the structure joined with the dynamic modulation allow to tailor the shape of the propagating pulse. The patterns that are imprinted in the electric field envelope are not destroyed by absoprtion. These are examples of quantum processing of DP. The possibility to create higly localized structures appears interesting in view of the observation of peculiar regimes for the polariton propagation [106].

Furthermore, an extension of the MB formalism to 2D geometries is promising to study the trapping and guiding of DP within structures with non-absorbing interfaces where to realize quantum billiards and polaritonic circuits.

Notation

The acronyms used through this thesis are summurized here.

- e.m. : electro-magnetic;
- OBE: Optical Bloch Equations;
- EIT: Electromagnetically Induced Transparency;
- MI: Mott Insulator;
- TM: Transfer Matrix;
- fBz: first Brillouin zone;
- MB : Maxwell-Bloch;
- SVEA: Slowly Varying Envelope Approximation;
- mSVEA: modified Slowly Varying Envelope Approximation;
- FDTD: Finite Difference Time Domain;
- DP : Dark Polariton;
- LP : Lower Polariton;
- UP : Upper Polariton;

Furthermore they are repeated the first time they appear in each chapter.

The physical constants that are used in this work are [103]

- Speed of Light: $c = 3 \cdot 10^8 \mathrm{m/s}$;
- Permeability of Vacuum: $\mu_0 = 4\pi \cdot 10^{-7} \mathrm{N/A^2}$;

- Dielectric constant of Vacuum: $\epsilon_0 = 8.854 \cdot 10^{-12}$ F/m;
- Reduced Planck's constant: $\hbar = 1.055 \cdot 10^{-34}$J s;

Bibliography

[1] N. Delone and V. Krainov. *Fundamentals of Nonlinear Optics of Atomic Gases.* Wiley, New York, 1988.

[2] C. Adams and E. Riis. Laser cooling and trapping of neutral atoms. *Prog. Quant. Electr. 21*, 1 (1997), 1.

[3] L. Pitaevskii and S. Stringari. *Bose-Einstein Condensation.* Oxford University Press, Oxford, 2003.

[4] F. Minardi *et al.* Frequency shift in saturation spectroscopy induced by mechanical effects of light. *Phys. Rev. A 60* (1999), 4164.

[5] I. Bloch. Ultracold quantum gases in optical lattices. *Nat. Phys. 1* (2005), 23.

[6] O. Morsch and M. Oberthaler. Dynamics of Bose-Einstein condensates in optical lattices. *Rev. Mod. Phys. 78* (2006), 179.

[7] G. Birkl, M. Gatzke, I. Deutsch, S. Rolston, and W. Phillips. Bragg scattering from atoms in optical lattices. *Phys.Rev. Lett. 75* (1995), 2823.

[8] F. Brennecke, S. Ritter, T. Donner, and T. Esslinger. Cavity optomechanics with a Bose-Einstein condensate. *Science 322* (2008), 235.

[9] E. Yablonovitch. Photonic band-gap crystals. *J. Phys: Condensed Matter 5* (1993), 2443.

[10] D. Smith, J. Pendry, and M. Wiltshire. Metamaterials and negative refractive index. *Science 305* (2004), 788.

[11] B. Svistunov and G. Shlyapnikov. Resonance optics of the low-temperature h-down and d-down quantum gases. *Sov. Phys. JETP 70* (1990), 460.

[12] H. Politzer. Light incident on a Bose-condensed gas. *Phys. Rev. A 43*, 11 (1991), 6444.

[13] O. Morice, Y. Castin, and J. Dalibard. Refractive index of a dilute Bose gas. *Phys. Rev. A 51*, 5 (1995), 3896.

[14] M. Greiner, O. Mandel, T. Esslinger, T. Hänsch, and I. Bloch. Quantum phase transition from a superfluid to a mott insulator in a gas of ultracold atoms. *Nature (London) 415* (2002), 39.

[15] M. Antezza and Y. Castin. Spectrum of light in a quantum fluctuating periodic structures. *Phys. Rev. Lett. 103* (2009), 123903.

[16] D. Coevorden, R. Sprik, A. Tip, and A. Lagendijk. Photonic band structure of atomic lattices. *Phys. Rev. Lett. 77*, 12 (1996), 2412.

[17] J. Klugkist, M. Mostovoy, and J. Knoester. Mode softening, ferroelectric transition and tunable photonic band structures in a point-dipole crystals. *Phys. Rev. Lett. 96*, 12 (2006), 1163903.

[18] M. Antezza and Y. Castin. Fano-hopfield model and photonic band gaps for an arbitrary atomic lattice. *Phys. Rev. A 80* (2009), 013816.

[19] F. Bariani and I. Carusotto. Light propagation in atomic Mott insulators. *J. Europ. Opt. Soc. Rap. Public. 3* (2008), 08005.

[20] G. Alzetta, A. Gozzini, L. Moi, and G. Orriols. An experimental method for the observation of r.f. transitions and laser beat resonances in oriented Na vapour. *Nuovo Cimento B 36* (1976), 5.

[21] E. Arimondo. Coherent population trapping in laser spectroscopy. In *Progress in Optics XXXV*. Elsevier, 1996, p. 257.

[22] S. Harris. Electromagnatically induced transparency. *Phys. Today 50* (1997), 36.

[23] M. Lukin. Trapping and manipulating photon states in atomic ensembles. *Rev. Mod. Phys. 75* (2003), 457.

[24] M. Fleischhauer, A. Imamoglu, and J. Marangos. Electromagnetically induced transparency: optics in coherent media. *Rev. Mod. Phys. 77* (2005), 633.

[25] I. Mazets and B. Matisov. Adiabatic raman polariton in a Bose condensate. *JETP Lett. 64*, 7 (1996), 515.

[26] M. Fleischhauer and M. Lukin. Dark-state polaritons in electromagnetically induced transparency. *Phys. Rev. Lett. 84* (2000), 5094.

[27] G. Juzeliunas and H. Carmicheal. Systematic formulation of slow polaritons in atomic gases. *Phys. Rev. A 65* (2002), 021601(R).

[28] A. Matsko *et al.* Slow, ultraslow, stored and frozen light. *Adv. At. Mol. Opt. Phys. 46* (2001), 191.

[29] M. Fleischhauer and M. Lukin. Quantum memory for photons: Dark-state polaritons. *Phys. Rev. A 65* (2002), 022314.

[30] L. Hau, S. Harris, Z. Dutton, and C. Behroozi. Light speed reduction to 17 meters per second in an ultracold atomic gas. *Nature 397* (1999), 594.

[31] C. Liu, Z. Dutton, C. Behroozi, and L. Hau. Observation of coherent optical information storage in an atomic medium using halted light pulses. *Nature 409* (2001), 490.

[32] U. Schnorrberger *et al.* Electromagnetically induced transparency and light storage in an atomic mott insulator. *Phys. Rev. Lett. 103* (2009), 033003.

[33] M. Yanik and S. Fan. Dynamic photonic structures: stopping, storage, and time reversal of light. *Stud. Appl. Math. 115* (2005), 233.

[34] M. Scully and M. Zubairy. *Quantum optics.* Cambridge University Press, Cambridge, 1997.

[35] C. Cohen-Tannoudji, J. Dupont-Roc, and G. Grynberg. *Atom-Photon Interactions. Basic Processes and Applications.* Wiley Science Paperback Series, New York, 1998.

[36] A. Yariv and P. Yeh. *Optical waves in crystals.* Wiley Interscience, New York, 1984.

[37] Z. Gaburro *et al.* Photon energy lifter. *Opt. Express 14* (2006), 7270.

[38] R. Hilborn. Einstein coefficients, cross sections, f values, dipole moments, and all that. e-print arXiv:physics/0202029.

[39] J. Jackson. *Classical Electrodynamics.* J. Wiley (2nd Edition), New York, 1975.

[40] J. Hopfield. Theory of contribution of excitons to the complex dielectric constant of crystals. *Phys. Rev. 112*, 5 (1958), 1555.

[41] C. Cohen-Tannoudji and J. Dupont-Roc. Experimental study of Zeeman light shifts in weak magnetic fields. *Phys. Rev. A 5*, 2 (1972), 968.

[42] J. Pendry. Photonic band structures. *J. Mod. Optic. 41*, 2 (1994), 209.

[43] B. Batterman and H. Cole. Dynamical diffraction of X-rays by perfect crystals. *Rev. Mod. Phys. 36* (1964), 681.

[44] N. Ashcroft and N. Mermin. *Solid state physics.* Brooks/Cole, 1976.

[45] P. Russell. Interference of integrated Floquet-Bloch waves. *Phys. Rev. A 33*, 5 (1986), 3232.

[46] P. S. Russell, T. Birks, and F. Dominic Lloyd-Lucas. Photonic Bloch waves and photonic band gap. In *Confined electrons and photons.* Plenum Press, 1995, p. 585.

[47] M. Weidemuller, A. Hemmerich, A. Gorlitz, T. Esslinger, and T. Hansch. Bragg diffraction in an atomic lattice bound by light. *Phys. Rev. Lett. 75*, 25 (1995), 4583.

[48] I. Deutsch, R. Spreeuw, S. Rolston, and W. Phillips. Photonic band gaps in optical lattices. *Phys. Rev. A 52*, 2 (1995), 1394.

[49] M. Lewenstein *et al.* Ultracold atomic gases in optical lattices: mimicking condensed matter physics and beyond. *Adv. Phys. 56*, 2 (2007), 243.

[50] M. Fisher, P. Weichman, G. Grinstein, and D. Fisher. Boson localization and the superfluid-insulator transition. *Phys. Rev. B 40* (1989), 546.

[51] D. Jaksch, C. Bruder, J. Cirac, C. Gardiner, and P. Zoller. Cold bosonic atoms in optical lattices. *Phys. Rev. Lett. 81* (1998), 3108.

[52] T. Akatsuka, M. Takamoto, and H. Katori. Optical lattice clocks with non-interacting bosons and fermions. *Nat. Phys. 4* (2008), 954.

[53] Y. Boucher. Transfer matrix of a Dirac-like singularity of the dielectric permittivity. *IEEE J. Quantum Elect. 33*, 2 (1997).

[54] Y. Chong, D. Pritchard, and M. Soljačić. Quantum theory of a resonant photonic crystal. *Phys. Rev. B 75* (2007), 235124.

[55] K. Kempa, R. Ruppin, and J. Pendry. Electromagnetic response of a point-dipole crystal. *Phys. Rev. B 72*, 20 (2005), 205103.

[56] T. Ikawa and K. Cho. Fate of the superradiant mode in a resonant Bragg reflector. *Phys. Rev. B 66* (2002), 085338.

[57] M. Artoni, G. La Rocca, and F. Bassani. Resonantly absorbing one-dimensional photonic crystals. *Phys. Rev. E 72*, 4 (2005), 046604.

[58] M. Artoni and G. La Rocca. Optically tunable photonic stop bands in homogeneous absorbing media. *Phys. Rev. Lett. 96* (2006), 073905.

[59] D. Petrosyan. Tunable photonic band gaps with coherently drive atoms in optical lattices. *Phys. Rev. A 76* (2007), 053823.

[60] M. Erementchouk, L. Deych, and A. Lisyansky. Optical properties of one-dimensional photonic crystals based on multiple-quantum-well structures. *Phys. Rev. B 71* (2005), 235335.

[61] M. Erementchouk, L. Deych, and A. Lisyansky. Spectral properties of exciton polaritons in one-dimensional resonant photonic crystals. *Phys. Rev. B 73* (2006), 115321.

[62] A. Moroz. Three-dimensional complete photonic-band-gap structures in the visible. *Phys. Rev. Lett. 83*, 25 (1999), 5274.

[63] I. Amato. Designing crystals that say no to photons. *Science 255* (1992), 1512.

[64] P. Vries, D. Coevorden, and A. Lagendijk. Point scatterers for classical waves. *Rev Mod. Phys. 70*, 2 (1998), 447.

[65] J. Wait. *Electromagnetic waves in stratified media.* Pergamon, Oxford, 1970.

[66] V. Kozlov, S. Wallentowitz, and S. Raghavan. Ultrahigh reflection from a medium with ultraslow group velocity. *Phys. Lett. A 296* (2002), 210.

[67] S. Rist, P. Vignolo, and G. Morigi. Photonic spectrum of bichromatic optical lattices. *Phys. Rev. A 79* (2009), 053822.

[68] S. Harris, J. Field, and A. Kasapi. Dispersive properties of electromagnetically induced transparency. *Phys. Rev. A 46* (1992), R29.

[69] H. Zoubi and H. Ritsch. Exciton-polariton scattering as signature of defects in cold atom optical lattices. *New J. Phys. 10* (2008), 23001.

[70] I. Mekhov, C. Maschler, and H. Ritsch. Light scattering from ultracold atoms in optical lattices as an optical probe of quantum statistics. *Phys. Rev. A 76* (2007), 053618.

[71] A. Imamoglu, H. Schmidt, G. Woods, and M. Deutsch. Strongly interacting photons in a nonlinear cavity. *Phys. Rev. Lett. 79*, 8 (1997), 1467.

[72] A. Gorshkov, A. André, M. Lukin, and A. Sørensen. Photon storage in Λ-type optically dense atomic media. i. Cavity model. *Phys. Rev. A 76* (2007), 033804.

[73] A. Gorshkov, A. André, M. Lukin, and A. Sørensen. Photon storage in Λ-type optically dense atomic media. ii. Free-space model. *Phys. Rev. A 76* (2007), 033805.

[74] A. Gorshkov, A. André, M. Lukin, and A. Sørensen. Photon storage in Λ-type optically dense atomic media. iii. Effects of inhomogeneous broadening. *Phys. Rev. A 76* (2007), 033806.

[75] N. Phillips, A. Gorshkov, and I. Novikova. Optimal light storage in atomic vapor. *Phys. Rev. A 78* (2008), 023801.

[76] M. Kiffner and T. Dey. Dynamic control of pulse propagation in electromagnatically induced transparency. *Phys. Rev. A 79* (2009), 023829.

[77] R. Shakhmuratov, A. Kalachev, and J. Odeurs. Instantaneous processing of slow light: amplitude-duration control, storage, and splitting. *Phys. Rev. A 76* (2007), 031802(R).

[78] R. Shakhmuratov and J. Odeurs. Increase of the fractional delay of the pulse in an electromagnetically-induced-transparency medium. *Phys. Rev. A 78* (2008), 063810.

[79] A. Patnaik, F. Le Kien, and K. Hakuta. Manipulating the retrieval of stored light pulses. *Phys. Rev. A 69* (2004), 035803.

[80] I. Carusotto, M. Antezza, F. Bariani, S. De Liberato, and C. Ciuti. Optical properties of atomic Mott insulators: From slow light to dynamical Casimir effects. *Phys. Rev. A 77* (2008), 063621.

[81] A. André and M. Lukin. Manipulating light pulses via dynamically controlled photonic band gap. *Phys. Rev. Lett. 89* (2002), 143602.

[82] M. Bajcsy, A. Zibrov, and M. Lukin. Stationary pulses of light in an atomic medium. *Nature (London) 426* (2003), 638.

[83] B. Ham and J. Hahn. Ultralong trapping of light using double spin coherence gratings. e-print arXiv:0901.1082.

[84] B. Ham and J. Hahn. Quantum manipulation of two-color stationary light: Quantum wavelength conversion. *Phys. Rev. A 76* (2007), 043832.

[85] R. Buffa, S. Cavalieri, and M. Tognetti. Coherent control of temporal pulse shaping by electromagnetically induced transparency. *Phys. Rev. A 69* (2004), 033815.

[86] R. Buffa, S. Cavalieri, E. Sali, and M. Tognetti. Laser-pulse compression by coherent control in a Doppler-broadened medium: analytical and numerical studies. *Phys. Rev. A 76* (2007), 053818.

[87] V. Arkhipkin and I. Timofeev. Temporal shape manipulation of intense light pulses by coherent population trapping. *Phys. Rev. A 73* (2006), 025803.

[88] L. Landau, L. Pitaevskii, and E. Lifshitz. *Electrodynamics in continuous media*. Pergamon Press (2nd Edition), Oxford, 1984.

[89] M. Anton, C. no, O. Calderon, and S. Melle. All-optical control of the time delay in a one-dimensional photonic bandgap formed by double-quantum-wells. *Opt. Comm. 281*, 4 (2008), 644.

[90] P. Kolchin, C. Belthangady, S. Du, G. Yin, and S. Harris. Electro-optic modulation of single photons. *Phys. Rev. Lett. 101* (2008), 103601.

[91] A. Messiah. *Quantum Mechanics*. Dover, New York, 2000.

[92] M. Fleischhauer and A. Manka. Propagation of laser pulses and coherent population transfer in dissipative three-level systems: an adiabatic dressed-state picture. *Phys. Rev. A 54* (1996), 794.

[93] M. Fleischhauer, R. Unanyan, B. Shore, and K. Bergmann. Coherent population transfer beyond the adiabatic limit: generalized matched pulses and higher-order trapping states. *Phys. Rev. A 59*, 5 (1999), 3751.

[94] C. Carroll and F. Hioe. Analytic solutions for three-state systems with ovelapping pulses. *Phys. Rev. A 42*, 3 (1990), 1522.

[95] G. Nikoghosyan and G. Grigoryan. Influence of relaxation on propagation, storage, and retrieving of light pulses in a medium with electromagnetically induced transparency. *Phys. Rev. A 72* (2005), 043814.

[96] L. Landau and E. Lifshitz. *Quantum Mechanics.* Pergamon Press, Oxford, 1977.

[97] M. Abramowitz and I. Stegun. *Handbook of Mathematical Functions.* Dover (9th Dover printing, 10th GPO printing), New York, 1964.

[98] S. Yoo. Wavelength conversion technologies for WDM network applications. *J. Lightwave Technol. 14* (1996), 955.

[99] S. Preble, Q. Xu, and M. Lipson. Changing the colour of light in a silicon resonator. *Nat. Photonics 1*, 5 (2007), 293.

[100] M. Boyd *et al.* Optical atomic coherence at the 1-second time scale. *Science 314* (2006), 1430.

[101] L. Karpa, G. Nikoghosyan, F. Vewinger, M. Fleischhauer, and M. Weitz. Frequency matching in light-storage spectroscopy of atomic Raman transitions. *Phys. Rev. Lett. 103* (2009), 093601.

[102] J. Brehm and W. Mullin. *Introduction to the structure of matter.* Wiley, New York, 1989.

[103] D. Steck. Alkali D Line data. http://steck.us/alkalidata, 2001.

[104] V. Ahufinger *et al.* Electromagnetically induced transparency in a Bose-Einstein condensate. *Opt. Comm. 211* (2002), 159.

[105] W. Ketterle, K. Davis, M. Joffe, A. Martin, and D. Pritchard. High densities of cold atoms in a dark spontaneous-force optical trap. *Phys. Rev. Lett. 70* (1993), 2253.

[106] J. Otterbach, R. Unanyan, and M. Fleischhauer. Confining stationary light: Dirac dynamics and Klein tunneling. *Phys. Rev. Lett. 102* (2009), 063602.

[107] V. Shatokhin, T. Thomas Wellens, B. Gremaud, and A. Buchleitner. Spectrum of coherently backscattered light from two atoms. *Phys. Rev. A 76* (2007), 043832.

Scientific Contributions

Publications

1. **FB** and I. Carusotto
   Light Propagation in Atomic Mott Insulators
   J. Eur. Opt. Soc.-Rapid. 3, 08005 (2008)

2. I. Carusotto, M. Antezza, **FB**, C. Ciuti and S. De Liberato
   Optical properties of atomic Mott insulators: from slow light to dynamical Casimir effects
   Phys. Rev. A 77, 063621 (2008)

3. **FB** and I. Carusotto
   Photon Wavepacket Manipulation via Space and Time dependent Electromagnetically Induced Transparency
   Submitted to *Phys. Rev. A*, e-print *arXiv:0908.0243*

Conferences, Schools and Workshops

2006

1. Dec,15. Joint Meeting Trento-Innsbruck *Ultracold Fermi Gases and Molecular States* at the Physics Departement, University of Trento.

2007

1. Jun,4-17. Workshop *Quantum Gases* at the Henry Poincar Institute in Paris. Granted by European Science Foundation (ESF) - Quantum Degenerate Dilute Systems (QUDEDIS) Network through *Short Visit Grant*.

2. Jun,22-Jul,2. Summer School *Advances on Nanophotonics II* at the Ettore Majorana Centre in Erice.
   Poster: Light Propagation in Atomic Mott Insulators.

3. Aug,27-Sep,7. Summer School *Novel Quantum Phases and Non-equilibrium Phenomena in Cold Atomic Gases* at the ICTP Centre in Trieste.
   Poster: Light Propagation in Atomic Mott Insulators.

4. Nov,30. Joint Meeting Trento-Innsbruck *Ultracold Bose and Fermi Gases* at IQOQI in Innsbruck.

2008

1. Mar,25-29. Conference *YAO 2008 (Young Atom Opticians)* in Florence.
   Talk: Light Propagation in Atomic Mott Insulators.

2. Jul,1-11. International School of Physics Enrico Fermi, Course *Quantum Coherence in Solid State System*, at Villa Monastero in Varenna.
   Poster: Scattering of Slow Light on Defects.

3. Oct,11-18. INFM School on *Physics in Low Dimensions* in Lucca.
   Poster: 1D Propagation of Slow Light via time-dependent Electromagnetically Induced Transparency.

2009

1. Feb,17-21. Conference *YAO 2009 (Young Atom Opticians)* in Vienna.
   Talk: Playing with Light in Atoms: Dynamic Electromagnetically Induced Transparency.

Visits

2008

1. Oct,8–10. Short Visit to the photonic crystal group of prof. Andreani in Pavia. Invited by Dr. Gerace.
   Talk: Dynamic Photonic Structures using Electromagnetically Induced Transparency.

2. Nov,16–26. Short Visit to the quantum optics group of prof. Imamoglu at ETH in Zurich. Invited by Visiting Prof. Carusotto.

2009

1. Jun,3. Short Visit to the photonic crystal group of prof. Andreani in Pavia. Invited by Dr. Gerace.
   Talk: Propagation of Slow Light via Time and Space Dependent Electromagnetically Induced Transparency.

2. Jun,24-28. Short Visit to the group of Non Linear Dynamics in Quantum Systems of prof. Buchleitner in Freiburg. Invited by Prof. Buchleitner.
   Talk: Photon Wavepacket Manipulation via Time and Space Dependent Electromagnetically Induced Transparency.

3. Jun,29-30. Short Visit to the quantum optics group of prof. Fleischhauer in Kaiseslautern. Invited by Prof. Fleischhauer.
   Talk: Photon Wavepacket Manipulation via Time and Space Dependent Electromagnetically Induced Transparency.

Aknowledgements

Dear friend,

I'm really tempted to switch to Italian language after fighting for more than one hundred pages with technical English[1], but still I will stand fast.

There is no doubt about the first person to cite: my Supervisor Dr. Iacopo Carusotto. It has been a great pleasure for me to work with him. In particular, since I met Iacopo three and a half years ago, I have always been impressed by his capacity to find out the fundamental physics of a certain system and then his ability in creating interesting links between optics, atoms and solid-state concepts. I arrived in Trento with a basic knowledge of optics, aiming to work on ultracold atoms and then by following him, I have discovered and enjoyed the amazing physics of slow light and other intriguing phenomena in radiation-matter interaction. The careful check of the results and the precision in the discussion of the physical concepts are the skills I tried to learn from him. The careful reading of this work is only the last among many useful attentions I received from him. I think I have been his first Master Student and (for sure) the first PhD candidate to defend the thesis under his supervision: this is a great honour for me.

It is worth mentioning the very important support of the CNR-INFM-BEC group in Trento. The group seminars were the occasions to keep in touch with the top level cold atoms physics and the financial support for going to conferences and schools gave me very interesting occasions. In particular, I want to thank Prof. Stringari for the instructive courses on Bose and Fermi gases he taught during my PhD and for the suggestion about the very nice school organized by SIF on Quantum coherence in solid state in Varenna. Discussions with Alessio Recati about the photon lifter effect in cold atoms were very useful and I also have to aknowledge his patience in giving information about burocracy and (even more) about

[1] I also have the idea that the majority of people that want to read (only) this part of the thesis are not that familiar with English, and maybe they know even less about Physics!

the city of Trento. The recent visit of our former colleague Mauro Antezza (we worked a little bit together in the proofreading of the manuscript on Casimir effect in Mott Insulator) raised interesting questions about the role of absorption in the atomic Mott Insulator. I aknowledge the help of Prof. Dalfovo who also accepted to be internal Referee of this thesis. I'm very grateful to Davide Sarchi who recently joined our group: we started working on the scattering problem in a 3D Mott Insulator; he is a nice and smart office mate and a source of many suggestions from physical research to job research. The triplet state of our office is completed by Marco Larcher, great basketball player, and (I wish him) future PhD student of the BEC group. I'm indebted to Beatrice Ricci who is able to solve all the problems I create whenever I visit some place! Last but not least I wish to express my gratitude to all the other people of the BEC group for the nice working days and pizzas, barbecues and parties we had together: Prof. Giorgini, Prof. Pitaevskii, Augusto Smerzi, Chiara Menotti, Sebastiano Pilati (PhD ad honorem!), Ingrid Bausmerth (I still remember the fantastic chicken you cooked the first year), Francesco Piazza, Gianluca Bertaina, Gentaro Watanabe, Ed Taylor, Jan Chwedenczuk (to correctly pronouce his name was one of the hardest challenge during the PhD), Philipp Hyllus. Among the different activities, I cannot forget the hystorical record of football matches of the BEC team with THREE WINS and NO DEFEATS which makes me really proud (together with the role of chef of the group barbecues).

Coming back to science, I am deeply grateful to Dario Gerace and Prof. Andreani for inviting me to Pavia and for the insightful discussions about defects in photonic crystals and scattering matrix formalism.

I wish to aknowledge the hospitality of the group of Prof. Imamoglu in ETH (Zurich) where I had the possibility to work with Iacopo and to learn something about the rich world of quantum dots.

I want to express my gratitude to Prof. Buchleitner, I met for the first time in the nice location of Erice for a summer school about Nanophotonics and he invited me in Freiburg where I was involved in intriguing discussions about coherent backscattering from atomic media with V. Shatokhin and T. Wellens. Over there, I also met D. Petrosyan who gave me very useful comments about light propagation in atomic lattices.

I gratefully thank Prof. Fleischhauer for the occasion to give a seminar in front of his group that raised fundamental questions with respect my recent work on pulse shaping and because he accepted to be external Referee of this thesis. I'm indebted to Dr. G. Nikoghosyan for the illuminating suggestions about the literature on EIT and to R. Unanyan and J. Otterbach for the discussion about Dirac-like dispersion of stationary polaritons.

I wish to thank Prof. La Rocca, I met in Varenna where he gave an in-

teresting overview of EIT and he also confirmed the growing interest in dynamical and inhomogeneous structures to manipulate light; it is a great pleasure for me that he accepted to be external Referee of the present work.

The Journal Club we started this year has been the occasion of enlighting discussions in the broad field of optics, from cavity optomechanics to polariton physics, and in particular useful hints from the experimental groups of Prof. Pavesi, Prof. Ricci and Mehr Ghulinyan are aknowledged. Prof. Ciuti, S. De Liberato, and V. Guarrera are also aknowledged for useful discussions. Financial support from INFN and ESF was crucial to attend a workshop in Paris and a school in Varenna. I'm deeply grateful to prof. Tubaro for the suggestions about Fourier Transform, Gaussian Integrals and differential equations that were crucial in the second part of this thesis (in particular for inter-band coupling integral).

I owe a big debt to all the PhD students who shared my adventure during these exciting three years, starting from the colleagues that welcomed me in the open space at the beginning of the first year (in particular M. Cristoforetti), and arriving to the students I met in the surprising *Physics PhD Workshop* of last December. I found that university is much more than simply an office. In particular, I want to mention the group of friends who have organized the outstanding PhD Barbecues: Paolo Armani, Marco Zanatta, Gianluca Bertaina (second time), Raffaele Millo, Giacomo Gradenigo, Ilaria Dorigatti, Ester Dalvit. Many thanks to Luisa Rossi Doria and Micaela Paoli: the precious secretaries of our PhD school!

I am particularly grateful to three friends I met in the Physics Department: Dr. Stefano Prezioso, Dr. Silvia Caponi and Prof. Marco Traini. We study different things, but I am always impressed by their enthusiasm for research, for understanding reality and by their *subversive and surprising way of living things*. In particular, I'm completely indebted to Marco for the hospitality during the writing of this thesis.

There was another great friend that showed to me a fascinating way to live: Nicola Fambri. Now he is no more among us, but he is still present: for this reason I want to dedicate this work to his memory.

There are a lot of friends (faces that now are in front of my eyes) that witness to me that each new day is a great Present (and also the occasion to do nice Physics): Gians (a mathematician...),Marco, Franz, Nicola Arber, Checco, Francy, Ester, Mary, Taddeo, Planck (not the one you, physicist, are thinking to), Roby, Michele, Lucy, Betta, Carol, Sacca, Panda, Enry, Lucas, Frodo, Nick, Fabri, Frengo, Federica, Beppe, Gabri, Luca, Duilio, don Roberto, Paola, Carla, Annalisa, Ciuffo, Giova, Elirosa, Irene, and many many others. It is crucial to remember the families who hosted me for dinners....a great cost!

Special thanks to Monto (a PhD in engineering at Politecnico in Milan) for the beautiful hiking in Valtellina and for his simple and sincere friendship. I'm also grateful to all the friends in Como: Davide, Andrea, Laura, Greta, Pippo, Riky, Silvia, Alberto, Valentina, Simone, Sofia, Giacomo, Marta....we haven't seen each other much during the last three years, but still the time we spent together was precious. Big thanks to Pietro and Cristina for the wonderful example they are giving me. I'm also indebted to Silvia and Maurizio, Luca and Jessica, Andrea and Laura, who asked me to be godfather of their own sons: Sofia, Ludovica and Angelo (my three Angels).

The thesis is dedicated to my Family that is the place where I come from and that is the place I belong.

Is this a conclusion? I think that it is more like a beginning...

≪Anche questa la manda direttamente il Padreterno?≫ domandò.
≪Tutto ci viene dal Padreterno≫ borbottò Peppone. ≪Tutto: il bene e il male. Tocca a chi tocca. E' toccata a noi.≫
[*Giovannino Guareschi*[2]]

[2]G. Guareschi. *Tutto don Camillo (Vol. Primo)*. Ed. BUR (Rizzoli), 2008, p. 396. Many thanks to Alberto and Carlotta Guareschi for their friendship.